Development of electrostrictive P(VDF-TrFE-CTFE) terpolymer for medical applications

Nellie Della-Schiava

N°d'ordre NNT : 2020LYSEI112

THESE de DOCTORAT DE L'UNIVERSITE DE LYON
opérée au sein de
L'Institut National des Sciences Appliquées de Lyon

Ecole Doctorale N° 162
Mécanique, Énergétique, Génie civil, Acoustique (MEGA)

Spécialité/ discipline de doctorat : Acoustique

Soutenue publiquement 03/12/2020, par :
Nellie Della Schiava

Development of Electrostrictive P(VDF-TrFE-CTFE) Terpolymer for Medical Applications

Devant le jury composé de :

Richard Liang, Professor, Florida State University, High Performance Material Institute. Rapporteur
Annie Colin, Professeur des Universités, ESPCI. Rapporteur
Masae Kanda, Associate Professor, Chubu University, Center of Applied Superconductivity and Sustainable Energy Research, Examinateur
Frederic Demoly, Maître de Conférences HDR UTBM, ICB-COMM, Examinateur
Olivier Rouvière, Professeur des Universités en radiologie, Université Claude Bernard Lyon 1 et Hospices civils de Lyon, Examinateur
Patrick Lermusiaux, Professeur des Universités, Chirurgien Cardiovasculaire, Hospices civils de Lyon, Examinateur

Pierre-Jean Cottinet, Maître de Conférences HDR, LGEF, INSA Lyon. Directeur de thèse
Jean-Fabien Capsal, Maître de Conférences, LGEF, INSA Lyon. Co-directeur de thèse
Minh-Quyen Le, Maître de Conférences, LGEF, INSA Lyon. Co-encadrant
Marie-Christine Baeitto, Directrice de Recherche CNRS, INSA Lyon. Invité

SIGLE	ECOLE DOCTORALE	NOM ET COORDONNEES DU RESPONSABLE
CHIMIE	CHIMIE DE LYON http://www.edchimie-lyon.fr Sec : Renée EL MELHEM Bat Blaise Pascal 3e etage secretariat@edchimie-lyon.fr Insa : R. GOURDON	M. Stéphane DANIELE Institut de Recherches sur la Catalyse et l'Environnement de Lyon IRCELYON-UMR 5256 Équipe CDFA 2 avenue Albert Einstein 69626 Villeurbanne cedex directeur@edchimie-lyon.fr
E.E.A.	ELECTRONIQUE, ELECTROTECHNIQUE, AUTOMATIQUE http://edeea.ec-lyon.fr Sec : M.C. HAVGOUDOUKIAN Ecole-Doctorale.eea@ec-lyon.fr	M. Gérard SCORLETTI Ecole Centrale de Lyon 36 avenue Guy de Collongue 69134 ECULLY Tél : 04.72.18 60.97 Fax : 04 78 43 37 17 Gerard.scorletti@ec-lyon.fr
E2M2	EVOLUTION, ECOSYSTEME, MICROBIOLOGIE, MODELISATION http://e2m2.universite-lyon.fr Sec : Sylvie ROBERJOT Bât Atrium - UCB Lyon 1 04.72.44.83.62 Insa : H. CHARLES secretariat.e2m2@univ-lyon1.fr	M. Fabrice CORDEY CNRS UMR 5276 Lab. de géologie de Lyon Université Claude Bernard Lyon 1 Bât Géode 2 rue Raphaël Dubois 69622 VILLEURBANNE Cédex Tél : 06.07.53.89.13 cordey@ univ-lyon1.fr
EDISS	INTERDISCIPLINAIRE SCIENCES-SANTE http://www.ediss-lyon.fr Sec : Sylvie ROBERJOT Bât Atrium - UCB Lyon 1 04.72.44.83.62 Insa : M. LAGARDE secretariat.ediss@univ-lyon1.fr	Mme Emmanuelle CANET-SOULAS INSERM U1060, CarMeN lab, Univ. Lyon 1 Bâtiment IMBL 11 avenue Jean Capelle INSA de Lyon 696621 Villeurbanne Tél : 04.72.68.49.09 Fax :04 72 68 49 16 Emmanuelle.canet@univ-lyon1.fr
INFOMATHS	INFORMATIQUE ET MATHEMATIQUES http://infomaths.univ-lyon1.fr Sec :Renée EL MELHEM Bat Blaise Pascal 3e etage infomaths@univ-lyon1.fr	Mme Sylvie CALABRETTO LIRIS – INSA de Lyon Bat Blaise Pascal 7 avenue Jean Capelle 69622 VILLEURBANNE Cedex Tél : 04.72. 43. 80. 46 Fax 04 72 43 16 87 Sylvie.calabretto@insa-lyon.fr
Matériaux	MATERIAUX DE LYON http://ed34.universite-lyon.fr Sec : M. LABOUNE PM : 71.70 –Fax : 87.12 Bat. Direction Ed.materiaux@insa-lyon.fr	M. Jean-Yves BUFFIERE INSA de Lyon MATEIS Bâtiment Saint Exupéry 7 avenue Jean Capelle 69621 VILLEURBANNE Cedex Tél : 04.72.43 71.70 Fax 04 72 43 85 28 jean-yves.buffiere@insa-lyon.fr
MEGA	MECANIQUE, ENERGETIQUE, GENIE CIVIL, ACOUSTIQUE http://mega.universite-lyon.fr Sec : M. LABOUNE PM : 71.70 –Fax : 87.12 Bat. Direction mega@insa-lyon.fr	M. Philippe BOISSE INSA de Lyon Laboratoire LAMCOS Bâtiment Jacquard 25 bis avenue Jean Capelle 69621 VILLEURBANNE Cedex Tél : 04.72 .43.71.70 Fax : 04 72 43 72 37 Philippe.boisse@insa-lyon.fr
ScSo	ScSo* http://recherche.univ-lyon2.fr/scso/ Sec : Viviane POLSINELLI Brigitte DUBOIS Insa : J.Y. TOUSSAINT Tél : 04 78 69 72 76 viviane.polsinelli@univ-lyon2.fr	M. Christian MONTES Université Lyon 2 86 rue Pasteur 69365 LYON Cedex 07 Christian.montes@univ-lyon2.fr

*ScSo : Histoire, Géographie, Aménagement, Urbanisme, Archéologie, Science politique, Sociologie, Anthropologie

ACKNOWLEDGEMENTS

TABLE OF CONTENTS

Part III. Experiments and results **70**

RESUME

Au XXIe siècle, les maladies cardiovasculaires sont devenues une cause majeure de mortalité, la première au monde, la deuxième en France après les cancers. En effet, les facteurs de risque cardiovasculaires ont augmenté de façon significative au cours des dernières décennies et ce phénomène se poursuit aujourd'hui. Ces facteurs sont responsables du développement de l'athérosclérose et mènent à des syndromes coronariens aigus, des crises cardiaques, des accidents cérébrovasculaires, des insuffisances rénales mais également à des maladies artérielles périphériques et à des anévrysmes artériels. Le traitement de première ligne de l'athérosclérose, indépendamment du territoire artériel concerné, est le traitement médical. Mais, si malgré le meilleur traitement médical, les symptômes sont importants pour les patients, le traitement interventionnel peut être considéré. Pour les anévrismes et pour la maladie artérielle périphérique, la chirurgie vasculaire est possible. La chirurgie vasculaire peut être divisée en deux catégories : la chirurgie ouverte conventionnelle et les techniques endovasculaires. Au cours des dix dernières années, les techniques endovasculaires sont devenues le traitement de première ligne pour la plupart de ces lésions artérielles. Elles sont devenues le traitement de première ligne, car elles permettent une réduction considérable de la morbi-mortalité chirurgicale et une grande réduction des coûts de santé.

Ce virage chirurgical a été possible grâce aux progrès technologiques considérables dans les matériaux. Pour tout geste endovasculaire, le chirurgien a besoin d'au moins un guide pour la navigation intra-artérielle. Il y a beaucoup de guides fabriqués et commercialisés par plusieurs industries (Terumo, Abbott, Cordis...). Ces guides diffèrent les uns des autres par leur diamètre, leur longueur, leur rigidité. Nombres d'entre eux ont une extrémité plus flexible sur une distance variable. Mais aucun d'entre eux n'est orientable. Donc, en fait, le guide n'est suffisant à lui seul que pour avancer en ligne droite. Mais dans le système artériel humain, il y a beaucoup de bifurcations, d'angulations... ce qui nous oblige à utiliser plusieurs matériaux (guides et cathéters angulés) pour cathétériser une artère cible. Ces manipulations peuvent entraîner des complications artérielles telles que perforation ou dissection artérielle et les coûts globaux sont élevés. Un guide orientable serait donc un dispositif très intéressant pour le chirurgien, le patient et la santé publique.

Les polymères électroactifs qui peuvent réaliser la conversion entre l'énergie électrique et l'énergie mécanique, et ce dans les deux sens, sont devenus l'un des matériaux intelligents les plus intéressants au cours des deux dernières décennies. En effet, ils ont de nombreux avantages: faible densité, excellentes propriétés électromécaniques, facilité de fabrication, biocompatibilité, permettant un grand potentiel d'applications dans les domaines des capteurs, des actionneurs, des robots biomimétiques et autres. Parmi tous ces polymères électroactifs, les poly(fluorure de vinyle) (PVDF) électrostrictifs ont été grandement étudiés en raison de leur haute performance électromécanique, et de leurs propriétés mécanique. Mais un problème majeur de ces polymères est l'exigence d'un champ électrique élevé pour obtenir les réponses souhaitées, ce qui n'est pas souhaitable pour certaines applications en particulier pour des applications médicales.

L'objectif de ce travail de thèse est de développer un guide intelligent car orientable pour la navigation intra-artérielle basé sur le terpolymère électrostrictif P(VDF-TrFE-CTFE). Tout d'abord, nous expliquerons les raisons ayant fait choisir ce polymère électroactif pour cette application donnée. Nous avons travaillé sur le processus de fabrication du terpolymère et sur sa caractérisation. Nous avons travaillé sur les figures de mérite des polymères pour développer une méthode pour obtenir des performances matérielles élevées et nous avons avec cette méthode évaluer celles du terpolymère nu et celles du terpolymère modifié avec du DEHP. Ensuite, pour obtenir de meilleures performances électromécaniques, nous avons évalué l'influence de différents plastifiants sur le comportement du terpolymère. Les étapes suivantes ont cherché à évaluer la possibilité d'utiliser le terpolymère à des fins médicales et nous avons testé pour cela sa résistance au processus de stérilisation et sa compatibilité cellulaire. Pour chaque étape, nous avons évalué le terpolymère pur et le terpolymère modifié et nous avons vérifié toutes leurs performances électromécaniques. Enfin, nous avons travaillé sur la modélisation de la structure et la conception du guide intelligent avec un prototype sous forme tubulaire.

Mots-clés : chirurgie endovasculaire, guide, polymère électrostrictif, plastifiant, figures de mérite, actionneur

ABSTRACT

In the 21st century, cardiovascular diseases became a major cause of mortality, the first in the entire world, the second in France after cancers. Indeed, cardiovascular risk factors have been increasing significantly over the past decades and this phenomenon is ongoing today. These factors cause atherosclerosis and lead to coronary acute syndrome, heart attacks, cerebrovascular accident, renal insufficiency but also to peripheral arterial disease (PAOD) and arterial aneurysms. First line treatment of atherosclerosis, regardless of arterial territory concerned, is medical treatment. But, if despite best medical treatment, symptoms are important for patients, interventional treatment may be considered.

For aneurysms and for PAOD, vascular surgery is possible. Vascular surgery can be divided into two categories: conventional open repair (COR) and endovascular techniques (ET). During the last ten years, ET became the first line treatment for most arterial injuries. ET has become the first line treatment because it allows a considerable reduction in surgical morbi-mortality and a great reduction in health costs.

This surgical shift was possible thanks to the considerable technological advances in materials. All ET needs at least a guide wire for intra-arterial navigation. There are a lot of guide wires fabricated and marketed by several industries (Terumo, Abbott, Cordis…). These guides differ from each other in their diameter, length, stiffness. Numbers of them have an extremity more flexible over a variable distance. But none of them is steerable. So actually, guide wire is sufficient only for straight navigation. But in the human arterial system, there are many bifurcations, angulations... which forces us to use several materials (guide wires and angulated catheters) to catheterize a targeted artery. These manipulations can lead to arterial complications such as perforation or dissection and global costs are high. A steerable guide wire would therefore be a very interesting device for the surgeon, the patient and the public health.

Electroactive polymers (EAPs) which can realize the conversion between electrical and mechanical energy in both ways, have been emerging as one of the most interesting smart materials in the past two decades. In fact, they have many advantages: low density, excellent electromechanical properties, ease of processing, biocompatibility, permitting a great potential of applications in the fields of sensors, actuators, biomimetic robots and so on. Among all of EAPs, poly(vinylidene fluoride)(PVDF) based electrostrictive polymers have been greatly investigated due to their high electromechanical performance, particularly strain and elastic energy density. But one major problem of these polymers is the requirement of high electric field to obtain the desired responses which is not safe for some applications particularly for medical applications.

The objective of this work is to develop a smart steerable guide wire for intra-arterial navigation based on the electrostrictive terpolymer P(VDF-TrFE-CTFE). First of all, we explain the reasons of choosing this EAP for this application. Then, we worked on the fabrication process of the terpolymer and on its characterization. We worked on Figures on merit of polymers to achieve a method to obtain high material performances and we evaluate with this method the neat and the modified terpolymer with DEHP. Then, to obtain better electromechanical performances we evaluated the influence of different plasticizers on the behavior of the terpolymer. The following steps evaluated the possibility to use the terpolymer for a medical use and we tested its resistance to the sterilization process and its cellular compatibility. For each step, we evaluated the neat and the modified terpolymer and we check all the electromechanical performances. Finally we work on modeling the structure and design of the smart guide wire with a tubular prototype.

Keywords : endovascular surgery, guide wire, electrostrictive polymer, plasticizer, figures of merit, actuator

ABBREVIATIONS

BDS : broadband dielectric spectroscopy
CNT : carbon nanotube
COR : conventional open repair
CP : conductive polymers
CTFE : chlorotrifluoroethylene
CuPc : copper-phtalocyanine
DBS : dielectric breakdown strength
DEHP : 2-ethylhexyl phthalate
DINP : diisononyl phtalate
DOF : degree of freedom
D_{outer} : outside diameter
DSC : differential scan calorimetry
DE : dielectric elastomer
E_c : coercive electric field
EAP : electroactive polymers
ET : endovascular techniques
FE : ferroelectric
FOM : figures of merit
GPa : Giga pascal
HAS : “haute autorité de santé”
IPG : ionic polymer Gel
IPMC : ionic polymer metal composite
IPN : inter-penetrating network
L: length
LCE : Liquid crystal elastomer
LME : laboratory mixing extruder
LZT : lead zirconate titanate
MEMS : micro electromechanical systems
MWNT : multi-walled carbon nanotubes
OLED : organic light-emitting diode
PANI : polyaniline
PAOD : peripheral arterial occlusive disease
PDMS : polydimethylsiloxane
PEEK : poly (ether ether Ketone)
P_r : remnant polarization
PPS : sulfonated polysulfone
PPy : polypyrrole
PT : polythiophene
P(VDF-TrFE-CTFE) : Poly(vinylidene fluoride-Trifluoroethylene-chlorotrifluoroethylene)

PU : polyurethanes
RPM : revolutions per minute
SPPSU : sulfonated polyphenylsulfone
SWNT : single-walled carbon nanotubes
T_c : curie temperature
T_m : melting temperature
TRL : technology readiness level

PART I:

Bibliographic study

PART I: Bibliographic study

I.1. Endovascular surgery, techniques and materials

In the 21st century, cardiovascular diseases became a major cause of mortality, the first in the entire world, the second in France after cancers. This is explained principally by changes in health behaviors.[1,2] Indeed, cardiovascular risk factors have been increasing significantly over the past decades and this phenomenon is ongoing today. Cardiovascular risk factors are represented by smoking, diabetes, obesity, dyslipidemia, hypertension and sedentary lifestyle. These factors cause atherosclerosis and lead to coronary acute syndrome, heart attacks, cerebrovascular accident, and renal insufficiency and so on. These pathologies are the main cause of cardiovascular deaths. But these cardiovascular risk factors lead also to chronic peripheral artery occlusive disease and arterial aneurysms.

An arterial aneurysm is an abnormal dilatation of an artery with an increased diameter of at least 1,5-fold the normal diameter. The main location is popliteal artery and abdominal aorta. For abdominal aorta, the main risk is arterial rupture and massive hemorrhage. In case of rupture, despite surgical progress, mortality rate is about 80 % because many patients do not reach hospital because of a sudden death.[3]

For popliteal artery, rupture is rather rare and not lethal but aneurysms cause a destruction of leg arteries and lead to acute ischemia with poor possibilities of revascularization and a high risk of major amputation.[4,5]

PAOD involve thousands of patients especially in high-income countries. The prevalence increases with age reaching almost 20 % for patients over 80 years old. So this pathology become more and more frequent due to the population ageing.[6-9]

This pathology is not directly fatal but this is a major cause of handicap because of many leg amputations. Moreover, atherosclerosis involve most of time several arterial territories and PAOD must lead to detection of coronary and cerebrovascular disease at least.

First line treatment of atherosclerosis, regardless of arterial territory concerned, is medical treatment including control of each cardiovascular risk factors, physical activity especially walking, associated with statin and antiplatelet therapy.[6]

If, despite best medical treatment, symptoms are important for patients, interventional treatment may be considered.[6,8]

For aneurysms and for PAOD, vascular surgery is possible. Vascular surgery can be divided into two categories: conventional open repair (COR) and endovascular techniques (ET). During the last ten years, ET became the first line treatment for most arterial injuries. This surgical shift was possible thanks to the considerable technological advances in materials.

ET has also become the first line treatment because it allows a considerable reduction in surgical morbi-mortality. Moreover, total in-hospital stays and number of days in intensive care units is significantly reduced permitting a reduction in costs and a faster resumption of professional and personal activities. For many endovascular interventions, ambulatory surgery is even possible. Actually, French government via its “Haute autorité de Santé” (HAS) edit recommendations about ambulatory surgery. This is a real public health issue.

ET is mini-invasive surgery with no scar that is also an advantage for the patient. Even if esthetic considerations seems not to be the priority for severe pathologies, for patients and for society it is a priority.

Here is an example to illustrate the differences between COR and ET. To treat an abdominal aortic aneurysm, COR consists of an exclusion of the aneurysm and an aortic replacement by an aortoiliac prosthetic bypass. This is a major surgery, with large laparotomy, with often the necessity of few days in an intensive care unit and a total in-hospital stay of at least a week. Peri-operative mortality is about 3 % and morbidity about 20 % with major possible complications as coronary acute syndrome, pneumonia, renal insufficiency…[10] This surgical procedure needs long and deep general anesthesia. Transfusions of blood cells are almost systematic. In post-operative period, despite new analgesic techniques and drugs, patients have quite severe abdominal pains, bowel motility disorders…

Figure 1 shows per-operative photographs illustrating this type of surgical procedure.

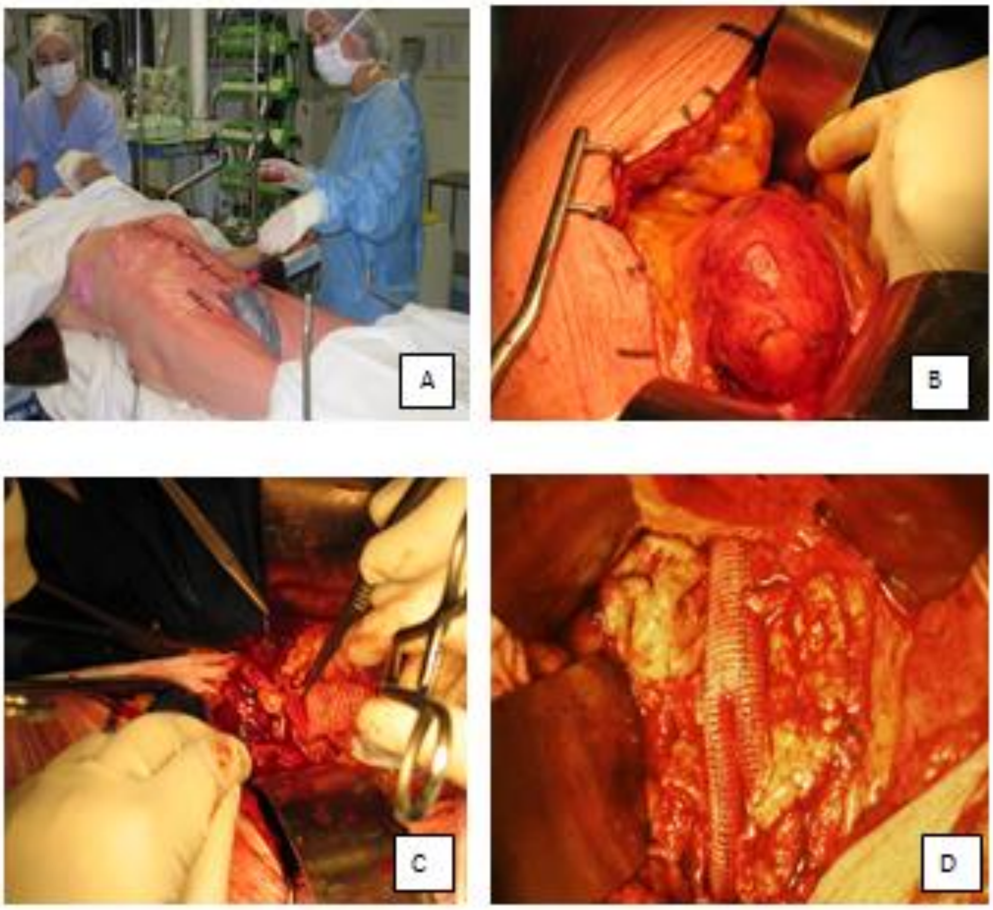

E

A. Installation, schemes of future scars
B. Median laparotomy for aneurysm exposition
C. Proximal anastomosis between prosthesis and aortic neck
D. Final result
E. xypho-pubic laparotomy scar

Figure 1. Open repair for abdominal aortic aneurysm

For the same pathology, ET consists of aortobiiliac endoprosthesis by bilateral femoral puncture. This surgical procedure has its own risks and complications as embolic acute limb ischemia, renal insufficiency, stroke, femoral pseudoaneurysm… but mortality is close to 0 % and morbidity is about 15 % with less severe complications.[10] Transfusions are usually no necessary because of low blood loss and no aortic clamping. There is no scar, only 2 small orifices in groin fold. This surgical procedure may be done under local anesthesia. No intensive care unit is necessary and total in-hospital stay is very short; ambulatory is even possible. There is very low pain or no pain in post-operative period.

Figure 2 shows per-operative photographs illustrating this surgical procedure.

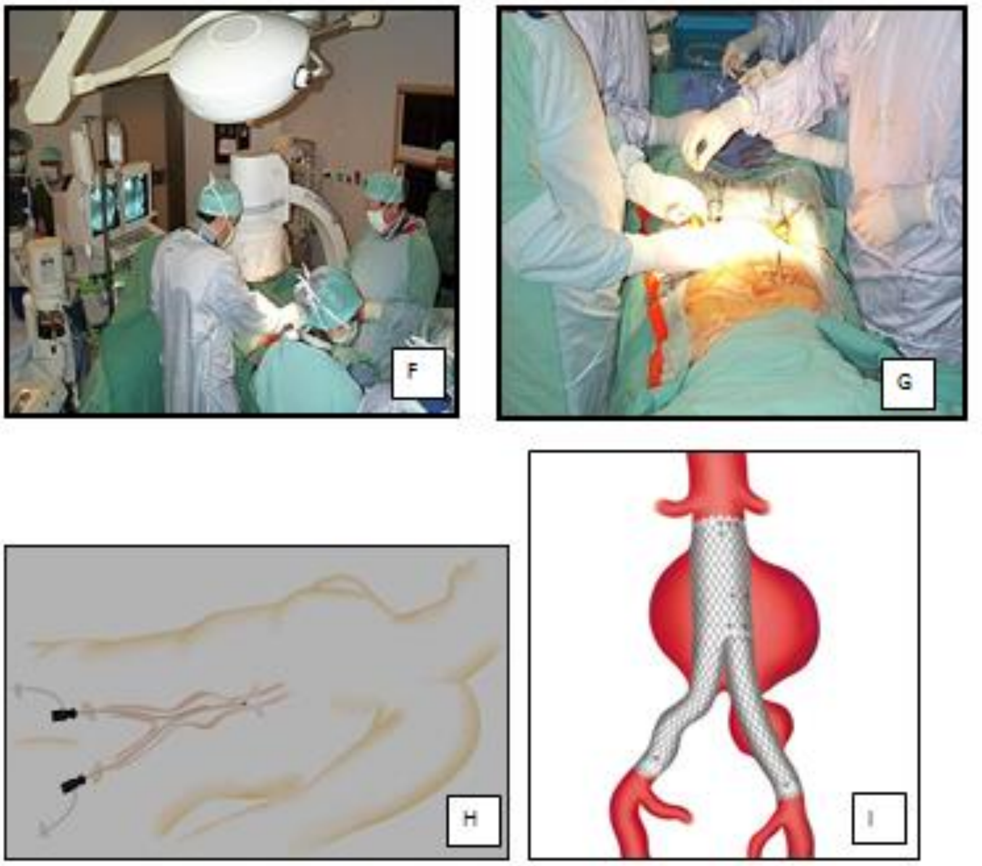

F. Preoperative installation in an hybrid room
G. Local asepsis of groin fold for femoral puncture
H. Intraarterial progression of the endoprosthesis
I. Final result
J. No scar, just 2 small orifices

Figure 2. Endovascular repair for abdominal aortic aneurysm

For PAOD, lesions are different but principles are the same. Lesions in PAOD are stenosis or thrombosis. Stenosis is a reduction of the lumen of the artery because of atheroma and thrombosis is the total occlusion of the lumen.

To treat these occlusive lesions, whatever the arterial territory, ET consists in balloon angioplasty and stenting. These techniques crush the atheroma on the arterial wall and reopen the arterial lumen and so improve the blood flow.

Figure 3 illustrates these techniques, with schemes and then with peroperative angiograms.

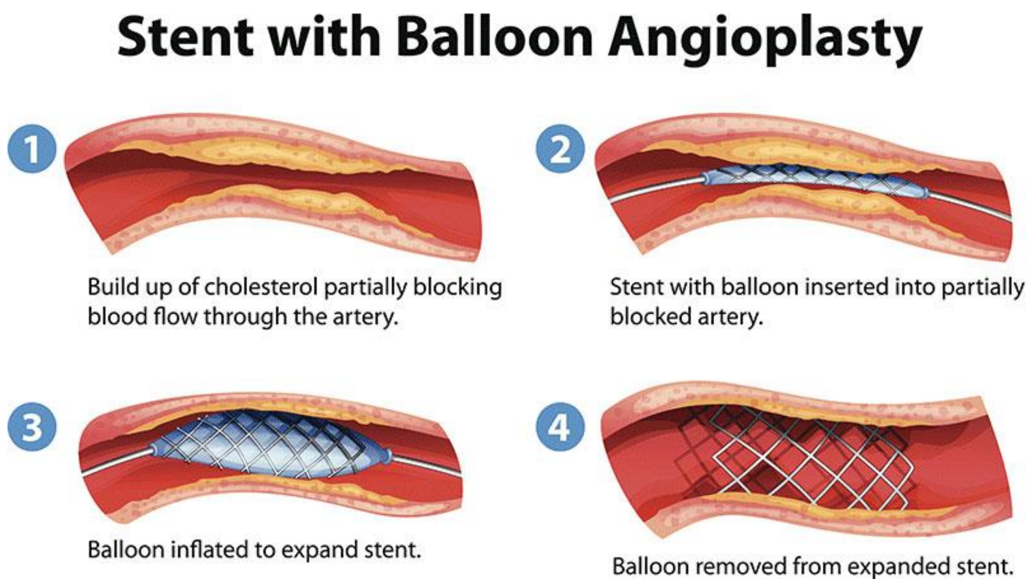

Figure 3. Endovascular techniques to treat arterial atheromatous lesions

In the following photographs (Figure 4), there is a thrombosis in the photo A, and in the photo B, the arterial flow is restored.

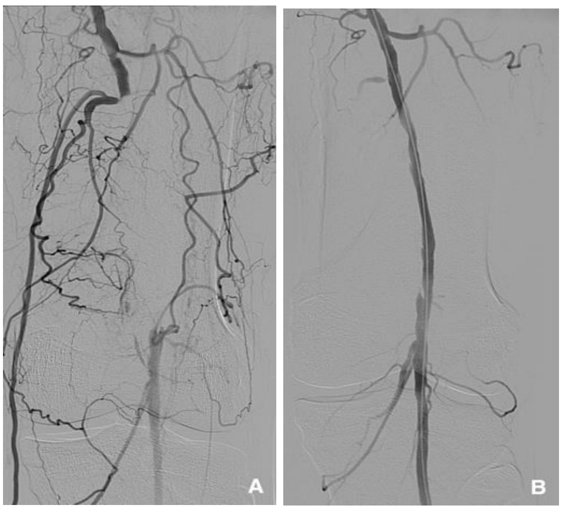

Figure 4. Per-operative angiograms showing successful endovascular treatment of a superficial femoral artery thrombosis.

In the following photographs (Figure 5), there is an iliac stenosis in the left image, successfully treated with a stent in the right image.

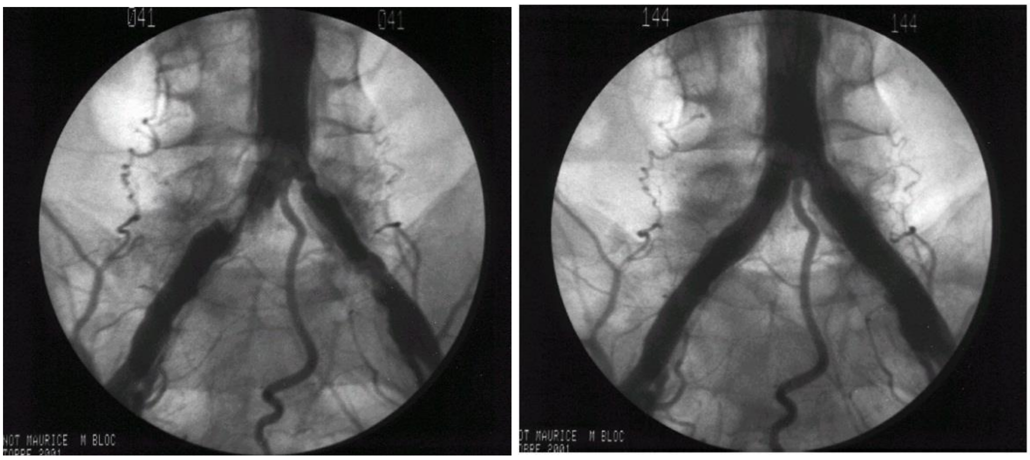

Figure 5. Successful endovascular tretament of an iliac artery stenosis.

For PAOD, COR consists in bypasses to shunt the pathologic arterial segment, with large scars, pains and difficulties to walk and to regain activities (Figure 6). Black segment correspond to the thrombosis, blue segment correspond to the bypass.

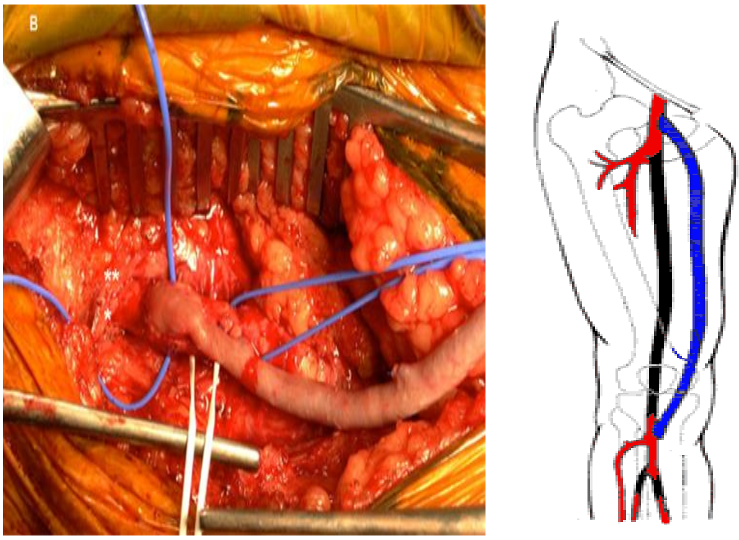

Figure 6. scheme and per-operative photo of a femoropopliteal bypass.

So with these examples, we understand that there are many advantages for ET. Nevertheless, a lot of materials and equipment are needed for ET contrary to COR.

All ET needs at least a guide wire for intra-arterial navigation.

Intra-arterial penetration is done more often by common femoral artery puncture. More rarely, radial or humeral or popliteal puncture may be done. For this step, we use a very simple and short catheter as illustrate in Figure 7.

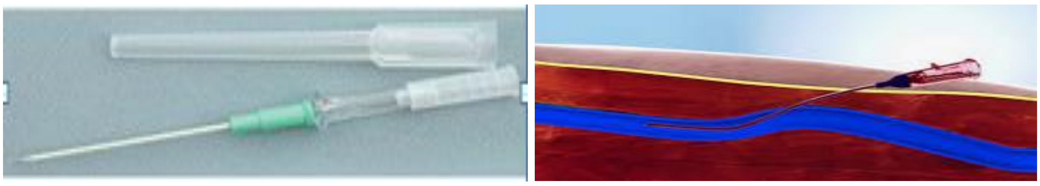

Figure 7. Angiocatheter and arterial puncture.

When this catheter is on the artery, blood reflux is obtained and we introduce in the catheter a guide wire as shown in Figure 8.

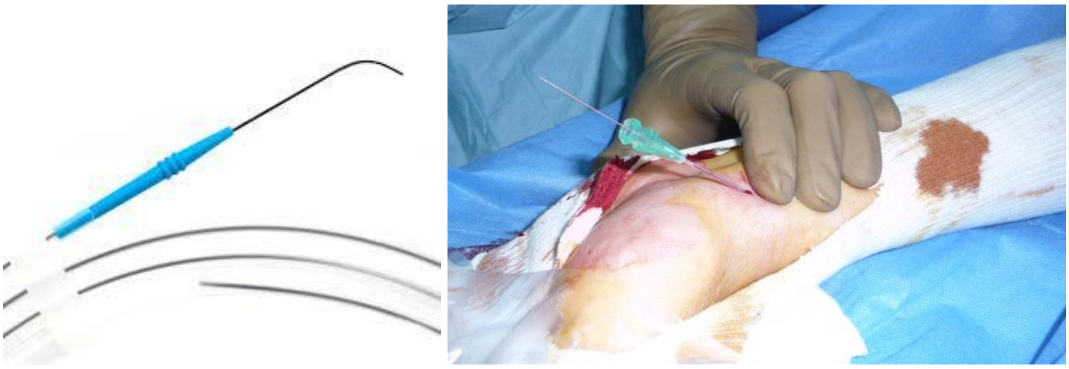

Figure 8. Guide wire in its packaging and then in the artery through the angiocath.

This guide wire allow us in first step to navigate into arteries. Guide wires are radio-opaque so we can see and follow them on radioscopy (Figure 9).

Figure 9. Per-operative radioscopy showing the guide wire in the iliac arteries.

As it has been show in Figure 8, most of the guide wires are curved on one of their extremity in order to reduce the risk of arterial perforation during guide wire advancement in arterial flow. There are a lot of guide wires fabricated and marketed by several industries (Terumo, Abbott, Cordis…) (Figure 10). These guides differ from each other in their diameter, length, stiffness. Numbers of them have an extremity more flexible over a variable distance.

Figure 10. Different guide wire in their packaging

But none of them is steerable. So actually, guide wire is sufficient only for straight navigation. But in the human arterial system, there are many bifurcations, angulations, as illustrates the simplified scheme in Figure 11.

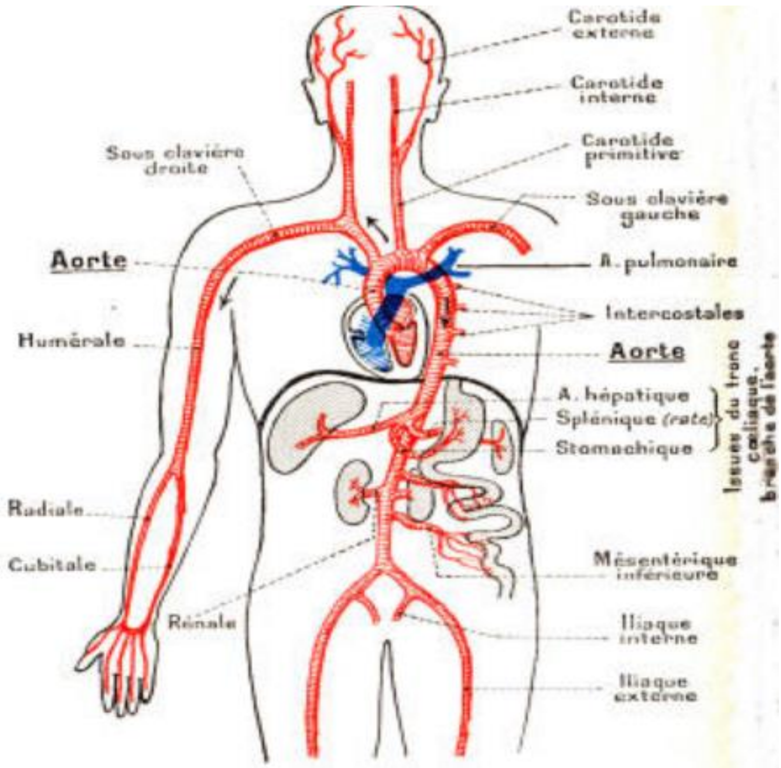

Figure 11. Simplify scheme of the human circulatory system

In angiograms of Figure 12, we see for example, on the right, angulation of more than 90 ° between abdominal aorta and renal arteries, and on the left, angulation between thoracic aorta and supra-aortic trunks.

Figure 12. Per-operative angiograms of thoracic and abdominal aorta and their respective branches.

To treat lesions of these arteries, we need to catheterize that means to enter in them. To direct the distal end of the guide wire, we need angulated catheters. There are many forms of catheters in order to catheterize arteries according to different angulations and diameter vessels. Figure 13 illustrates the different types of catheters or probes.

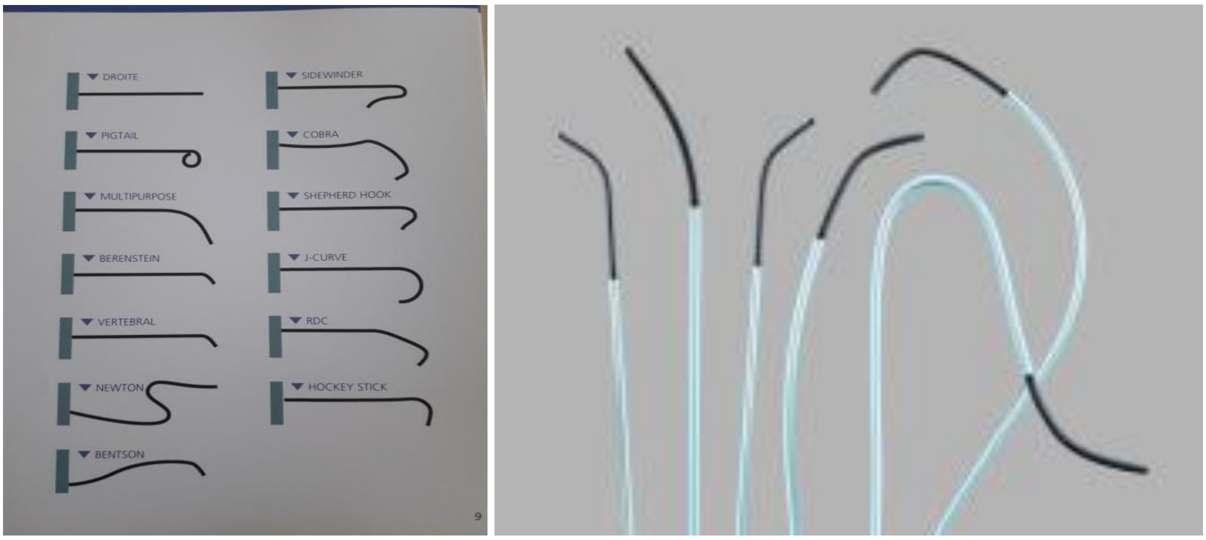

Figure 13. Different forms of catheters for intravascular catheterism

We introduce the catheter of choice on a soft guide wire until the ostium of the targeted artery identified on angiogram. We remove the guide wire and we block our catheter in the ostium. When the catheter is stabilized in the targeted artery, we gently push the soft guide wire in the artery. Then we remove the angled catheter and we put onto the soft guide wire a new straight catheter to change the soft guide wire for a more stiff. Figure 14 illustrates the procedure, and the complexity for the surgeon.

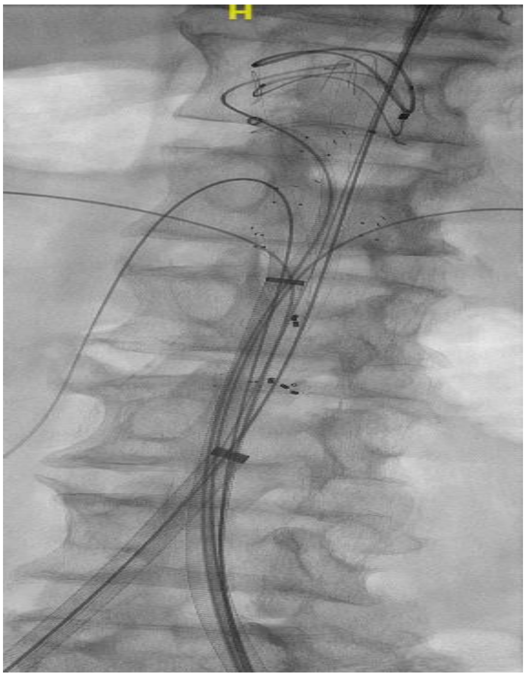

Figure 14. Per-operative radioscopy showing multiple guidewires in the targeted arteries.

These steps need several manipulations with possible risks. The main risk is to fail to catheterize. Indeed, when we push the guide, the force applied may roll back the angled catheter and we must try again. It's not a real complication for the patient but this lengthens the operating time what can be harmful for the patient.

For the patient directly, the main risks are arterial perforation or arterial dissection. Dissection is a lesion of the arterial wall with a short-term risk of stenosis or thrombosis and a long term risk of aneurysm. The consequence may be an acute or subacute ischemia of the organ or member perfused by the dissected vessel. If the vessel is the superior mesenteric artery, dissection causes a mesenteric ischemia with important risk of bowel necrosis and death. If it is the renal artery, dissection causes renal insufficiency. If it is leg artery, dissection causes limb ischemia with a risk of amputation.

On the other hand, perforation may cause a hemorrhage. If hemorrhage is important or difficult to control, death is possible.

For each guide manipulation, push and pull, these risks exist.

So it is very important to reduce the number of intra-arterial manipulations. For this, steerable guide wires may be a good solution, avoiding or reducing the use of angled catheters. But such guides do not exist.

To obtain the same goal, i.e navigate into angled vessels without manipulations of push and pull with catheters, it exists several different researches but no commercialized product.

Main works concern robotic researches. The goal is, from the preoperative CT-scan, to program the guide wire's route to go from the arterial puncture to the targeted artery with coordinates x, y and z in the 3 planes of space. And the robot can mechanically push the guide wire until this final destination. To obtain the displacement of the guide wire in angled vessels, electromagnetic sensors are under study and development (Figure 15). Electromagnetic tracking seems to be a promising tool to improve navigation of endovascular instruments. This technology is used in many studies for catheterization techniques in EVAR.[11,12] They are still mostly performed in vitro,[13-15] although some teams have tested this device in vivo on swines.[16,17]

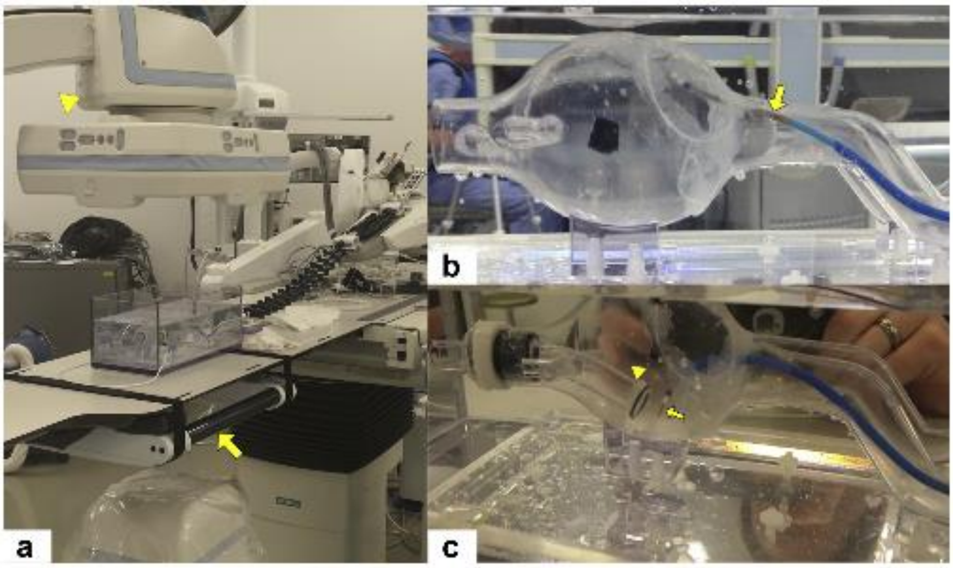

Figure 15. Electromagnetic tracking for endovascular navigation in an AAA phantom with the 9F Magellan Robotic Catheter (Hansen Medical Inc)

But catheters for the instance used for electromagnetic navigation have large diameter. They are catheters and not guide wires. So works on steerable guide wires seem to be very complementary.

There is another work very recent and interesting about electromagnetic steerable guide wire developed by Zhao et al (Massachusetts Institute of technology MIT) published in Science Robotics.[18] The goal is medical, for neuroradiology but we can totally imagine the use of this new device for vascular surgery. This technology is in development for the treatment of acute stroke to help to clear blood clots in the brain. The core of the guide wire is a flexible nickel alloy coated with a slippery hydrogel and the guide wire is steered with magnets (Figure 16). This is in vitro studies for the instance. This good result may be confirmed in in vivo model. No product is yet commercialized.

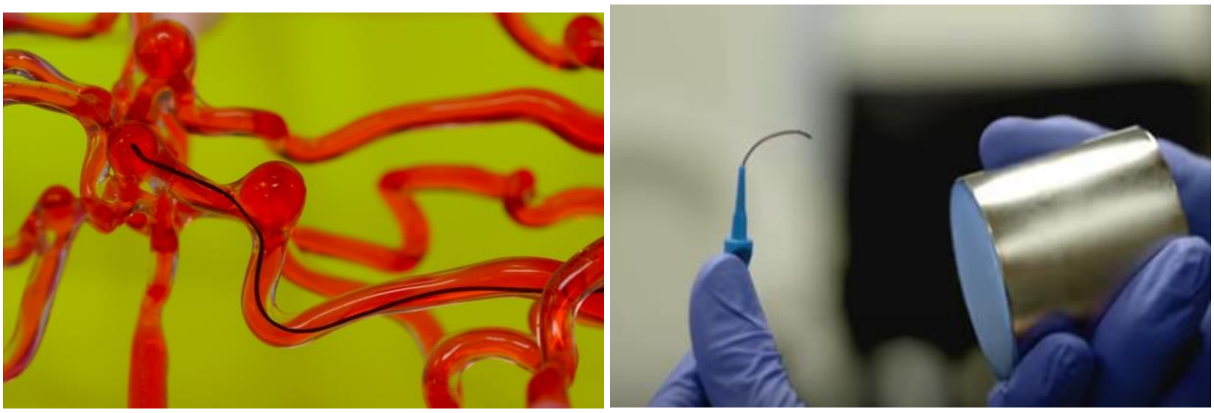

Figure 16. Illustrations of Zhao et al works about magnetic steerable guide wire.

Medtronic enterprise developed and commercialized a steerable catheter for a new technology for the treatment of abdominal aortic aneurysm with short neck named APTUS (Figure 17). It is a catheter quite stiff, with a large diameter, in which the surgeon introduces another catheter on which there are screws to fix the endoprosthesis in the short neck. This device named APTUS HeliFX TM®. Here is an illustration of this device. To obtain the orientation of the extremity of the catheter, the surgeon uses an electronic handle. With this we can obtain an angulation of at least 90 °. But this system doesn't permit the navigation into arteries. It is usable only in large diameter vessel as aorta.

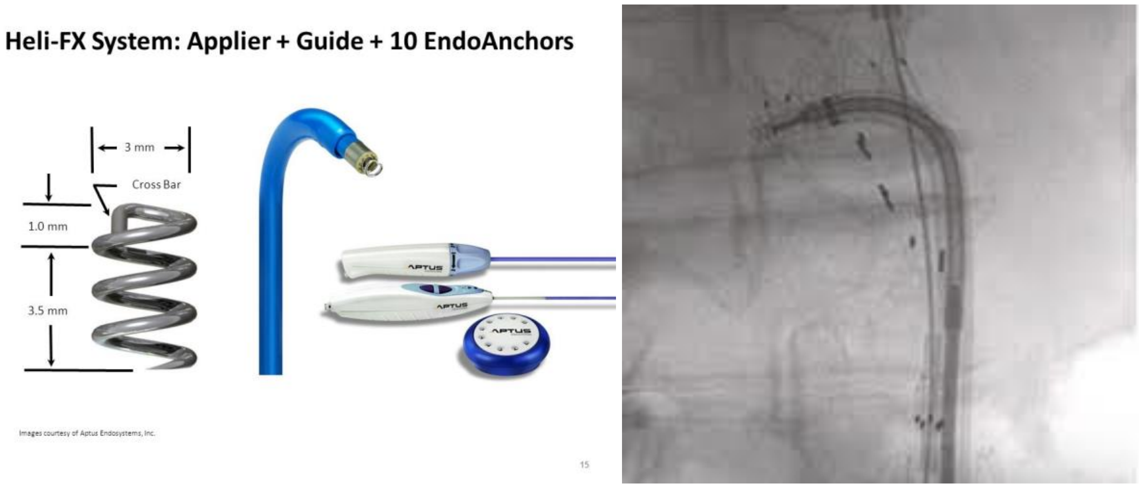

Figure 17. APTUS HeliFX system, Medtronic Vascular Inc.

We only talk about peripheral vascular surgery, but guide wires are also used in a very large scale, for interventional cardiologists, neurologists, radiologists, urologists… Every day in the world, thousands of guides are used in these different medical specialties.

By reducing operating time and costs and medical complications, steerable guide wires seem to be a real public health issue.

I.2 Electroactive polymers (EAP

A very good bibliographical research was carried out in the thesis of Xunqian YIN, with whom we collaborated during preliminary work for this thesis. This part takes up again the synthesis which was presented in the manuscript of Xunqian YIN "Modification of electrostrictive polymers and their electromechanical applications" https://tel.archives-ouvertes.fr/tel-01278439/document (page 26 to 63 of the following manuscript).

I.2.a. Introduction and historical background

Since 19st century, several publications have studied the transformation of the mechanical vibration into electrical energy. Most of these researches work concern classical piezoelectric ceramic materials. More recently, EAP seem to be promising.[19] They can be sensors but also actuators. They are promising particularly for actuation because of huge deformations through external electric fields. In fact, even if piezoelectric ceramics remain more efficient in terms of energy conversion by weight unit, their stiffness and brittleness limit their use. Moreover, ceramics require high temperatures contrary to EAP.[20] So rapidly various applications including actuators and sensors, robotic, storage devices, medical devices, acoustic transducers, high energy weapon systems...seem to be compatible with EAP. Haptic feedback, especially for handheld touchscreen devices and peripherals, is also a current new market.[21]

EAP emerged back in 1880, with Wilhelm Roentgen works. In his experiment, a 16 x 100 cm natural rubber strip with one end fixed and the other hand attached to a mass was subjected to an electric field across the rubber band and an elongation was observed.[22] Then, Sacerdote formulate a theory on strain responses to an applied electric field in 1889.[23] In 1925, Eguchi discovered the first piezoelectric polymer named electret.[24] A electret is a dielectric material with a quasi-permanent electric charge or dipolar polarization. Electrets can generate voltage when subjected to stress and deformation in response to an applied electric field. However the low deformation limits its applications as actuator and it is widely used as sensors or transducers such as an electret microphone. But it is only in 1949 with Katchalsky's work that real stimulated polymers are obtained for the first time. It was chemically stimulated polymers.[25] In 1969, Kawai was also able to demonstrate that polyvinylidene fluoride (PVDF) exhibits a large piezoelectric effect.[26] In 1971, Bergman also reported the piezoelectric effect of PVDF.[27] The piezoelectric,[28] pyroelectric,[27,29] ferroelectric,[30,31] electrostrictive[32,33] properties and transition behaviors[34] of PVDF were extensively investigated during 1970s and 1980s. Ferroelectric materials are materials possessing a spontaneous polarization which can be switched by an applied external electric field. The traditional ferroelectric materials are inorganic ceramics.

In 1977, other type of EAP, conducting polymer of polyacetylene, was discovered by Hideki Shirakawa et al.[35] During the 1980s, a great number of other polymers had been studied and had been shown a piezoelectric effect.[36,37] Ionic polymer metal composite (IPMC) was shown to have actuator properties in 1992 by Oguro et al in Osaka.[38]

On the other hand, Zhang et al, have developed fluorinated copolymers of which the energy density was significantly increase.[39] More recently, other significant classes of EAP have emerged whose carbon nanotube actuators developed by Baughman et al since 1999.[40]

It's only from the 1990s that scientists and industrial firms began to study electrically stimulated polymers for industrial applications. And actually we can say that EAP are one of the most interesting smart materials in the past two decades.

There are many applications. For example, in 2002, an aquarium of swimming robotic fishes was fabricated by Eamex Corporation in Osaka (Figure 18); that is the first commercial EAPs product. What makes it remarkable is that the brightly colored plastic fishes propelling themselves through the water in a fair imitation of life without any mechanical parts : no motor, no drive shaft, no gears, not even a battery.

Figure 18. The first reported commercial EAPs

Because of great increasing researches works and industrial uses, in order to enhance the cooperation among researchers, investors and users, Yoseph Bar-Cohen, one of the EAPs field's pioneers, organized the first EAPs conference through the International Society for Optical Engineering (SPIE) as a part of the Smart Structures and Materials Symposium in 1999.[41] Since then, the EAP actuators & devices (EAPAD) conference is held annualy and it has become the largest communicating platform for researchers and investors involved in the field of EAPs. Besides, a website named Worldwide EAP (WW-EAP) Webbub was built to gather and archive related information about the development of all EAPs. A semi-annual WW-EAP newsletter has been published electronically with short summary from authors worldwide to provide a snapshot of the latest advances related of this field such as materials, processing approach, analytical modeling, and applications and so on.

In 2006, he develops a classification of polymers, accepted and used for science community. This classification is the reference about EAP.[42]

Recently, many high-tech companies have invested more financial resources to accelerate the transfer process of EAPs technology. In 2004, Artificial Muscle Inc. was spun out of SRI international to commercialize EAPs technology. On 2014, Parker Hannifin Corporation, the global leader in motion and control technologies announced that it purchased intellectual property and licenses from Bayer Material Science LLC and its AMI business unit. The acquired EAPS technology will be used in new and existing Parker products and services in medical devices and it will strengthen Parker's smart material development capabilities. According to the IDTechex Research report "Electroactive polymers and devices 2013-2018", the EAPS potential market would be US$ 245 million in 2013 and this value will increase up to US$ 2,25 billion by 2018.

For instance, with touchscreens everywhere, haptic for consumer portable touch screen devices and peripherals is going to be the next big application and potentially the first large scale implementation of EAP actuators. Prototypes and evaluation studies have been just recently made. Figure 2 presents the world's next-generation ultrathin and flexible keyboard via EAPs by Novosentis, Inc. The Awake™ keyboard (Figure 19) has a super-slim profile and appealing design with haptic keys. It is designed to replace the bulk mechanical keyboards. Novosentis, Inc. won the 2014 CES (Customer Electronics Show) Innovation Awards in the embedded technologies category with this product.

Figure 19. Haptic keyboard via ultrathin and flexible EAPs technology by Novosentis, Inc.

In general, EAPs are very attractive materials and have a wide range of applications. In the next section, a short presentation of the common EAPs materials and their recent developments will be done; the classification of EAP has been realized using the proposed method of Bar-Cohen.

I.2.b. Types of EAP

Generally, EAP are defined as lightweight, flexible organics compounds, capable of changing size and shape through electrical field. Comparing to ceramics, they are easier to process into large area films, and they are a good ability to be molded into a desirable dimension.

There are numerous types of EAP but most of them fall into 2 categories, ionic (involving mobility or diffusion of ions) or electronic (driven by electric field or coulomb forces) polymers. Table 1 reports main types of EAP according to Bar-Cohen classification.

Electronic EAP	**Ionic EAP**
-Dielectric elastomer EAP	-Conductive Polymers
°Acrylics	-Electrorheological Fluids (ERF)
°Silicones	-Ionic polymers gel (IPG)
°Polyuréthanes (PU)	-Ionic Polymer metallic composite (IPMC)
-Electrostrictive Graft elastomers	-carbon nanotubes (CNT)
-Electrostrictive paper	
-Electro-viscoelastic Elastomers	
-Ferroelectric polymers	
-Liquid crystal elastomers (LCE)	

Table 1. Main types of EAP

I.2.b.i. Ionic EAP

Their actuation is caused by the displacement of ions inside the polymer. Electric field applied leads to a displacement of ions inside the polymer with then a change in solvent volume near each electrode. Cations migrate to the cathode while anions, which are immobile in the polymer, undergo an attractive force of the anode. In the same time, water molecules diffuse to regions with high concentrations of positive ions to equilibrate charges distribution. As a consequence, region near the cathode expands in volume and the region near the anode decreases in volume. All these mechanisms lead to a flexion of the ionic polymer to the anode. Their structure is equivalent to an alkaline battery that is two electrodes separated by electrolytes. Figure 20 shows an example of the global structure of a ionic polymer.

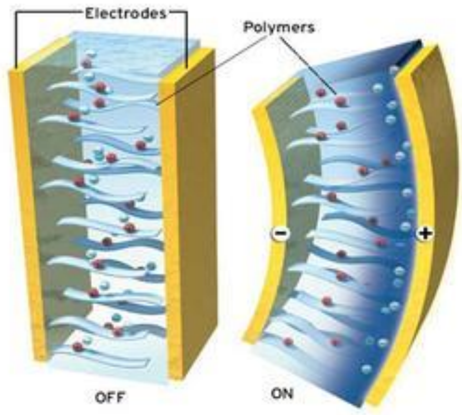

Figure 20. Example of ionic polymer structure

Only a few volts are needed for actuation, but the ionic flow implies a higher electrical power needed for actuation and energy is needed to keep the actuator at a given position. I introduce and briefly detail main ionic EAP in the following text.

I.2.b.i.1.Ionic polymer metallic composite

IPMC are highly active actuators. They show very large deformation in the presence of low applied voltage and exhibit low impedance. They need a humid environment to obtain better properties but they can be used in dry environment as well if they are self-contained encapsulated actuators. They may be modeled as both capacitive and resistive element actuators. Their main applications are biomechanics and biomimetics applications with the actuation as artificial muscles.[43]

IPMC consist in a thin ionomeric membrane with noble metal electrodes plated on both surfaces. It also contains cations to balance the charge of anions fixed to the polymer backbone. A schematic representation is shown in Figure 21.

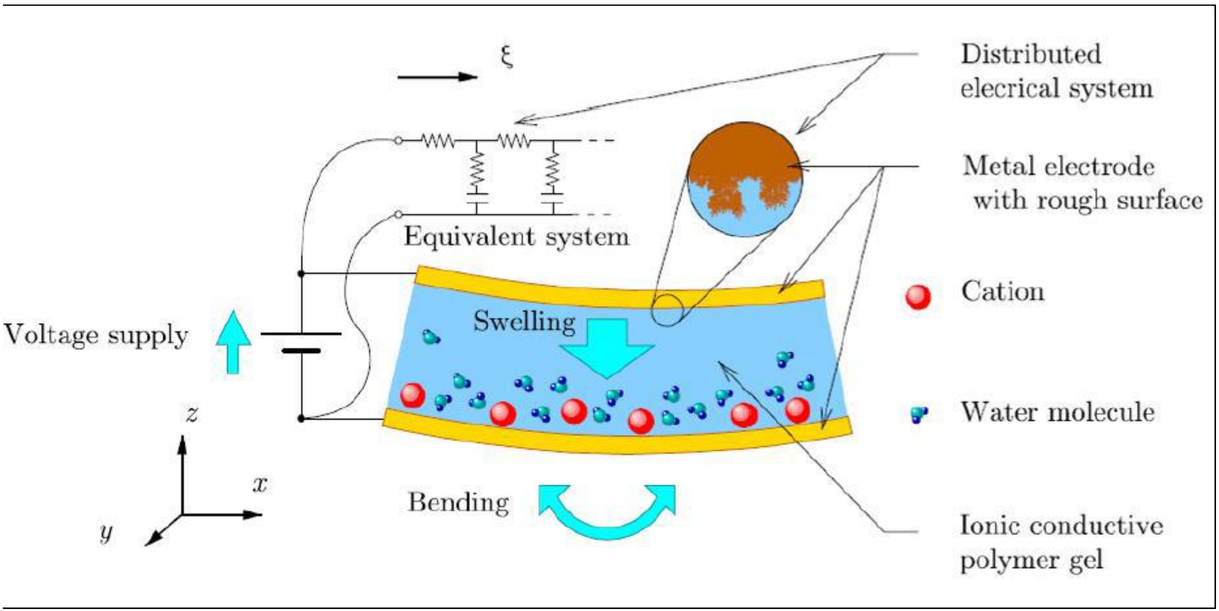

Figure 21. Physical structure of IPMC

IPMC work through electrostatic attraction between the cationic counterions and the anode.

There are two main material used as ion-exchange membrane : perfluorinated alkenes with short side-chains terminated by hydrophilic ionic groups and styrene/divinylbenzene-based polymer with ionic groups substituted from the phenyl rings. Perfluorinated alkenes are generally chosen. The chemical structure of these polymers combines a hydrophobic Teflol-like backbone with short side chains terminated by hydrophilic sulfonic acid (Nafion®) (Figure 22)or carboxylated groups (Flemion®) .[44]

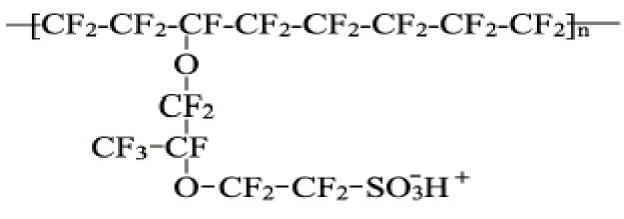

Figure 22. Chemical structure of Nafion

IPMC were initially developed as a solid polymer electrolyte for water electrolysis by Takenaka and Millet.[45,46] The fabrication method of IPCMs involves a two-step process : the first in-depth composite process and the secondary surface electroding process. In the first step the Nafion membrane is immersed into a precursor salt solution containing the noble metal cations for the permeation of metal cations and exchange with H^+ and then a reduce agent

($NaBH_4$ or $LiBH_4$) is introduced into the solution to reduce the metal cations into atoms, leading to a Nafion/metal composite. In order to improve the conductivity, a layer of metal is deposited on the initial metallic surface with the same chemical reduction reaction in the second stage. The metal particles distribute homogeneously within the polymer membrane and predominate near the two surfaces with a typical depth of 1 at 10 µm.[47] Pretreatment including roughening the surfaces with sandpaper and cleaning the Nafion membrane are required to improve the adhesive strength and to reduce the resistance of the deposited electrode. An extra ion-exchange of H^+ in the IPMCs membrane with the other desired counter ions such as Li^+ or Na^+ is applied to fabricate different type actuators. With an applied voltage on two sides of IPMCs, the mobile cations with associated water migrate along the water-channels from the anode to the cathode resulting in a volume expansion in the cathode side and contraction in the anode side and finally a bending of the IPMCs to the anode side as shown in Figure 23.

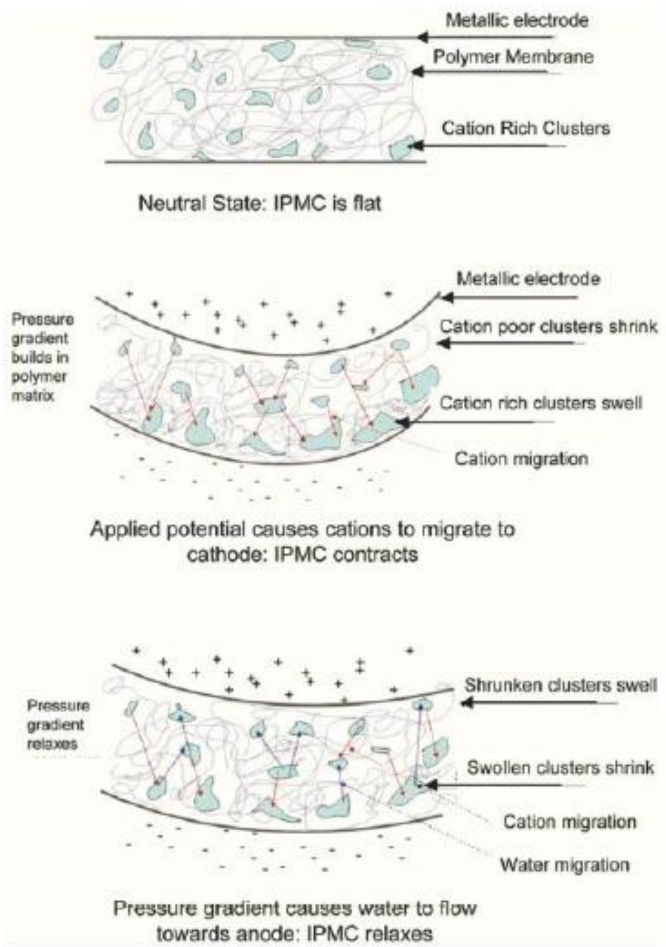

Figure 23. Schematic illustration of the actuation mechanism of IPMCs.

The performance of the IPMCs actuator is obviously determined by the nature of the ion-exchange membrane and mobile cations, the electrode materials and structures, and the level of hydration solvent saturation.[48,49]

Actuation strains of above 3 % have been reported for IPMCs under applied voltage of 7V. [50] One example of application is dust wiper in one NASA's mission to address the issue of dust on Mars.[51] (Figure 24)

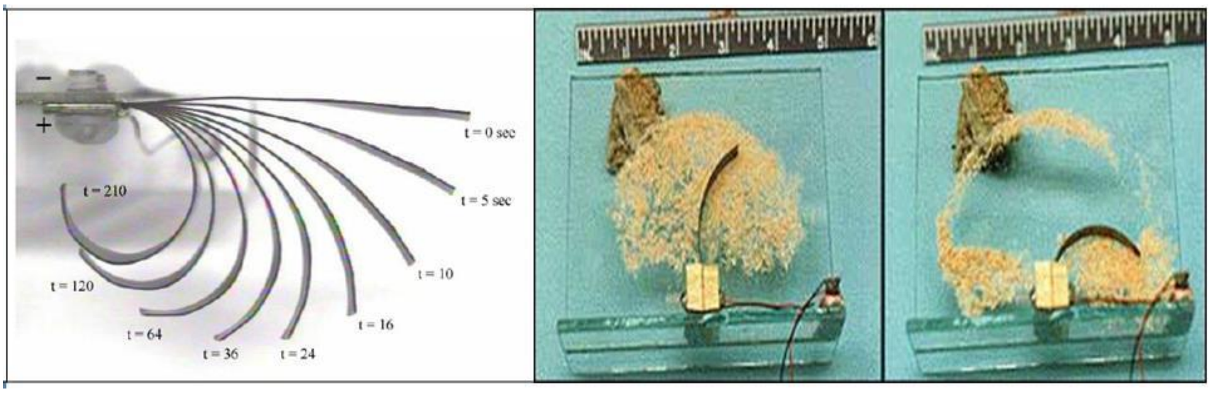

Figure 24. Actuation of a Flemion-based IPMC strip as a function of time in seconds [51]

But the practical applications of IPMCs are restricted by the low flexibility, strain resistance, and high cost of noble metal electrode layer. Moreover, the Nafion membrane has low blocking force, environmental-unfriendliness, and back relaxation under direct current voltage. To improve IPMCs actuation and to enlarge applications, recent development of the new generation of IPMCs focus on new ion-exchange membrane materials, solvent and electrode materials with high performance. Non-fluorinated hydrocarbon polymers instead of Nafion have been used. A lot of sulfonated and a few carboxylated polymers with good ion-exchange capacity, proton conductivity, low cost and environmental-friendly have been synthetized for new IPMCs including sulfonated poly(ether ether Ketone) (PEEK), acrilyc acid copolymers… Recently Tang et al developed sulfonated polysulfone (PPS) and sulfonated polyphenylsulfone (SPPSU) membranes which show enhanced ionic exchange capacity and water uptake capacity and also fast response.[52,53]

Many other researches are made on IPMCs and many advances are obtained. But drawbacks such as long response time, low and narrow available frequency range and low output power limit their wide applications.

Medical and industrial products based on IPMCs as biomimetic nanosensors, nanoactuators, nanotransducers and artificial muscles are extensively being developed by Environmental Robots Inc., the current world's leader company of IPMCs products.[54,55]

I.2.b.i.2.Ionic Polymer Gel (IPG)

They are particularly unique because they can be tailored to respond to a lot of various stimuli. In 1970s, the phase transition of an IPG, characterized by its abrupt volume change, was found by Tamagawa.[56] Stimuli demonstrated to induce changes in physical properties are diverse as temperature, pH, solvent or ionic composition, electric field, light intensity…

The deformation of such polymer gels is extremely high. Some ionic gels can even change their volume by thousand times.

For example, Figure 25 shows the shape change of an anionic gel with time under the electric field.

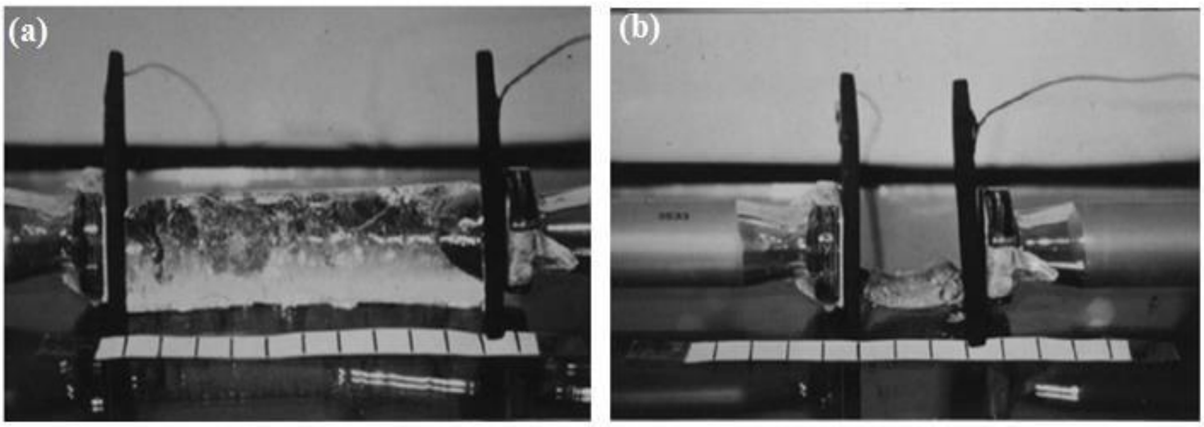

Figure 25. Poly(2-acrylamido-2-methyl-1-propanesulfonic acid) gel before (a) and after (b) imposing an electric field of 15V for 10 hours [57]

I.2.b.i.3.Conductive polymers (CP)

CPs was discovered in 1977 by Shirakawa et al with oxidized iodine-doped polyacetylene. For this work, they were awarded the Nobel Prize in Chemistry.[35]

CPs are electronically conducting organic materials. They are conjugated polymers which have backbones of contiguous sp^2 hybridized carbon centers. A molecule wide delocalized set of orbitals provides the possibility of the long-range mobility of electrons.

Actuation is possible due to the electronically change of oxidation state in the polymer. The flux of ions into and out of the polymer backbone causes deformation. With appropriate dopants, such as hydrogen chloride or sulphuric acid, CP exhibit chemically and electrochemically controllable electronic conductivities. A CP sandwich is composed of 2 CP layers separated by an electrolyte. When an electric field is applied, a reversible exchange of ions takes place between the CP and the electrolyte which leads to oxidation or reduction reactions in the CP which induces significant changes in its volume. Figure 26 shows a schematic representation of actuation mechanism for polypyrrole (PPy).

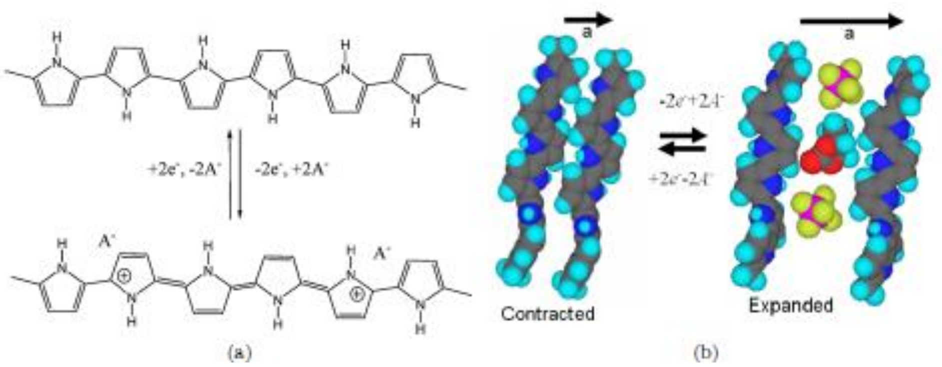

Figure 26.Schematic representation of actuation mechanism for PPy. (a) the oxidized and reduced states of a PPy chain (58);(b) the uptake and expulsion of ions PF_6^- (yellow/purple) and concomitant solvent (red/blue/grey) between PPy chains.[59]

For CP doped with bulky immobile anions, cations are inserted and deinserted and polymer will expand in reduced state. While for CP doped with small size anions, anions are inserted and deinserted and therefore polymer will expand in oxidized state.[60]

The most widely used CPs for actuators are PPy, pilyaniline (PANI) and polythiophene (PT).

They are a wide range of applications such as batteries, supercapacitors, solar cells and organic light-emitting diodes (OLEDs) because of their electromechanical performances. Actuation strains are large, ranging from a few percent to about 40 %.[61] Moreover, low operate voltage (1-2 V) is sufficient to obtain deformation. But they have low electromechanical coupling (< 1%), low strain rate due to relative low ion transport and the internal resistance between the electrolytes and the polymer.[62]

They have also a good biological compatibility and medical devices are possible with CP such as cochlear implants or blood vessel connectors.[63]

I.2.b.i.4.Carbon nanotubes (CNTs)

Since discovery of multi-walled carbon nanotubes (MWNT) in 1991 by Iijima [64] and single-walled carbon nanotubes (SWNT) two years later,[65] CNTs have emerged as materials of considerable interest for various high-tech applications due to their excellent mechanical and electrical properties. SWNT can be viewed as a sheet of graphite rolling into a cylinder and MWNT is composed of concentric SWNT of different diameters with an interlayer spacing of 0,34 nm. Nanotube properties are highly dependant on its nano-scale atom arrangement, tube diameter and length, and macro-scale material structure. CNTs are very strong and stiff. Based on experimental and theoretical results, the Young's modulus of a SWNT should be as high as 640 Gpa with a strain-to-failure about 5,8 % which is about 10 times higher than any other type of continuous fiber.[66] However, the properties for MWNT are much lower. The actuation of CNTs results from the charge injection based quantum chemical effects and double-layer electrostatic effect. As is depicted in Figure 27, charges are injected into SWNT electrodes by an applied potential and balanced by the ions from electrolyte, forming a so-called double layer.[58]

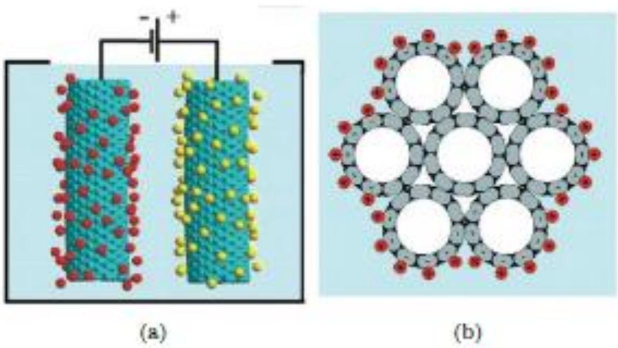

Figure 27.Schematic illustration of actuation mechanism of CNTs artificial muscles. (a) an applied potential injects charge into two SWNT electrodes which are immersed in electrolyte and the injected charges are compensated by ions from the electrolyte;(b) charge injection at the surface of a nanotube bundle.[58]

The injected charges cause dimension changes in covalent C-C bond, leading to the actuation behavior of CNTs. For low charge density, quantum mechanical effect is dominant to the strain while both quantum chemical effect and electrostatic double layer charging contribute to the strain for high charge density.

Figure 28 shows the first reported biomorph cantilever based CNT actuator operated in aqueous NaCl electrolyte.[40]

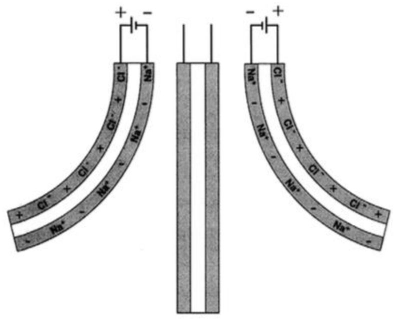

Figure 28. Biomorph cantilever based CNTs actuator operated in aqueous NaCl electrolyte [40]

It consists of two strips of MWNT bulky paper adhered to two opposite sides of a scotch. Electron injection induced expansion and hole injection induced contraction result into the bending behavior of CNT actuator. A maximum strain of 0,2 % and a stress of 0,75 MPa were observed.[40]

Vohrer et al showed that actuator performances of CNTs are not only dependent on the material itself but also affected by used electrolyte, applied voltage and so on.[67] The performances of CNTs actuators are highly dependent on the mechanical properties of the used CNTs assemblies. The inherent extremely Young's modulus combined with the predicted strain (1% for SWNT in aqueous electrolyte) contributes to high stress generation and unexpected work density per cycle. However, the actual performances of CNTs actuators are much lower than the predicted ones. For example, the typically strain for SWNT actuators is between 0,06 and 0,2 %.[68] And maximum observed isometric SWNT actuator stress is 26 MPa.[69] One major cause for this discrepancy is the poor stress transfer between nanotube bundles since the nanotubes are joined by mechanical entanglement and Val de Waals force within CNTs assemblies, which also result into the common creep behavior of CNTs actuators.[70] Therefore, one challenge for improving actuation performances of CNTs actuator is to convert available nanotube powder into useful assemblies with high mechanical property, creep resistance as well as conductivity. Because of difficulties to control the purity and high cost during the synthesis process of SWNT, most CNTS actuators are made of MWNT.

Figure 29 shows the development of CNTs materials for actuator applications. MWNT forest, which comprises approximately parallel nanotubes resembling trees in bamboo forest (Fig 29b),[69] is synthetized by chemical vapor deposition on an iron catalyst-coated substrate using acetylene gas as the carbon source. Zhang et al. reported the mechanically drawn high-oriented, strong, transparent, and conductive ultrathin CNTs sheet and spun-twisted multi-functional CNTs yarns from MWNT forest.[71] The fabrication process of CNTS sheets and yarns is shown in Figure 29c and Figure 29d respectively. The diameter of CNTs yarns is typically between 1 and 60 µm, depending upon the width of the forest sidewall used for spinning. Two-ply or four-ply yarns are obtained by over twisting a single yarn and the two-ply yarn with opposite twist direction, respectively as shown in Figure 29e-g.

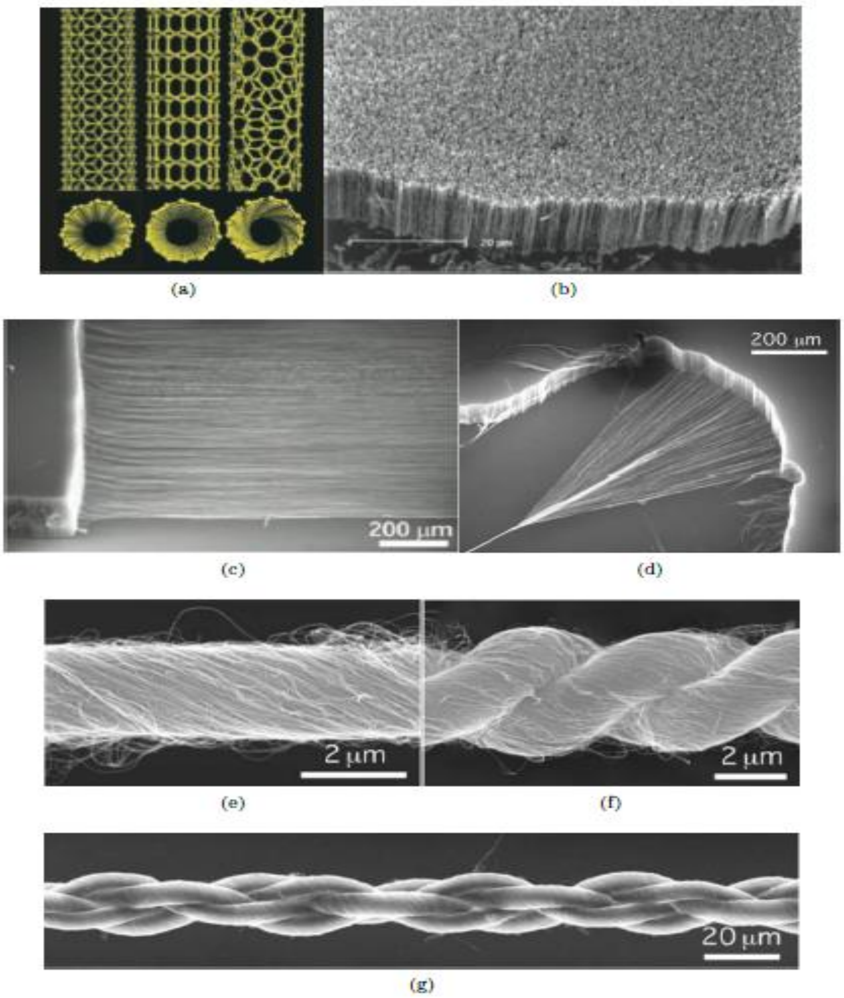

Figure 29. Photos illustrating development of CNTs materials. (a) structures of SWNT: armchair (left), zigzag (middle), chiral (right); (b) scanning electron microscope image of MWNT forest; (c) mechanicaly drawm ultrathin CNTs sheet; (d) the preparation process of CNTs yarns, (e) single, (f) two-ply and (g) four-ply yarns.[69-71]

These prepared CNTs yarns exhibit high creep resistance, high electrical conductivity, increased strain-to-failure (as high as 13 %) and enhanced tensile strength (up to 460 MPa).[71]

In addition to the cantilever-based CNTs actuators, rotational actuation for CNTs was first reported by Fennimore et al.[72] More recently, Foroughi et al developed and electrolyte-filled CNTs yarn based tensile and rotational actuator.[73] The basic configuration is shown in Figure 30. Three electrodes (reference electrode, actuating CNT yarn electrode and counter-electrode from left to right) were used and half length of the MWNT yarn was immersed into the electrolyte with a paddle in the middle of the yarn. As is depicted in Figure 30b and Figure 30c, the untwist behavior of the yarn resembles a helically wound finger cuff toy, where simultaneous yarn contraction and torsional rotation occur to increase the volume. The actuator provides a reversible 15 000 rotation and a fast action of 590 revolutions per minute. A large torsional stork of 250°/mm of the actuator length, a peak work density per cycle of 61 W/kg and strains up to 1 % were observed.

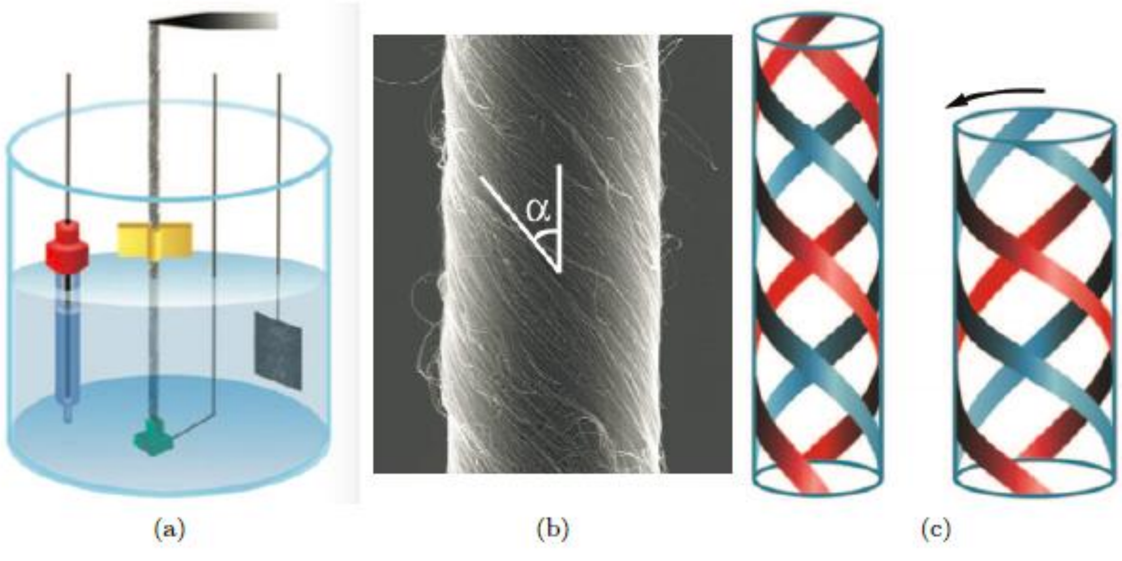

Figure 30. Schematic illustration of rotational actuation of CNTs artificial muscles : (a) a simple three-electrode configuration of torsional CNTs actuator; (b) scanning electron micrograph of a carbon nanotube yarn that was symmetrically twist-spun from a MWCNT forest; (c) effect of yarn volume expansion during charge injection, behaving like a helically wound finger cuff toy. The amount of yarn untwist during yarn volume expansion is indicated by the arrow.[73]

Another issue is to develop CNTs actuators without aqueous electrolyte. As is known, the use of aqueous electrolyte will lead to low work density and difficulty to realize the miniaturization of the actuation system. A hybrid CNTs actuators with an introduce guest (paraffin waxes) which can be electrically, chemically and photonically driven in air was demonstrated by Lima et al in 2012.[74] Torsional and tensile actuation of these hybrid muscles result from dimensional changes of a yarn guest caused by different external stimuli. This artificial muscle provides fast and large stroke tensile and torsional actuation with a high work density. Lee et al reported an all-solid tensile and torsional actuator in which the liquid electrolyte was replaced by poly(vinylydene fluoride-hexafluoroproplylene) P(VDF-HFP) based solid gel electrolyte. A large torsion stroke of 53°/mm at a low voltage of 5V and useful tensile stroke (1,3 % at 2,5 V) were obtained.[75]

Due to its thermal and chemical stability, CNTs actuators can work at a wide temperature range and hard chemical environment.[69,71]

Possible eventual applications for CNTs muscles are in micro electromechanical systems (MEMS) devices, such as controlling valves and stirring liquids in micro-fluid circuits and in medical catheters.

I.2.b.ii. Electronic EAP

For electronic EAP, the actuation is caused by external electric field, electrostatic forces between two electrodes and/or interaction between dipoles inside the material, squeezing the polymer. Figure 31 shows the typical structure of an electronic polymer.

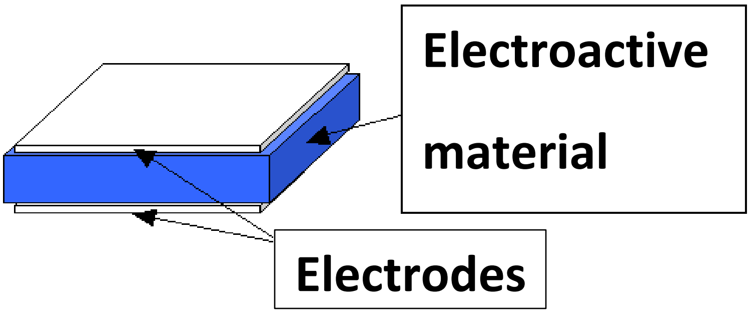

Figure 31. Typical structure of an electronic polymer

One of their main advantages is that they can be manipulated in air. Coupling may be linear (piezoelectric polymer) or non linear (electrostriction, electrostatic forces). In the following sections, several types of electronic EAP are reviewed. Electrostrictive polymers and dielectric elastomers (DE) are the leading electronic EAP.[41]

I.2.b.ii.1.Dielectric elastomer

The actuation behavior of DEs was first observed in a natural rubber strip that was charged and discharged by Roentgen in 1880.[22] However, at this moment, Roentgen attributed the observed volume changes to the thermal effect of electric field.

Dielectric elastomer actuators consist of a polymer sandwiched between two compliant electrodes. A schematic model of a dielectric polymer actuator system is presented in Figure 32.

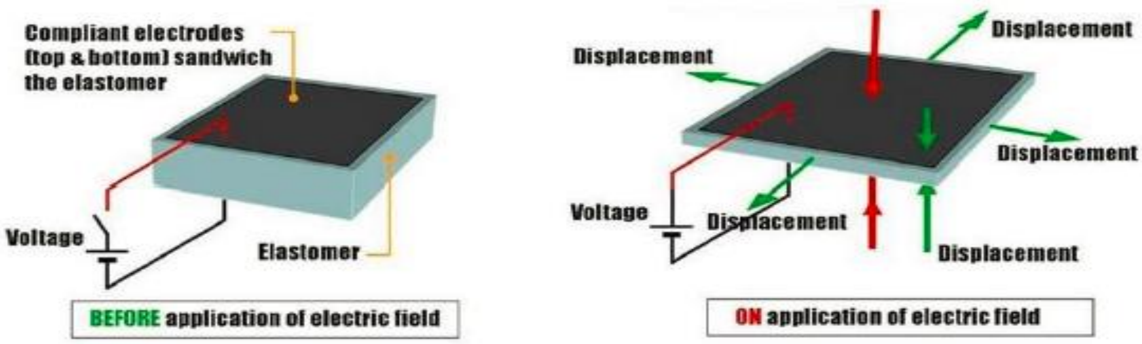

Figure 32. Dielectric elastomer actuator system

When a voltage difference is placed across the 2 electrodes, the polymer is compressed and stretched in area by the electric field pressure since the material is incompressible.[76] The Maxwell strain in a dielectric polymer with compliant electrodes results from the electrostatic forces generated between free charges on the electrodes and is proportional to the square of the electric field. Thus, it may be argued that actuators based on this EAP technology, are more properly considered to be electrostatic. However, the dielectric and mechanical properties of the polymer determine the magnitude of the stress and the strain response. In order to obtain a high Maxwell stress, DEs should have a high dielectric permittivity and operate at a relatively high electric field. The corresponding actuation strain is dependent on the Young's modulus of the elastomer. To ensure a high performance actuation with high elastic energy density, the DEs have to meet the requirements such as high dielectric permittivity, high breakdown strength and a moderate Young's modulus.

The investigation of DEs actuators began in 1990s.[77,78] The generated strain is up to 30 to 40 %. The performance is mainly limited by three failure: pull-in, dielectric breakdown and mechanical break.[79] The pull-in failure is a fundamental limit of materials with a pure linear elasticity which behave as the material's mechanical instability and collapse due to the electromechanical instability when the thickness strain is over 33 %. In 2000, a great breakthrough of DEs actuators with significantly enhanced actuation performance was made by Pelrine et al.[80] In their work, biaxial or uniaxial stretch was used to prestrain the DEs films, resulting actuated area strains up to 117 % for silicone elastomers and up to 215 % for acrylic elastomers respectively. It has been demonstrated that prestrain can provide an increase of dielectric breakdown strength (DBS) which can be explained by thermodynamic stability criterion and it likely prevents pull-in failure.[58] Since then, prestrain is an efficient approach to achieve high performance DEs actuators with area strain level exceeding 100 %.

Figure 33 shows the actuation of a circular dielectric elastomer made of acrylic elastomer.

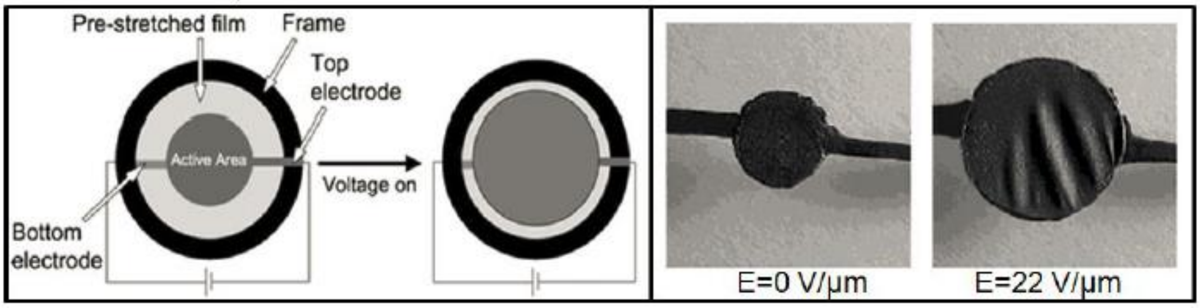

Figure 33. Circular strain test of acrylic dielectric elastomer (81)

The commonly investigated DEs mainly include three different materials: acrylates, silicones and polyurethanes (PU).

DEs based commercially available 3M VHB acrylics have shown the most promising strains up to 300 to 400 % in area for prestrained films. Furthermore, the elastic energy density (3,4 J/cm^3, about 400 times higher than natural muscles), stress (up to 8 MPa) and electromechanical conversion efficiency (60-90 %) are all extraordinarily high.[82] The acrylates have a low Young's modulus (1-2 MPa) enable that they can be prestrained on the order of 200-300 %, much higher than the other elastomers for which prestrain is limited to less than 50 %. However there are some drawbacks for acrylate elastomers which limited their commercial applications such as their sensitivity to temperature as well as slow response time owing to the viscoelasticity of the polymer network.[83]

Other DEs are silicones. They are the basis of the commercial products from Bayer Material Science under intense investigation. Silicone elastomers consist of a silicon-oxygen backbone with two side groups covalently attached to Si atoms. Compared to acrylate elastomers, silicone elastomers show a moderate actuation performance due to its low dielectric permittivity which results from its non-polar nature and low modulus (0,1-1 MPa). The maximum electromechanical coupling efficiency which is in the range of 63-79 % is a little lower than that of acrylates.[84] Moreover, the self-reinforcing behavior decreases the application of prestrain as an efficient way to improve the actuation performance. In spite of this, silicon elastomers feature higher resistance than acrylates leading to a lower leakage current, low viscoelasticity contributing to a fast response and stable actuation owning to less sensitivity to the environment conditions. More importantly they are bio-compatible. And therefore, silicone elastomers have great potential for medical actuation applications.

Among the class of DEs, PUs elastomers are of great interest due to their significant electrical-field strains (due to polar nature) but also for their flexibility, light weight, high chemical and abrasion resistance and high mechanical strength under relatively low electric field.[58,85] Moreover, processing is quite easy to large area films and they are able to be molded into various shapes. Finally, they have a good biocompatibility with blood and tissues. PU can generate a strain above 10 % under a moderate electric field. They can therefore be considered as potential actuators.[86]

To resume this class of EAP, Table 2 presents the different properties of main DE films.

Elastomer materials	Film thickness (μm)	Strain at break (%)	Young's modulus at 50 % (MPa)	Relative dielectric constant at 1/8 Hz	Breakdown strength (MV/m)
Polyurethane TPU LPT 4210 UT 50	50	421	3.36	6.0	218
Polyurethane Bayfol EA102	50	300	1.44	7.1	130
Silicon proprietary	45	422	0.25	2.4	80
Acrylate VBH 4905	498	879	0.04	4.5	31

Table 2. Properties of several DE films.[83]

Many efforts have been made to improve the performances of DEs actuation devices. The main drawback of acrylate limiting their overall efficiency, the maximum response frequency and response speed is its sensitivity to temperature and its viscoelasticity. The addition of low molecular weight plasticizers can widen the temperature range, increase the response frequency and decrease the modulus without sacrifice the elasticity.[87] The volatilization or migration nature of plasticizers which will limit the lifetime of DEs devices can be solved by reactive plasticizers or monomers which can be grafted to the existing elastomer network or react together to form an inter-penetrating network (IPN).[88] An IPN within acrylate elastomer was made by Ma et al. Without externally applied prestrain, the IPN containing 3M VBH films underwent a thickness strain up to 75 % with a stress of 5,1 MPa, an energy density of 3,5 MJ/m^3, coupling efficiency of 94 % and a DBS of 420MV/m so good performance.[89]

For DEs, one other key issue is to reduce the high operating voltage to remove the danger associated with the high voltage and consequently increase their commercial viability. There are two main ways to reduce the operating voltage: increasing the dielectric constant and reducing the thickness of the elastomer films. The reduction of thickness can benefit of keeping the dielectric breakdown and dielectric loss but suffers from increased inhomogeneities and recued output force. Many works have been done to enhance the dielectric constant via physical approach such as incorporation of particles with high dielectric constant or conductive materials into polymer matrix or by chemical modification such as introduction of polar groups into polymer network. For the physically modified elastomers, various kinds of fillers including organic/inorganic, metallic/ceramic materials have been investigated. Titanium dioxide, polarizable conjugated poly-3-hexylthiophene are examples. By this method, dielectric constant increase but dielectric loss and reduction of DBS as well as increase in Young's modulus are negative consequences. One possible way to solve this problem is the filler-polymer matrix interface modification.[90,91]

Besides composite approach, chemical graft of polar groups offers another method to improve the DEs performance. As shown in Figure 34, push-pull dipoles are chemically grafted to polydimethylsiloxane (PDMS) elastomer network through silicone crosslinking chemistry. The resulting elastomer possess an homogeneous structure at molecular scale, yielding an increased dielectric constant (from 3 to 5,9) and decreased elastic modulus (from 1900 to 550 kPa) and contributing to an improvement of the actuation response of more than six times.[92]

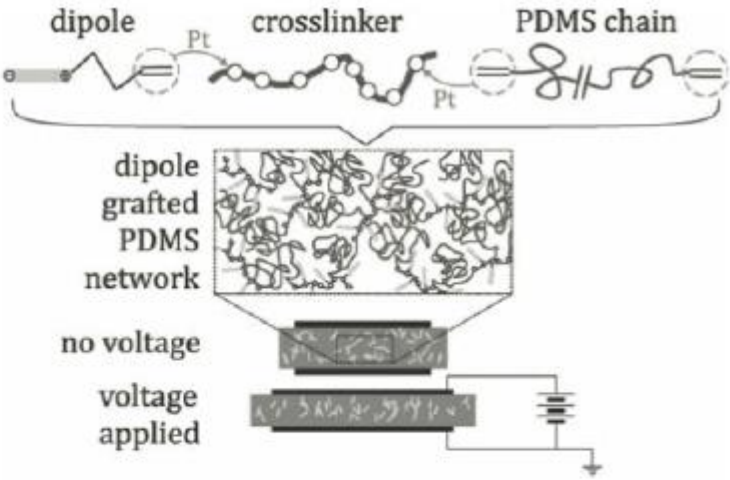

Figure 34. Schematic illustration of dipole functionalization of the PDMS elastomer network and actuation mechanism [92]

In addition, compliant electrodes also play a very important role in the actuation performance of DEs actuator devices. A good electrode must closely adhere to the elastomer films and follow the deformation without constraining it either mechanically or electrically.[83] In fact, electrodes should maintain high conductivity at large strain, have negligible stiffness (softer than elastomers), good stability and fault tolerance. A review written by Rosset et al in 2013 presents much detailed informations about these electrodes and their properties.[93] The improvement of electrodes materials will promote the commercial applications of DEs actuators.

DEs films may have various configurations such as rolled, tube, unimoprh, bimorph, stretched-frame, spider…[58] Among them, two most interesting device designs are the spring roll and stacked actuator since both of them are able to effectively couple the deformations of DEs to provide linear actuation.

With all these possible configurations, DEs have many applications such as MEMS, robot, force and strain sensors. They have already some commercial products. For example, Bayer Material Science has developed EAP actuator with DEs which can enhance the sound dimensions of headphones.

I.2.b.ii.2.Electrostrictive graft elastomer

The electrostrictive graft elastomer is one the more recent type of EAP developed in the NASA Langley research Center in 1999. They exhibit electric-filed induced strain above 4 % that is far smaller than the 300 at 400 % with dielectric elastomer but much larger than the 0,2 %

achieved with ceramics as LZT. The most important thing for this type of EAP is that there is no hysteresis in this material. But they require quite high electrical field so their use is for the moment still limited. Figure 35 shows the structure of the graft elastomer and the induced strain under electrical field.[94]

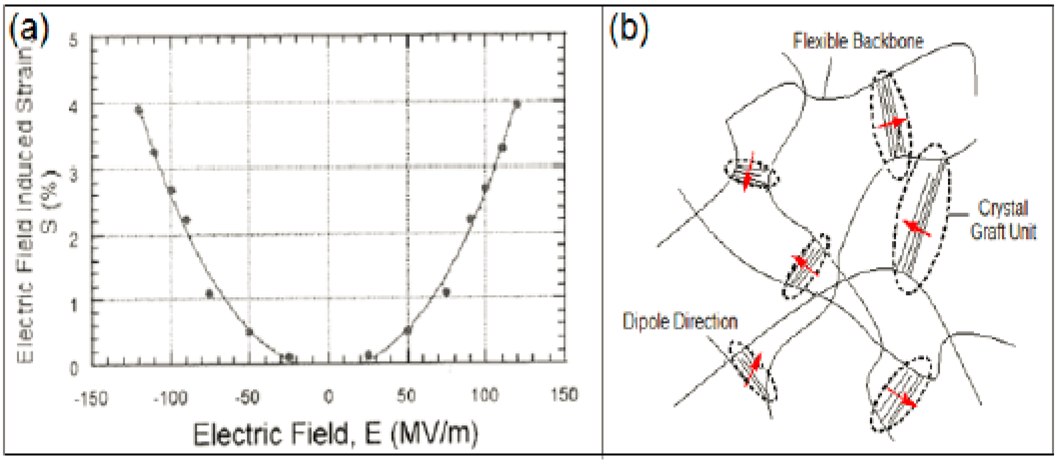

Figure 35. (a) electrical-field induced strain on the graft elastomer, (b) structure of the graft elastomer [94]

From a microstructural point of view, the graft elastomer consists of two different components: flexible backbone chains and side chains attached to the backbone, called grafts.[95] These grafts can crystallize to form physical cross-linking sites for a three-dimensional elastomer. This generates electric field responsive polar crystal domains. The polar crystal domains are primary contributors to electrostrictive mechanical functionality. When the material is under the electrical field, the polar domains rotate to align themselves in the field direction due to the driving force generated by the interaction between the net dipoles and the applied electric field. The rotation of grafts induces the reorientation of backbone chains, leading to deformational changes. In the absence of electric field, the polar domains orientation randomize, leading to dimensional recovery. The dimensional change generated demonstrates a quadratic dependence on the applied electric field.

I.2.b.ii.3.Liquid crystal elastomer

LCE are unique molecular materials because of the large anisotropies in many of their properties such as the dielectric, optical and mechanical anisotropies. As early as 1975, De Gennes and his co-worker Chung predicted that the reorientation of LC molecular (known as mesogens) during a phase transition could lead to a mechanical strain and stress.[96] However, the liquid crystal has a crystalline ordering only in one dimension, perpendicular to the layer planes. In the 2 other dimension, they have a liquid-like structure. Therefore, static forces are impossible to build inside liquid crystal and they can neither sustain nor exert mechanical stress. LCE, just as the name implies, combine the orientational ordering properties of LC and the elastic properties of elastomers. By incorporating mesogens into a flexible polymer backbone or as a side chains, the reorientation capacity of mesogens is sufficiently kept, and meanwhile, the free flow of mesogens is prevented by their bonds to the polymer network. The stress or strain originating from mesogens changes upon external thermal or electrical stimuli can be transferred to the bulk LCEs via the bond and backbone to perform mechanical work. As a result, LCEs can be used to produce electric field-induced actuation.

The basic actuation principle of LCE is shown in Figure 36. In LCEs, the polymer chains experience an anisotropic environment due to the introduction of the anisotropic mesogens of LC. When such an elastomer loss its anisotropy upon the external stimulus, an isotropic chain conformation will be adopted again and the sample as a whole will have to change its shape.[97]

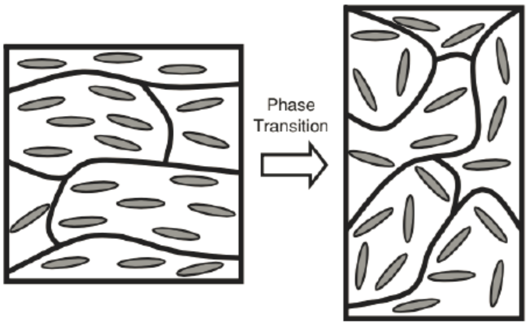

Figure 36. Schematic illustration of actuation principle of LCEs.[97]

There are two different categories of LC depending on the phase present: nematic and smectic as shown in Figure 37. In smectic C phases, the mesogens are additionally titled towards the normal layer. Smectic A phases exhibit a layered structure with the mesogens parallel to the normal layer. In the nematic phase, the mesogens have a short-range order and are aligned parallel in a uniform direction.

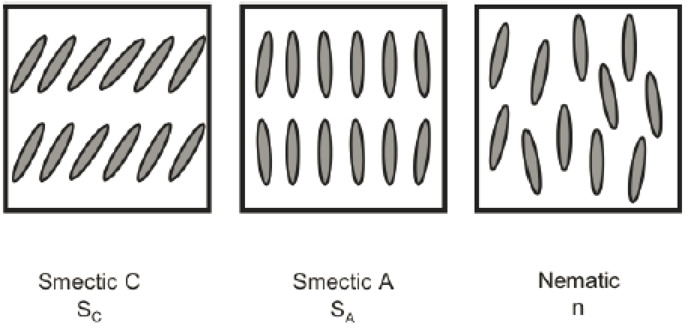

Figure 37. Different types of LC.[97]

LCEs can be chemically synthetized with three distinguished structures: the mesogens are introduced into the main chain of the polymer or can be attached as side chains via flexible spacer at the ends (end-on) or in the middle (side-on) of mesogens. One of the most particularities of LCEs is that LCEs can be activated thermally, optically and electrically.[98-100] Thermally activated LCEs display length changes up to 400 %,[101] but their response rate is limited to the heat diffusion process and also there is the thermal relaxation problem.[58]

In the following paragraph only focus on the electrically stimulation. Given the dielectric anisotropy properties, the intrinsically polarized mesogens can reorientate them in the presence of electric field, generating the bulk LCEs stress and strain.[102] Electric field can be applied en LCEs very quickly contributing to a fast electromechanical response. The response speed of LCEs is greatly dependent on the used mesogens, but also on the polymer structure and the degree of cross linking. The chemical structure and actuation mechanism of ferroelectric LCEs are shown in Figure 38.[103] The large electrostrictive strain originates from the combination of electroclinic effect of the ferroelectric (FE) LC and polysiloxane network. The reported Young's modulus of FE LCEs is below 3 Mpa and the corresponding elastic energy density is below 0,002 J/cm^3. Nematic anisotropic LCEs seem to have better performances than smectic anisotropic LCEs.[103]

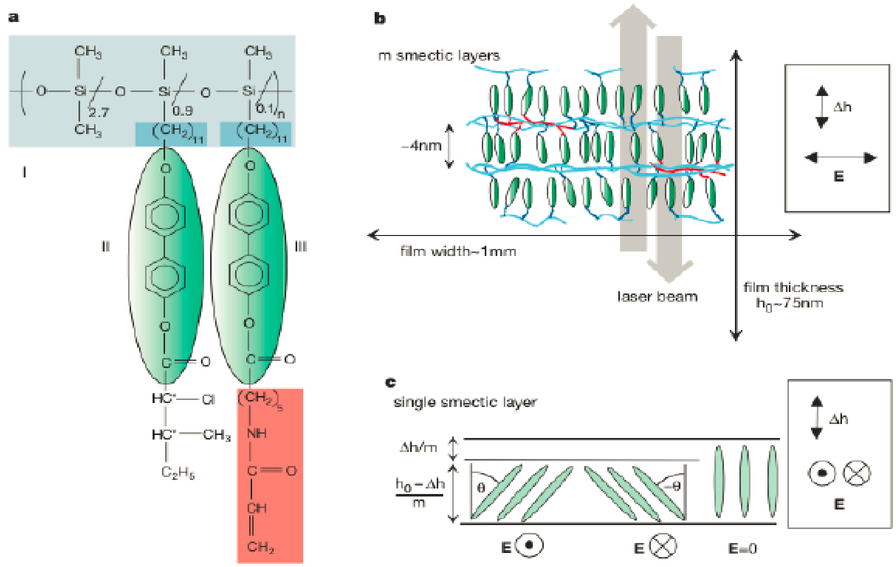

Figure 38. The electroclinic effect in ferroelectric LCE. (a) the chemical structure of FE LCEs. I (blue) = the polysiloxane backbone; II (green) = the core of the chiral mesogen; III (red) = the crosslinkable end group of the mesogen. (b) scheme of measurement geometry. (c) the electroclinic effect [103]

To conclude about LCEs, actuators based electrically activated LCEs feature fast response speed (10 ms) at a relative low electric field, strain less than 10 % and a low elastic energy density due to the low Young's modulus.[103]

The possibilities of applications are wide and range from MEMS (valves in microfluidic systems, artificial muscles in robot…) to propulsion systems and active smart surfaces.[97,104]

I.2.b.ii.4.Piezoelectric polymer

A piezoelectric polymer can be defined as a polymer in which the application of an electric field reverses the direction of spontaneous polarization. PVDF and its copolymers (see following section) are the most promising materials of this class of EAP. Kawai et al published the first description of the piezoelectric properties of PVDF in 1969.[26] Their electrostrictive strain is nearly 2 %. It is not very large but very much larger than traditional electrodriven sensors/actuators which usually generate an electrostrictive strain around 0,2 %. Moreover, some of them have a high elastic modulus (around 1 GPa) and the field-induced strain can operate at very high frequencies (higher than 100 kHz). But large electric fields, around 200MV/m, are more often required, compared with ceramics as LZT. Their main applications are sensors, actuators and underwater acoustic transducers.[105]

I.2.b.iii. Fluorinated polymers and the terpolymer P(VDF-TrFE-CTFE)

From a structure-property point of view, a piezoelectric material should be a crystalline material lacking a symmetric center. The highly electro-negative fluoride atom with a very small van der Waals radius (1,35 Å), which is only slightly larger than of hydrogen (1,2 Å), can form a highly polar fluoride-carbon bond with a dipole moment of μ = 6,4 x 10^{-30} C.m, and consequently, the fluoride polymers can form multiple crystalline structures through molecular design and material process conditions.

Recently, emerging researches have been carried on the fluorinated polymers since work of Lovinger et al on PVDF polymer. Lovinger described for the first time the structure of molecular chains and chains conformations.[36] PVDF is a semi-crystalline polymer with its crystal phase limited to 50-60 % which the ferroelectric behavior originated from. Generally, the mostly common molecular conformation consists of four main crystal forms, α, δ, γ, and β, depending on the dipole orientation which are show in detailed in Figure 39. The two most common chain conformations are *trans-gauche-trans-gauche TGTG* conformation and *all-trans* conformation. For *all-trans* conformation, all the dipoles align in the same direction essentially perpendicular to the molecular axis, contributing to the most highly polar conformation in PVDF. While for *TGTG* conformation, due to inclination of dipoles to the chain axis, it has dipole moment both parallel and normal to the chain axis.[106]

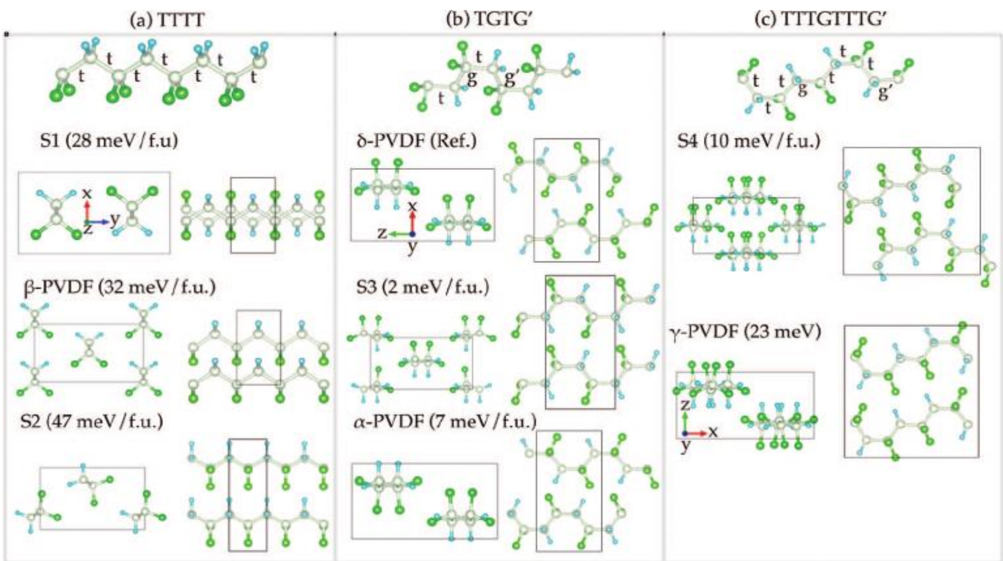

Figure 39. Top and side views of low-energy crystal structures of PVDF found in USPEX searches starting from (a) TTTT chain; (b) TGTG chain; (c)TTTGTTTG chain. The energetics relative to the ground state (δ -PVDF) are also shown. Gray, cyan, and green spheres represent the carbon, hydrogen and fluorine atoms, respectively.[106]

The PDVF films with different crystal form strongly depend on the polymer processing methodologies. α and β forms are the most common phases for practical ferroelectric and piezoelectric applications and the other two phases exist only at some special conditions. For instance, the α form can be obtained by cooling from the polymer melt while γ has a $TTTG^{+}TTTG^{-}$ chain conformation and often obtained by solution-casting from polar solvents at temperature below 100 °C and annealing at high temperature. The dipole moment cancel out in the α-form, leading to a nonpolar form, while the 3 other forms are ferroelectric. Beta- form is the main form with piezoelectricity. To obtain preferentially β form, PVDF films must be mechanically stretched for circular times and poled under high electric field at high temperature. Alpha form has lattice dimensions of a = 4,96 Å, b = 9,64 Å and chain direction c = 4,62 Å. Beta form has lattice dimensions of a = 8,58 Å, b = 4,90 Å and c = 2,56 Å.

Unfortunately, PVDF crystallizes directly into a non-polar α-phase rather than ferroelectric β-phase from the melt crystallization or solution cast. Even there are ferroelectric β-phase domains in stretched PVDF, these crystallites are randomly oriented within bulky PVDF, displaying the absence of overall piezoelectricity for the bulky PVDF. In order to obtain piezoelectricity, PVDF thick films have to be mechanically stretched several times of its original length and poled under an electric field more than 100 MV/m at an elevated temperature.

As we can see, the processing to make PDVF is complex leading this polymer less potentially used in the practical implementation, let alone its low field-induced strain and weak electromechanical coupling behavior.

But these disadvantages of PVDF can be improved by a P(VDF-TrFE) copolymer strategy. Unlike PVDF, the copolymer P(VDF-TrFE) exhibits a directly formed β-phase from melt crystallization and solution cast. It has been demonstrated that copolymer with a VDF content from 12,5 to 85 % always shows the ferroelectric β-phase and cannot be transformed into an α-phase by any thermal treatment.(107) Moreover, a high room temperature dielectric constant (15 at 1 kHz) which is about two times higher than that of both PVDF and TrFE is observed for 55 % VDF copolymer due to its high content of head-to-tail sequences.

The copolymer underwent the ferro-paraelectric transition, involving *all-Trans* phase transition to nonpolar substitution of T*rans* to *Left* conformation at high temperature. The TrFE molecules acting as defects in PVDF polymer chains contribute to a decreased Curie

Temperature (T_c) with the increased TrFE content and the T_c is below melting temperature T_m which is different with the pure PVDF as shown in Figure 40.

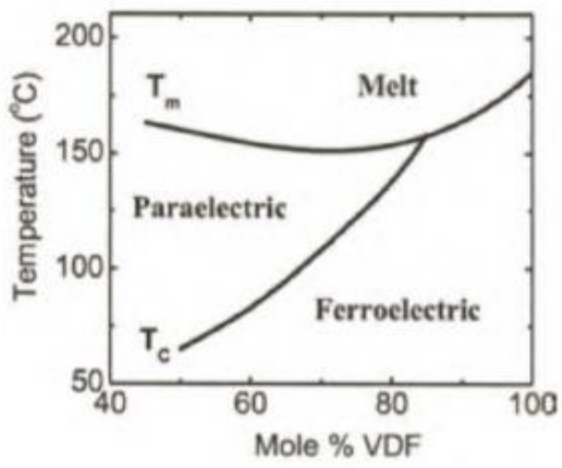

Figure 40. Phase diagram of PVDF and P(VDF-TrFE) polymers.[108]

During this phase, a large lattice constant along the molecular chain but a small unit cell dimension of all *Trans* conformation switched to a significant shortened lattice constant with an expansion of unit cell dimension. The differences in crystal unit cell aroused the macroscopic strain when there is a ferro-paraelectric phase transition. This phase transition is reversible under a relatively low poling electric field (< 70 MV m^{-1}).[109] P(VDF-TrFE) copolymer benefit a jump dielectric permittivity and piezoelectricity due to enhanced ferroelectricity in the crystal phase. Furthermore, large polarizability should also depend on the orientation of dipole moments because the orientational polarization is more important than electronic and atomic polarizations in the crystals.[110] When the c-axis of the crystal form is parallel to the external electric field, all the dipole moments will distribute in a perpendicular plane to the electric field, reaching a maximal dipolar polarization, and thus high ferroelectric behavior. The favored crystal orientation also strongly depends on the processing conditions, which in turns affected the dielectric constant and a large strain.[110] However, the large strain induced by such a transition is always accompanied by a relative large hysteresis due to large energy barrier during the dipole orientations. Such scenario may certainly undermine the development of out-performed electromechanical devices.

A possible approach to solve this problem of large hysteresis is to reduce or eliminate the energy barrier by reducing the size of large polarization domains to a nanometer scale. In

1998, Zhang et al reported a high energy electron-irradiated P(VDF-TrFE) 50/50 (50 % mol VDF) with a large longitudinal (or thickness) strain more than 4 % and very little strain hysteresis in response to an applied electric field of 150 MV/m at room temperature.[111] It has been demonstrated that, the electron-irradiation breaks up the long-range polar regions into micro non-polar domains (nanometer-size *all-trans* chains interrupted by *trans and gauche* bonds) and transforms the normal ferroelectric material into a relaxor ferroelectrics as shown in Figure 41. Due to the reduction of polar regions, the hysteresis features a slim loop with smaller remnant polarization (P_r) and coercive electric field (E_c) than ferroelectric P(VDF-TrFE) copolymer. As a result, this polymer cans response at a wide temperature and frequency range.

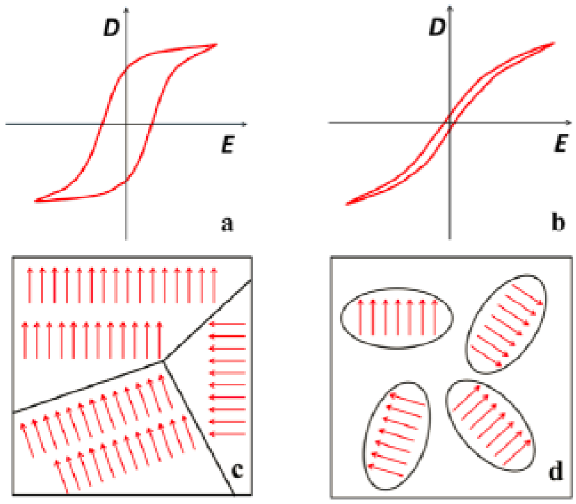

Figure 41. Schematic diagrams of the comparison of hysteresis loops and microscopic crystalline structures for ferroelectric (a,c) and relaxor ferroelectric terpolymers (b,d).

The electrostrictive properties of irradiated P(VDF-TrFE) were further investigated by Zhang's group.[112,113] Owning to the large anisotropy in the response along and perpendicular to the polymer chain, the transverse strain can be tuned by film stretching. The transverse strain of the stretched film along the stretch direction can reach comparable with the longitudinal strain. In addition to high strain response, irradiated copolymers also have high elastic energy density ($YS_m^2/2$ = 0,5 J/cm^3) and mechanical load capability (20 MPa) because of the high Young's modulus (Y = 0,4 GPa) and high strain level (maximum strain 5%). In comparison, the corresponding strain and the elastic energy density for copolymer are 0,15 % and 0,0045 J/cm^3. Moreover, a relatively high longitudinal electromechanical coupling factor k_{33} of 0,33 [112] and a high transverse coupling factor k_{33} of 0,45 [113] were also observed for irradiated copolymer. Since the energy conversion efficiency is proportional to the square of the coupling factor, such an improvement is really significant.

But high energy irradiation is not commercially available approach to produce fluoride based EAPs due to its high cost and undesirable side effects to the polymer. Thanks to the richness of fluorinated polymer chemistry, a relatively simple and low-cost alternative method by introducing a bulky monomer such as chlorotrifluoroethylene (CTFE) or chlorofluoroethylene (CFE) into the P(VDF-TrFE) chain to transform a normal ferroelectric copolymer into a relaxor ferroelectric terpolymer has been developed by PiezoTech S.A France and it is now commercially available.[114] The electromechanical properties of P(VDF-TrFE-CTEF) and P(VDF-TrFE-CFE) were investigated. A thickness strain of 4 % under an electric field of 150 MV/m at room temperature was observed for terpolymer P(VDF-TrFE-CTFE) 65/35/10,[115] and a thickness strain of 4,5 % was achieved for terpolymer P(VDF-TrFE-CFE) 62/38/4 at a relative low electric field of 130 MV/m.[116] The enhanced electromechanical response compared to P(VDF-TrFE) results from the defects modification effects of the third monomer. The introduction of CTFE or CFE reduced the polar *all-trans* conformation into room temperature stable non polar-phases, in which random or oriented nano-polar regions (with *all-trans* conformation) were surrounded by a mixture of *trans* and *gauche* bonds. The large lattice strain associated with the reversible molecular conformation change from TGTG and T_3GT_3G' to *all-trans* induced by electric field, coupled with expansion and contraction of the crystalline domains, generate the large electromechanical strain response.[116] Although CFE and CTFE can do the transformation into ferroelectric relaxor terpolymer, CFE monomers seem to be more efficient. A higher fraction of 10 mol% for CTFE is required to achieve the same reduction of hysteresis.[116] It is important to note that the introduction of the third monomer will alos lead to a decreased crystallinity and corresponding decreased elastic modulus which is not favorable to achieve a high elastic energy density. Therefore, P(VDF-TrFE-CFE) terpolymer possesses a higher elastic energy density and electromechanical coupling factor than P(VDF-TrFE-CTFE) terpolymer. Moreover, the introduction of the third monomer also give rise to enhanced dielectric properties with a dielectric constant larger than 45 which is 3 times higher than that of P(VDF-TrFE). Table 3 resume comparisons of electromechanical properties of several piezoelectric materials.

Materials	Y (GPa)	S_m (%)	$YS_m^2/2$ (J/cm^3)	k_{33}
Piezoceramic	64	0.2	0.13	-
Piezo P(VDF-TrFE)	4	0.15	0.0045	0.27
Irradiated P(VDF-TrFE)	0.4	5	0.5	0.30
P(VDF-TrFE-CTFE)	0.4	4	0.32	0.28
P(VDF-TrFE-CFE)	1.1	4.5	1.1	0.55

Table 3. Comparisons of electromechanical properties of several piezoelectric materials [111,115,116]

One obvious persistent drawback of fluorinated polymer is that relatively high electric field should be applied to generate high strain or mechanical deformation. It is well recognized that electrostrictive strain S has quadratic correlation with induced electric field E, being positively proportional to dielectric constant ε'.

Conductive metal-ligand,[117] nano-sized carbon particles,[118] grapheme nanosheets…[119] were embedded into the terpolymer matrix in an attempt to enhance these dielectric properties.

In 2002, Zhang et al reported an all-organic composite materials based on electrostrictive copolymer P(VDF-TrFE) in which an organic filler copper-phtalocyanine (CuPc) oligomers with very high dielectric constant (> 10^4) were dispersed into the copolymer matrix by solution casting method.[117] The new composite material exhibits a significantly enhanced dielectric properties (dielectric constant of 225 and loss factor of 0,4) and elastic modulus almost the same as the polymer matrix. An elastic modulus of 0,75 GPa, a strain about 2 % and an elastic energy density of 0,13 J/cm^3 which corresponds to the breakdown strength were observed for 40 wt% CuPc composite. In 2004, Huang et al, made a very flexible P(VDF-TrFE-CTFE)/PANI all-organic composite, with a PANI volume fraction of 0,251, with a very high dielectric constant up to 7000.[120] Consequently, a strain of 2,65 % with an elastic energy density of 0,18 J/cm^3 were observed under an electric field of 16 MV/m, which is nearly ten times lower than for polymer matrix. Zhang et al also showed a strain of nearly 2 % and an elastic energy density of 0,028 J/cm^3 under a field of 54 MV/m with P(VDF-TrFE)/CNTs composite.[121] One problem for these composites is the decreased breakdown strength which limits the capability to get a much better electromechanical response of fluorinated polymers.

To conclude, we can say that fluorinated polymers have high room temperature relative dielectric constant (~50) which is the highest among all the known polymers, high induced polarization (~0,05 C/m) and high electric breakdown field (>400 MV/m).[122] Therefore, electroactive fluoride polymers can generate a high electrostrictive strain (> 7 %), and high stress (~45 MPa) with relatively high modulus (> 0,4 GPa) and a high elastic energy density up to 1,1 J/cm^3. Moreover it has been also observed that the large strain is nearly constant in the temperature range from 20°C to 80°C. Finally they can response very fast with a wide operating frequency range from low frequency to 100 KHz.[123]

Based on these excellent properties, fluoride polymers have a wide range of potential applications. Organic electronics such as solar cells, memory devices, generators and printed sensors and so on have been for example under investigation.

I.3 Figures of merit of EAP, definitions

To evaluate the performances of EAPs and compare them, some important FOM may be defined.[124]

Strain (S) is the size deformation normalized by the original size in the direction of actuation. The most reported strain in the literature is the thickness strain or longitudinal strain (S_3), the transverse strain (S_1) and sometimes the area strain. The maximum strain (S_m) is used to describe the deformation capability of an EAP actuator. It is important to note that the maximum strain is generally obtained at free load and not at the peak stress.

Stress (T) gives the typical force per cross-sectional area. The peak stress is the maximum force generated by EAPs actuators and it is achieved when the displacement of the actuator is completely blocked. Blocking force is measured as follows : the actuator length before operation is recorded; the actuator is displaced without a load to the nominal displacement and then pushed back to the initial position with an increasing external force. The minimum force required for pushing back which is equal to the force generated by actuator is the blocking force that is to say, the maximum block stress is the stress under which EAPs can maintain position.

Work density or elastic energy density is the amount of mechanical work generated in a one actuation cycle normalized by the volume or mass of the actuator, in which the power supply, packing electrolyte, counter electrodes are not included. The volumetric and gravimetric energy density can be described as $YS^2{}_m/2$, $YS^2{}_m/2\rho$, respectively, where ρ is density of actuator materials.[111]

Efficiency or electromechanical coupling refers to the ratio of converted mechanical work (energy) to the input electric energy.

Response time or strain rate is the parameter to describe the response speed of EAP actuators. It is the average change in strain per unit time during an actuator stroke. The maximum strain rate is usually achieved at high frequency at which the strain is very small.

Operation voltage is the voltage required to actuation of EAPs.

Cycle life is the number of useful strokes that EAPs materials are able to undergo.

I.4. Comparison between ionic and electronic EAP

To resume, the currently leading EAP are listed in table 4 with a summary of their own advantages and disadvantages, and some of their main applications. Table 5 shows the figures of merit of several EAP materials that we have described in previous sections.

EAP Type	Advantages	Disadvantage	Applications
Ionic	°Bi-directional actuation depending on voltage polarity ° Low voltage requirement (1-5 V) °Bi-stability (in some of them) °Large strain	°wetland required for electrolytes °encapsulation/barrier layer required °Low electromechanical coupling efficiency °Strain not holded under direct current voltage °Slow response (fraction of a second) °relatively low actuation force °Electrolysis in aqueous system at > 1,23 V	°Catheters °Automotives devices ° Prosthetic devices °Active noise and vibration °peristaltic pumps
Electronic	°rapid response (milliseconds)	°High voltage raquirements (around 100MV/m)	<u>°Actuators :</u>

	°strain holded under DC voltage °Large actuations forces °High mechanical energy density °Long operation time °Use in the air possible	°No effect of voltage polarity	-haptic feedback for portable consumer electronics -Overear headphones °<u>Sensors :</u> -pressure -percolation °<u>Energy harvesting and generation</u> (wave energy)

Table 4. Advantages and disadvantages of electronic and ionic EAP, with some of their main applications

EAPs	Strain (%)	Stress (MPa)	Work density (kJ/m^3)	Efficiency (%)	Strain rate (%/s)	Voltage (V)	References
CPs	2	3~-5 Max 100	100	1	<1	1-2	[61,121]
CNTs	0,2	1-26	2-40	0,1	0,6 Max 19	1-2	[67,68,69,121]
IPMCs	0,5- 8	3	5,5	3	3,3-10	1-2	[121]
Des	20-380	0,3-1,6 Max 8	10-150 Max 3400	>15 Max 94	>450 Max 34000	>1000 E>150MV/m	[82,89,121]
LCEs	2-4	Low	2-20	75	1000	<1000 E<25MV/m	[102,121]
Fluoride polymer	7	20-45	320 Max > 1000	30-55	>2000	>1000 E<150MV/m	[111,113,115,116,121]
Biological muscle	20-40	0,1-0,35	Max > 40	Max 40	Max > 50		[121]

Table 5. Comparison of properties of main EAP (ionic and electronic) actuators.

No polymer surpasses another one, each one having their own advantages and disadvantages. So choice of EAP depends on desired application.

The main advantage of ionic EAP is the requirement of a very low voltage. The main disadvantages are the necessity of an aqueous system and their slow responses.

In contrast, the main advantages of electronic EAP are the high mechanical energy density and the possibility of be used in the air and the rapid responses. The main disadvantage is the necessity of high electric field activation.

Another way to classify EAP is based on actuation mechanisms. Dielectric elastomers and piezoelectric polymers produce actuation through polarization. Conducting polymers and gel polymers produce actuation through ions/mass transportation. Liquid crystal elestomers and shape-memory polymers produce actuation through phase change.

Among various electronic EAP, piezoelectric polymers, particularly flurorinated polymers are potentially good candidates for the processing of electromechanical actuators, because of their high energy density. Following section will studied them in more details.

I.5. Work mechanism of electronic EAPs

For electrical EAPs, the electromechanical response can be linear as the typical piezoelectric polymers or nonlinear such as Maxwell stress effect. Piezoelectric and electrostrictive effect arise from reorientation of dipole moment within material in response to external applied electric field. Maxwell effect arises from the electrostatic attraction of charges with opposite signal of two sides electrode of polymer film. In this section, a brief definition of work mechanisms of these polymers will be given.

I.5.a.Piezoelectric effect

The piezoelectric effect is the basic electromechanical effect of crystalline materials without symmetric center. There are 32 point groups for crystallines and 20 of them are non-symmetric. Dimension of these crystalline materials change in response to external stimuli such as electric field. These changes result in a change in electric polarization and hence give rise to occurrence of piezoelectric effect or even pyroelectric (with spontaneous polarization) and ferroelectric effects (with electrically reversible spontaneous polarization).

Piezoelectric effect is a linear electromechanical effect where the mechanical strain (S) and stress (T) are coupled with electric field (E) and displacement (or area charge density, D), expressed as following :

$$S = d\,E$$

$$D = d\,T$$

where d is the piezoelectric coefficient. The effect in the first equation is known as the converse piezoelectric effect and the second as the direct piezoelectric effect. Adding the linear elastic (Hook's law) and dielectric relations into the first equation, we can have the constitutive piezoelectric equations:

$$S_{ij} = d_{kij}E_k + s^E_{ijkl}T_{kl}$$

$$D_i = \varepsilon^T_{ik}E_k + d_{ikl}T_{kl}$$

Where s^E_{ijkl} is the elastic compliance, ε^T_{ik} is the dielectric permittivity and i,j,k,l = 1 – 3. Depending on the different boundary conditions, the constitutive piezoelectric equations have three other forms, which can be referred to the "IEEE standard on piezoelectricity" for detailed investigation.

I.5.b.Electrostrictive effect

Unlike piezoelectric effect, electrostrictive effect is a quadratic dependence of strain and stress on polarization (P), which exists in all dielectric materials :

$$S_{ij} = Q_{ijkl}P_kP_l$$

where Q_{ijkl} is the charged related electrostrictive coefficient. For an isotropic polymer,

$$S_3 = Q_{33}P^2$$

$$S_1 = Q_{13}P^2$$

where S_3 and S_1 are the strains along and perpendicular to the polarization direction, also known as the longitudinal and transverse strain, respectively. For an isotropic incompressible polymer, experiment and theoretical investigations demonstrate that $S_3 < 0$ and $S_1 > 0$. Hence, the electric field induced polarization will lead to a contraction along polarization direction and an expansion in the direction perpendicular to polarization direction.

For linear dielectrics, the polarization density can be expressed as a function of the dielectric permittivity and electric field :

$$P = (\varepsilon - \varepsilon_0)E = (\varepsilon_r - 1)\varepsilon_0 E$$

where ε_0 is the vacuum dielectric permittivity (= 8,85 x 10^{-12} $F.m^{-1}$) and ε_r is the relative dielectric permittivity. Therefore,

$$S_E = Q(\varepsilon_r - 1)^2 \varepsilon_0^2 E^2 = M'E^2$$

where M’ is the electric field related electrostrictive coefficient.

Most polymers exhibit nonlinear dielectric properties and as a result, the induced strain especially at high electric field exhibits saturation rather than a quadratic relationship as described in the last equation.

I.5.c.Maxwell effect

When an electric field is applied to a thin dielectric film, charges with different signals on two electrode sides will attract each other, resulting into an electrostatic force which is known as the Maxwell stress. It has been demonstrated that the Maxwell stress across the thickness is proportional to the product of the dielectric permittivity and square of the applied electric field.(58,78) And the Maxwell strain in the thickness direction can be expressed as:

$$S_M = \frac{1}{2}\frac{\varepsilon_r \varepsilon_0}{Y} E^2 (1 + 2v) = M'' E^2,$$

where Y is the Young’s modulus of the dielectric materials, Ʋ is the Poisson’s ratio, and M’’ is the as-defined Maxwell coefficient.

PART II:

Objectives of the PhD

II.1. Project concept and objectives

II.1.a. Challenge for public health

Diseases of the heart and circulatory system (cardiovascular disease or CVD) are the main causes of death in Europe: accounting for over 4 million deaths each year. Nearly half (47%) of all deaths are from CVD[1]. The CVD burden in Europe is exacerbated by its rapidly ageing population. With ageing, the prevalence of many cardiovascular diseases increases exponentially, especially Coronary Heart Disease (CHD), Valvular Heart Disease (VHD), Atrial Fibrillation (AF), heart failure and hypertension. The resulting economic as well as human costs for Europe are tremendous. Overall CVD is estimated to cost the EU economy almost 196 billion € a year.

In the last half century, medical technology has led to a significant improvement in both clinical diagnosis and management of CVD. This, together with a change in the lifestyle of European citizens, has resulted in a consistent decrease in death rates from CVD over the past two decades in most of the European countries. The advancement of techniques for minimally invasive management of CVD has contributed vitally to improving the prognosis of these patients and this is clearly reflected in their incorporation into the clinical guidelines.

The goal of this research concern the development of intelligent wire guide technologies that will accelerate the paradigm shift from costly, burdensome surgical treatments to cost-effective and patient-friendly minimally invasive interventions. It will also enable the creation of new advanced treatments for currently complex surgical procedures. This will allow for more individuals to be treated thereby contributing further to the trend of decreasing death rates and improvement in quality of life.

Since the 1940s when the first human cardiac catheterization and hemodynamics measurements were made there has been tremendous progress in the development of tools and techniques for performing measurements and interventions through percutaneous approaches. Wire guide and related instruments provide a delivery system for diagnostic and therapeutic devices through the vasculature of the body or small directed punctures externally. Consequently, methods that have high risks of complications including cardiopulmonary bypass, and large cardiothoracic incisions, are avoided. The patient also benefits from a dramatically reduced hospital stay and for some procedures, same day discharge in an outpatient workflow. With these significant advantages in mind, clinicians are developing methods to perform increasingly complex interventions via percutaneous and transcatheter routes. Most currently performed are percutaneous coronary interventions to open occluded vessels with a dilation balloon (and followed often by deployment of a stent). These are gradually being performed in more critical, smaller vessels, longer chronic occlusions and at vascular junctions or bifurcations. Other examples of complex interventions include endovascular aneurysm repair, endovascular stroke interventions, closure devices implantation for structural heart disease, etc. Thousands of guides have been used every day worldwide by radiologists, urologists, neuroradiologists, cardiologists and so on. This new innovative device could be commercialized worldwide and sold in thousands of copies every day.

II.1.b. Challenges in interventions

Coupled with the advancement in novel therapeutic devices, is the need for effective guidance and delivery systems. Unlike the simpler procedures, complex interventions require precise deployment and a careful monitoring of complications, as they can be irreversible and fatal. There is a need for more information and the ability to respond rapidly and accurately to the information. To ensure precise treatment it is necessary for the clinician to:

- have real-time, multi-variable information regarding the structure and function of the anatomy
- track precisely and accurately the position and orientation of the devices used in the intervention
- steer precisely and accurately the devices used in the intervention

II.1.c. Technical challenge : Limited availability of advanced functionality

The need in intervention can be translate in three technical challenges.

Sensing/imaging

For local information at the position of the intervention in the body, there are only a few examples of wire guide with sensors (eg. pressure, force and temperature) or imaging devices (eg. intracardiac echo, intravascular echo and optical coherence tomography). These sensors/imagers are based on bulk technology and further miniaturization is limited. The tremendous effort required to reduce the size of these bulk devices into a wire guide form factor yields expensive devices. Thus these devices are not readily adopted in Europe, despite the fact that they have clearly demonstrated clinical value. There is a strong need for sensors and imaging devices based on intrinsically miniaturizable technologies that can be readily integrated into small intelligent wire guides.

Tracking

In addition to sensors that provide information to guide therapy deployment, an important type of sensor is that used for tracking the position of tools relative to crucial anatomic locations. Currently tracking is most often performed through direct visualization from external imaging systems (eg. X-ray fluoroscopy). In the case of commonly used fluoroscopy, the lack of soft tissue contrast limits the localization of tools relative to the heart and vessels. Furthermore ubiquitous use of X-ray delivers radiation dose to the patient and physician, which accumulate for the generally long aforementioned procedures (>2h, until 6 or 8hours). There is a need to provide precise non-/reduced ionizing radiation dose tracking methods that are accurate in order to provide physicians with the confidence that they are applying the therapy in the desired location and not causing collateral damage to surrounding critical structures.

Steering

To obtain accurate local information from sensors, precise control of measurement devices is crucial for unlimited access to difficult areas in the body (eg. tortuous, high bending angles). Similar access and steering is needed for accurate, predictable deployment of therapeutic devices to ensure low physician effort and minimize repeat attempts. In the majority of interventions, tools are used without steering functionality. Clinicians maneuver the “passive” wire guide thanks to the contact with between the tip of the guide and the vascular wall surfaces. This can result in vessel trauma and the method cannot be used in the open spaces of the heart chambers. In heart chambers, catheters and related tools are generally steered through simple mechanical pull wire systems. These have the disadvantage that they have restricted directionality, limited shape control, large force requirements and are difficult to miniaturize. In peripheral arteries, we usually use angulated preformed catheters. The choice of the catheter depends on the angulation and the diameter of the targeted vessel. This results in poor deployment precision, restricted access and an overall increase in procedure time because of many manipulations. There is a need for the creation of new steering technologies that can readily and accurately control a wire guides tip into unlimited contours. This will enable improved steering in currently used procedures and allow for steering to guide other interventions for greater efficiency and safety.

II.2. PhD Objective and contribution

The main goal of this PhD is to develop a technology platform (Figure 42) that will enable advanced sensing and steering functions to be integrated into millimeter size in-body of wire guide for emerging complex minimally invasive cardiovascular and related diseases interventions. However, the emergence of an intelligent guide wire cannot be achieved without the development of other technological bricks (imaging, tracking), but behond the scope of this PhD thesis.

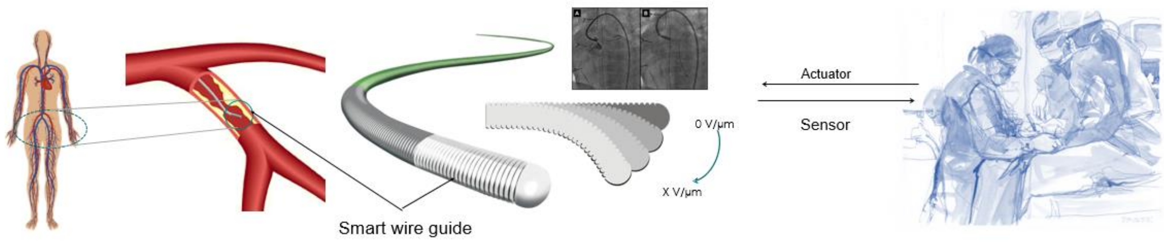

Figure 42. Schematic illustration of working principle for smart wire guide

Wire guide maneuverability has a strong influence on both the procedure time as well as the risk of complications such as vessel perforation. However, in the majority of cases, conventional, non-steerable wire guide are used. These passive wire guides typically have a no traumatic preformed distal tip (with the form of a J), which provide the rails over which catheters are deployed. Currently available steerable catheters are mainly used in the field of electrophysiology to treat heart arrhythmias. Pull wire based wire guide have a number of disadvantages:

1. Steering is limited to simple bending. Complex wire guide shapes or multiple wire guides segments are difficult if not impossible to realize.

2. Miniaturization is limited, especially for catheters with multiple steerable segments.

3. Pull wires extend over the entire length of the wire guide leading to less accuracy and resolution of tip positioning.

4. Pull wire based steering relies on a proximal applied torque to the wire guide shaft and restricts the ability of the catheter to follow a tortuous path of the vessels

5. The force exerted by the pull-wire for tip bending has to be guided by the catheter shaft, limiting small bending radii of the tip.

On-going developments in the field of smart materials enable the development of actuators that have the potential to be small, powerful and rapid enough to locally actuate the tip, or segments, of a wire guide. Among these, the project will investigate promising materials such as electro-active polymers. Prototypes of structures bent with such actuators have been shown in the literature (see chapter 2). The use of smart material actuators integrated into the wire guide could overcome the current drawbacks of pull wire based actuation by providing these benefits:

1. Actuation forces only act on the segment to be bent, thereby enabling the use of a shaft with a small bending stiffness.

2. Stick-slip phenomena are fully or drastically reduced.

3. Individual segments can be electronically and independently actuated

4. Many actuators or segments can be integrated in the wire guide allowing for complex movement.

5. The stiffness of such materials can be electronically altered resulting in segments that can switch between being stiff for good push-ability and soft for flexibility on demand.

This would potentially enable the realization of wire guide, with high accuracy of tip control, with the ability to perform complex navigation tasks. Further miniaturization of wire guide would be possible enabling minimally invasive vascular surgery in smaller vessels and in more difficult to reach areas of the human body. The challenges in realizing smart material actuators for steering include the appropriate physical form for effective motion, the material-control electronics interface and the control mechanism. The PhD will build and evaluate electroactive polymers actuators for precisely steering a wire guide tip. Optimization of electrostrictive polymers will be investigated for robust steering. The materials will be processed into forms effective for translation into mechanical energy (e.g. polymer films and stacks).

Then, we will focus on the possibility of use the device so the polymer into human vessel, so we will focus on the biocompatibility. The influence of process of sterilization for medical device will be investigated but also the cellular viability when cells are in contact with the materials. Finally this PhD provides a frame work will help the selection of optimization of electroactive polymer for the development of medical device, for cardiovascular surgery.

Figure 43 summarized the PhD structure around the development and optimization of EAP for smart wire guide.

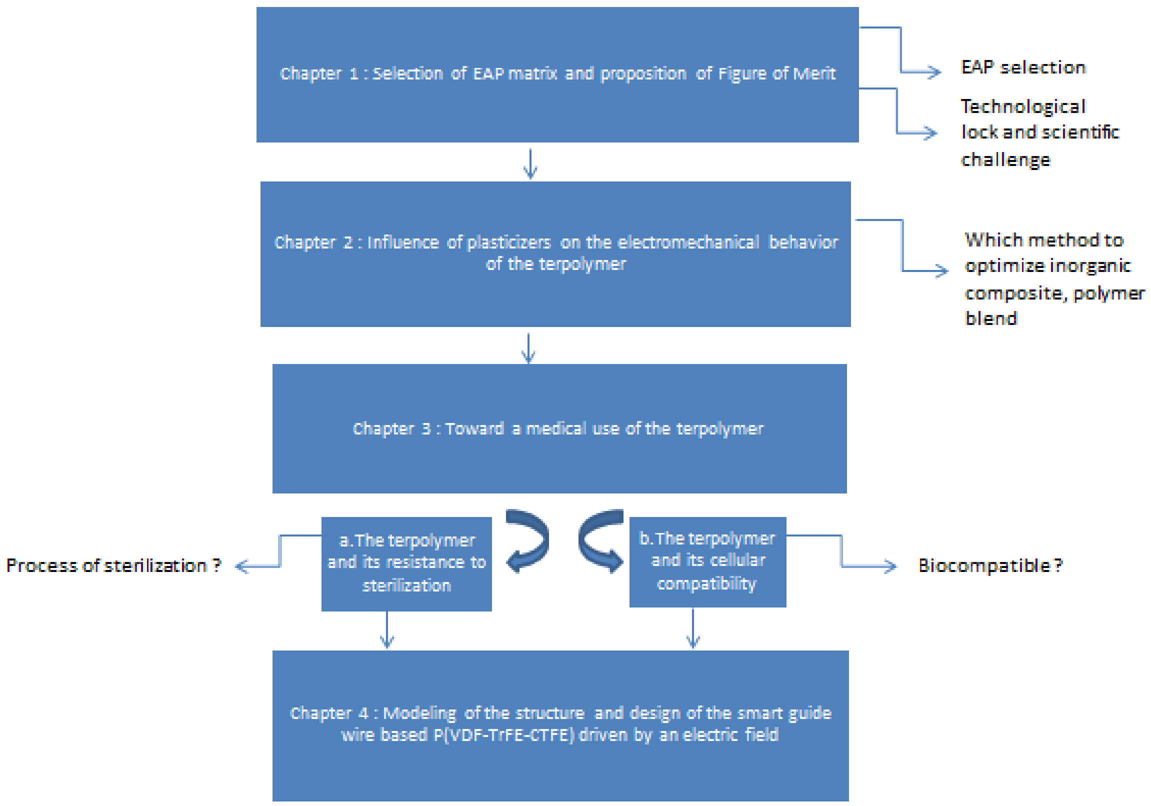

Figure 43. Overview of PhD structure

PART III:

Experiments and Results

Chapter 1: Selection of EAP matrix and proposition of Figure of Merit

This chapter repeats the works published during the thesis in the paper "Enhanced Figures of Merit for a High-Performing Actuator in Electrostrictive Materials", Polymers 2018, 10(3), 263; https://doi.org/10.3390/polym10030263, by **N. Della Schiava,** K. Thetpraphi, MQ Lê, P. Lermusiaux, A. Millon, JF Capsal et PJ Cottinet.[124]

III.1.a. Polymer selection : application needs and difficulties of selection

In the first bibliographic part, we described a lot of EAP with multiple applications. As we have seen, each EAP have its own electromechanical properties, advantages and drawbacks. There are also other classes of material which can be electroactive as ceramics. There is no perfect material to obtain this phenomenon. The choice of the material may be guided by the desired application. We must find the best compromise between advantages and drawbacks for the targeted application. And then we have to work on this material to improve these own properties to permit an efficient application. FOM can be a precious guide for the choice.

In our work, we want to perform a steerable guide wire for intravascular navigation. So first of all, the polymer used must be biocompatible. Moreover, high pushability, torque and flexibility are required qualities for the device.

Because of arterial bifurcation with angulation of more than 90 °, we need important bending angles. Hutchins et al, realized a study on the typical curvature and angle in human vessels.[125] Measurements were made of parent and branched vessel diameters from post-mortem human arteries. The included angle between branches varied from 32 to 124 degrees.

External electric field needed to obtain this angulation must be the smallest possible. Indeed, standard 60601-1 imposes a limit on the amount of current that flows in a medical device. The current in the human body is highly regulated because 1,5mA can cause atrial or ventricular fibrillation in the human. According to the standard 60601-1, we can say that the device cannot use a current superior to 50µA. [126]

The polymer must have great performances at low frequencies because we need quite slow deformation. In fact, the time response of the actuator is directly linked with the physical properties of the surgeon since the guide wire is controlled and moved by the surgeon. The typical reaction time of humans is about 180 ms because of time delay in human vision and the needing time between nerve impulses and muscles movement.[127] So the time response of the actuator does not exceed around 100 ms.

Miniaturization of the design must be possible. In fact, usual intravascular guide wires diameters ranged from 0,889 to 0,3556 millimeters.

Finally, the fabrication process may be easy, short, possible into the lab and low-cost.

Even though ceramics remain most of time more efficient in terms of energy conversion by weight unit, ceramics are stiff and brittle, their fabrication need high temperatures and is difficult.

Contrary to ionic polymers, electric EAP doesn't need wet state. Responses are more rapid; actuation forces and mechanical energy density are higher. So for the desired application, dielectric and electrostrictive polymers seems interesting candidate. Figure 429 show the electrostrictive coefficient of different dielectric material function of the density extract for the CES Edupack database. It is interesting to note that there is large quantities of potential candidate. For realized the selection in link with the application it is important to identify the key parameters in link with the application.

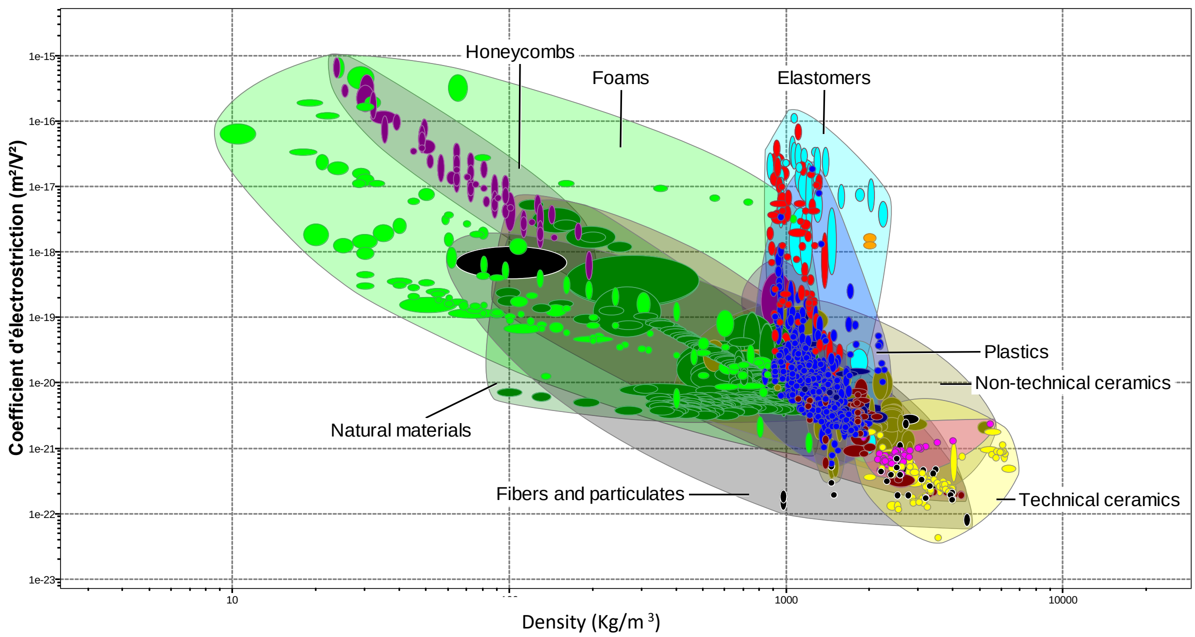

Figure 424. Ashby diagram electrostrictive coefficient function of the density without selection

III.1.b. Proposition of Figure of Merit

The well-known model of electrostrictive material can be written by expression as follows:

$$\begin{cases} S_{31} = M_{31}.E^2 + s^E.T_{31} \\ D_{ij} = \varepsilon.E + 2.M_{31}.E.T_{31} \end{cases} \quad (1)$$

where *S* is the strain, *T* is the stress, *D* is the electric displacement, *E* is the electric field, *M* is the electrostrictive coefficient, *s* is the compliance, and *ε* is the permittivity of the polymer. It is noteworthy that S_{31} denotes the transverse strain corresponding to the ratio of change in the length of the sample (direction of axis 1) under an applied electric field along the thickness direction (axis 3). A similar explanation can be made for other parameters, like T_{31} and D_{31}. Figure 45 illustrates the direction of the applied electric field as well as the deformation.

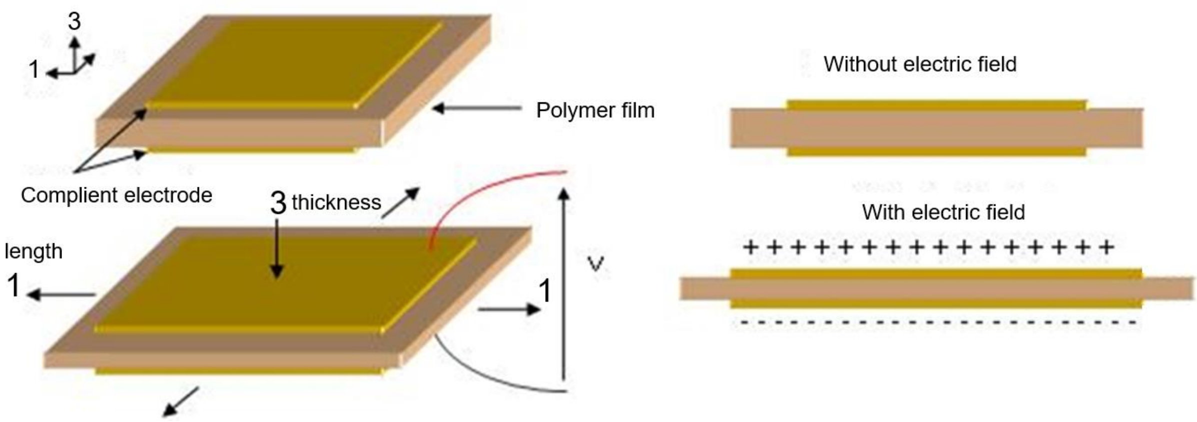

Figure 45. Schematic representation of the electrostrictive actuation principle

Without stress (i.e. $T_{31} = 0$), the electrostrictive transverse strain under an electric field can be simplified as Eq (2):

$$S_{31} = M_{31}.E^2 \quad (2)$$

where the electrostrictive coefficient M_{31} depends on the permittivity and the Young modulus of material as expressed as Eq. **Erreur ! Source du renvoi introuvable.** :

$$M_{31} \propto \frac{\varepsilon_0.\varepsilon_r}{Y} \quad (3)$$

where ε_r is the relative permittivity of the polymer et ε_0 is the vacuum permittivity.

It was revealed from Eqs **Erreur ! Source du renvoi introuvable.**–**Erreur ! Source du renvoi introuvable.** that in order to enhance the resulting strain without increasing the electric field, one can whether increase the permittivity, decrease the Young modulus or both.

Therefore, the FOM of the strain is defined by

$$\mathrm{FOM}_{\mathrm{strain}} = \frac{\varepsilon_0 . \varepsilon_r}{Y} \tag{4}$$

Nevertheless, the electrostrictive strain response of the polymer is not the only key issue that needs to be studied. Another alternative parameter permitting to assess the actuation performance of the electroactive material is the blocking force that can be easily determined at zero strain.

Substituting $S_{31} = 0$ in Eq. **Erreur ! Source du renvoi introuvable.** yields:

$$T_{31} = Y.M_{31}.E^2 \tag{5}$$

Combining Eq. **Erreur ! Source du renvoi introuvable.** and Eq. **Erreur ! Source du renvoi introuvable.** makes it possible to induce the FOM of the blocking force for a given electric field

$$\mathrm{FOM}_{\mathrm{force}} = \varepsilon_0 . \varepsilon_r \tag{6}$$

Again, the above equation demonstrates further advantage of increasing the permittivity for achieving better actuation performance.

Besides the strain and the blocking force, another critical parameter also affecting the electromechanical coupling of the polymer is the mechanical energy density W_m which is given by the following expression:

$$W_m = \frac{1}{2} Y.S_{31}^2 \tag{7}$$

Substituting Eq. **Erreur ! Source du renvoi introuvable.** into (4) yields

$$W_m = \frac{1}{2} \frac{\left(\varepsilon_0 . \varepsilon_r\right)^2}{Y} E^4 \tag{8}$$

Finally, the FOM of the mechanical energy density can be defined as

$$FOM_{energy} \frac{\left(\varepsilon_0.\varepsilon_r\right)^2}{Y} \quad (9)$$

In actuator applications based on electroactive polymers, the strain response, the blocking force, and the mechanical energy density under low electric field can be simultaneously enhanced by increasing the dielectric permittivity of the polymer. For a better electromechanical coupling, especially in low-frequency actuator applications, a decrease in the Young's modulus should be involved but it must be limited in order not to drastically change the elasticity as well as the compliance of the material. Consequently, for an improvement of electrostrictive property, the increase in strain must be higher than the decrease in the elasticity modulus of the material.

Erreur ! Source du renvoi introuvable.6 summarizes the FOM of an electrostrictive actuator based on three critical parameters comprising the strain response, the blocking force, and the mechanical energy density.

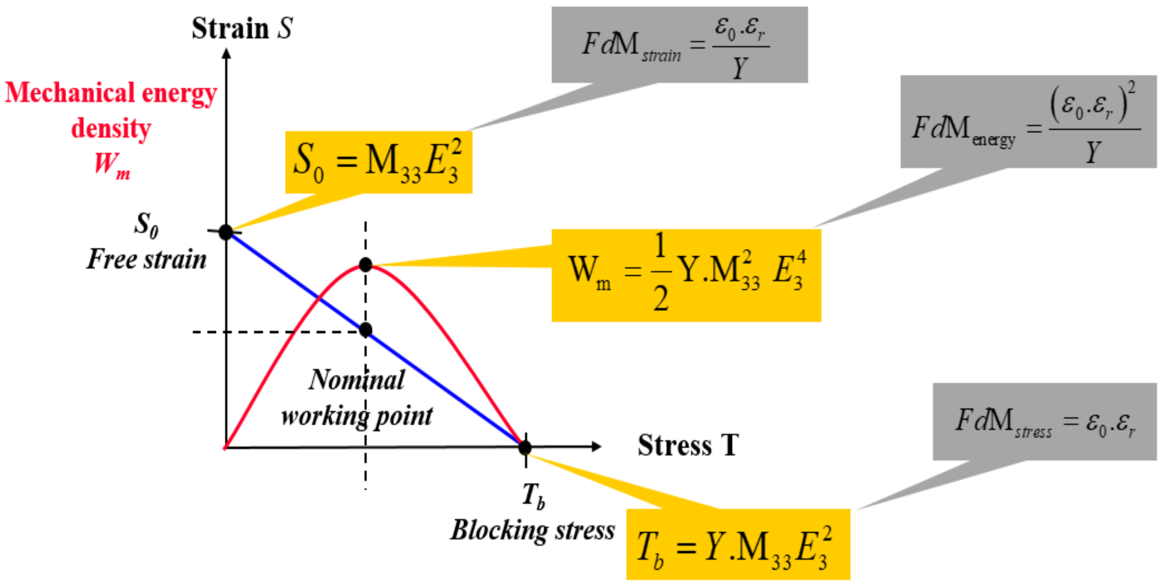

Figure 436. Pertinent parameters and figures of merit for an electrostrictive polymer

The strain S_{31} can be deduced from the deflection measurements of a unimorph under quasi-static conditions according to the following expression:

$$\delta_0 = \frac{3L^2}{2e}\frac{2AB(1+B)^2}{A^2B^4+2AB(2+3B+2B^2)+1}S_{31} \quad (10)$$

where δ_0 is the cantilevered tip deflection, $A=Y_{substrate}/Y_{poly}$ and $B=e_{substrate}/e_{poly}$ with $Y_{substrate}$, Y_{poly}, $e_{substrate}$ and e_{poly} depict the Young modulus of the substrate, the Young modulus of the polymer, the substrate thickness, and the polymer thickness, respectively; e and L are respectively the sample thickness and length. As illustrated in Figure 46, the transverse strain S_{31} corresponds to the ratio of change in length of the sample (axis 1) under an applied electric field along the thickness direction (axis 3).

It is noteworthy that the model based on Eq. (1) is only available for relatively small deflections. Consequently, all materials explored in this study will be excited under electric fields with which the tip deflection of the unimorph does not exceed 3 mm.

An ideal electrostrictive material is not only assured by a high figure of merit, but also by the electrical breakdown that occurs when the dielectric strength of the material is exceeded. In practical situations, each material has its ideal operation electric field that directly affect to the limit of strain range.

To better clarify this issues, we introduce here three different kinds of composites, i.e. a pure polymer, two modified polymers A and B possessing higher electrostriction coefficient compared to the pure polymer but their electric field breakdown is different. Figure 47 illustrates the linear relationship between the strain and the electric field square of these three composites, where the slope of each curve represents the electrostriction coefficient M_{13}. As observed, the M_{13} value of the sample A is higher than the other samples, leading to better strain response for a given electric field. Nonetheless, its electrical breakdown is relatively low, reducing drastically the strain range and as a result, limiting the electromechanical conversion. This kind of material is suitable for applications where low input voltage is mandatory. The pure material, on the other hand, exhibiting large range of electrical breakdown but its electrostrictive property is quite poor, involving in extremely high applied electric field for reaching sufficient strain. The sample B seems to be good compromise between the electrostrictive behavior and the electrical breakdown limit. However, we cannot conclude that this material is the most appropriate choices in any practical applications, neither does the material A with its highest electrostrictive coefficient. Again, it should be keeping in mind that the choice of each material is strongly affected by the intended use. For a better improvement of the electromechanical properties, it is important to ensure the fair balance between the various parameters including the strain, the blocking force, the electric field range, etc. The weighting given to each criterion effectively depends on the application area as the final purpose is not only to achieve the greatest electrostrictive behavior, but also to have reasonable electric field range.

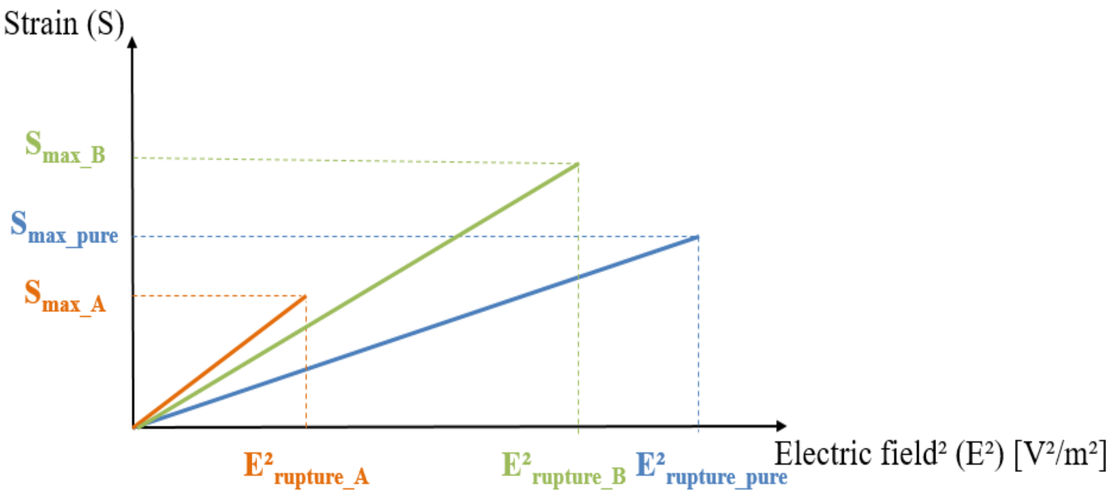

Figure 447. Strain versus electric field squares for different electrostrictive composites.

Finally, the efficient method proposed in this work for a performance comparison of different electrostrictive materials is to reference their characteristics to those of a standard material (e.g. the pure polymer). All criteria should be based on the FOM of the strain, the blocking force, and the energy density as well as the allowable maximal voltage imposed by the final application.

Table 6 depicts the characteristics of different electroactive polymers including the neat and the modified terpolymer. We will see on the following sections that the modified terpolymer shows excellent result in term of force, strain and mechanical energy density where its figure of merits are largely higher than those of the others polymers.

Type	**PDMS** [21]	**PU** [22]	**Nylon** [23]	**Pur Terpo.** [7]	**Modif. Terpo.** [7]
ε_r @ 1Hz	2.5	4.3	5	35	150
Y (MPa)	2	20	2 000	100	30
FOM_{energy} (F^2/N)	$2.44\ 10^{-28}$	$0.72\ 10^{-28}$	$0.01\ 10^{-28}$	$9.58\ 10^{-28}$	$586\ 10^{-28}$
FOM_{force} (F/m)	$2.21\ 10^{-11}$	$3.80\ 10^{-11}$	$4.42\ 10^{-11}$	$30.9\ 10^{-11}$	$133\ 10^{-11}$
FOM_{strain} (Fm/N)	$1.11\ 10^{-17}$	$0.19\ 10^{-17}$	$0.22\ 10^{-19}$	$0.31\ 10^{-17}$	$4.42\ 10^{-17}$
Breakdown field (V/µm)	200	50	30	150	140

Table 6. Characteristics of neat and modified terpolymer among various other EAPs.

For validate the proposed approach a selection based on FOM, experimental studies have been realized. The next part of this chapter will be dedicates to the presentation of fabrication process of EAP films and experimental test bench.

III.1.c. Fabrication process and characterization test bench

III.1.c.i. Film elaboration and actuator preparation

P(VDF-TrFE-CTFE) fluorinated terpolymers with a composition of 65/35/8.9 were synthesized by Piezotech S.A.S (Arkema group, France). The ratio between the VDF and CTFE contents was optimized in order to maximize the electromechanical properties [128,129]. Films were made by solution casting. In a first step, P(VDF-TrFE-CTFE) was dissolved in Methyl Ethyl Ketone (MEK, Sigma–Aldrich) solvent with a polymer-to-MEK mass fraction of 14% at 80°C and stirred for 1h to ensure complete dissolution. Then, the solution was cooled at room temperature for 2h. Finally, the mixture was cast onto a glass substrate using a Doctor Blade (Elcometer) and the solvent was allowed to evaporate. The films were placed in an oven at 70°C for 1h to totally remove the solvent, followed by an annealing at 103°C (which corresponds to the onset of the melting peak determined by DSC) during 1h to enhance the crystallinity process. A schematic of the temperature annealing process is shown in Figure 48. The dimension of all prepared films was 1cm-4cm-80µm, corresponding to their width-length-thickness.

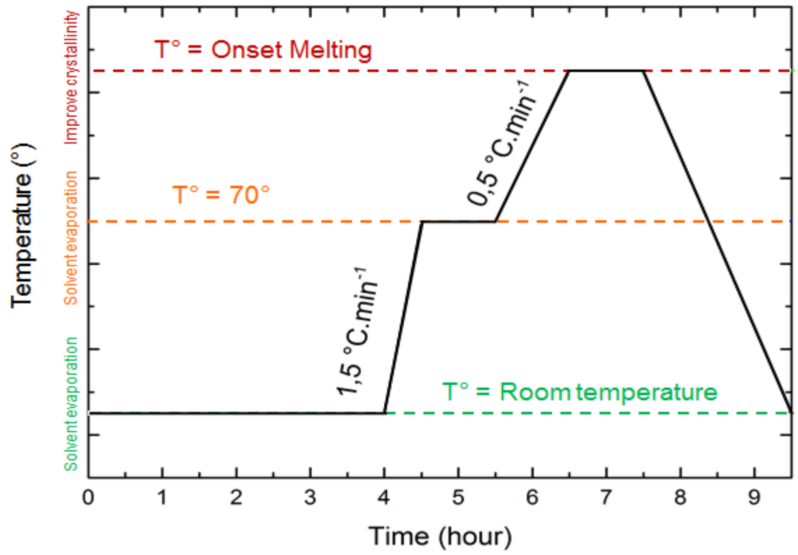

Figure 458. Evaluation of the temperature during the annealing of polymers.

For a simple electrical measurement, 25-nm-gold electrodes were sputtered on both sides of the samples using a Cressington Sputter Coater (208HR). On the other hand, for the electromechanical characterization, the whole sample comprised three layers that were fabricated with a polyethylene terephtalate (PET) substrate, adhesive, and electroactive films onto which gold electrodes were deposited by sputtering through a mask. The electroactive film was attached to the 100µm-thick PET film using a transfer adhesive (25µm-thick Scotch 3M ATG 924) between the terpolymer and the Mylar substrate

The PET was chosen due to its interesting characteristics, like flexibility, simple implementation, commercially available and low cost.

The samples were then laminated at the room temperature for 15 minutes using a D&K 4468H laminator in order to optimize the bonding of the polymer to the substrate. It is noteworthy that there is no need to pre-stretch the electroactive specimens before they were attached to the PET substrate. This property can be considered to be one of the most advantages of the developed material. Simple process fabrication, compared to CNT Buckypaper actuators, and possibility to be 3D printed in flexible electronic application are other advantages. Figure 49 illustrates the fabrication procedure of the bender actuators.

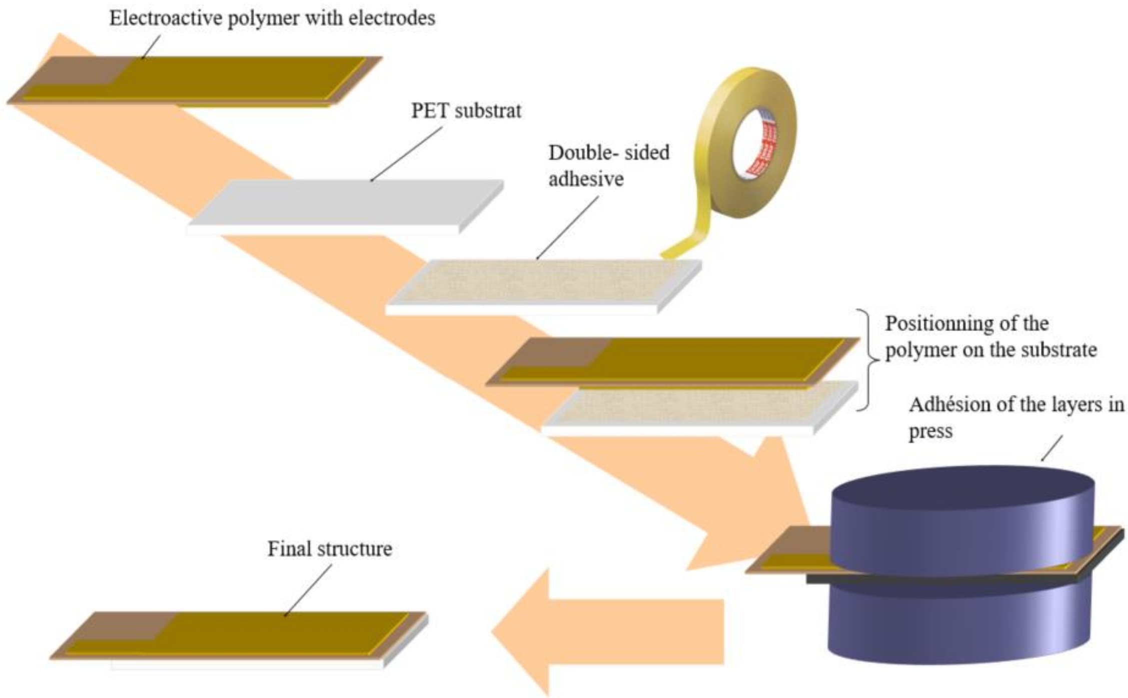

Figure 469. Fabrication process of P(VDF-TrFE-CTFE) composite actuator

III.1.c.ii. Characterization techniques

First, *Differential Scanning Calorimetric (DSC) measurements* of several polymers were performed with a DSC 131 EVO calorimeter from Seteram Instrumentation. All samples were heated to 200°C for 5 minutes, after which they were cooled to room temperature at rate of 10°C/min, and maintained at room temperature for 5 minutes. Next, the samples were heated again to 180°C at rate of 10°C/min and the measurement was recorded. The whole procedure was performed twice to confirm the reproducibility of the measurements. For all composites, the enthalpy of the melting peak was calculated from the area of the melting peak normalized to the material mass fraction.

Second, *Electrical characterizations* were performed at room temperature thanks to a Solartron SI 1255. The characterizations were performed under 1Vac with a frequency range of 0.1 Hz to 1 MHz. In order to better assess the performance of the dielectric response, all films were made with the same thickness for each set of measurements. An evaluation of the output current I versus the electric field E was investigated, allowing us to estimate the dielectric displacement. Indeed, thanks to the $I(E)$ data, software based on a simple linear model of the Ohmic conduction was employed to extract the dielectric displacement as a function of the electric field.

Next, values of the Young modulus were determined at room temperature using a homemade *Dynamic Mechanical Analysis* (DMA) setup, as shown in Figure 50. Experimental measurements were performed at a 0.1Hz frequency at which the electromechanical characterization was performed. Tensile specimens were 6 cm in total length and 1 cm wide with an effective length of 4 cm. One end of the film was fixed with a rigid clamp whereas the other end was held with a mobile one. Both clamps were fitted with gold electrodes that were fixed to the outside sample surface. A Newport table microcontroller and a force sensor were respectively used to measure the displacement and the force, which enable to infer the strain and stress of the sample. The Young modulus values were then calculated from the slope of the dynamic stress versus strain measurements.

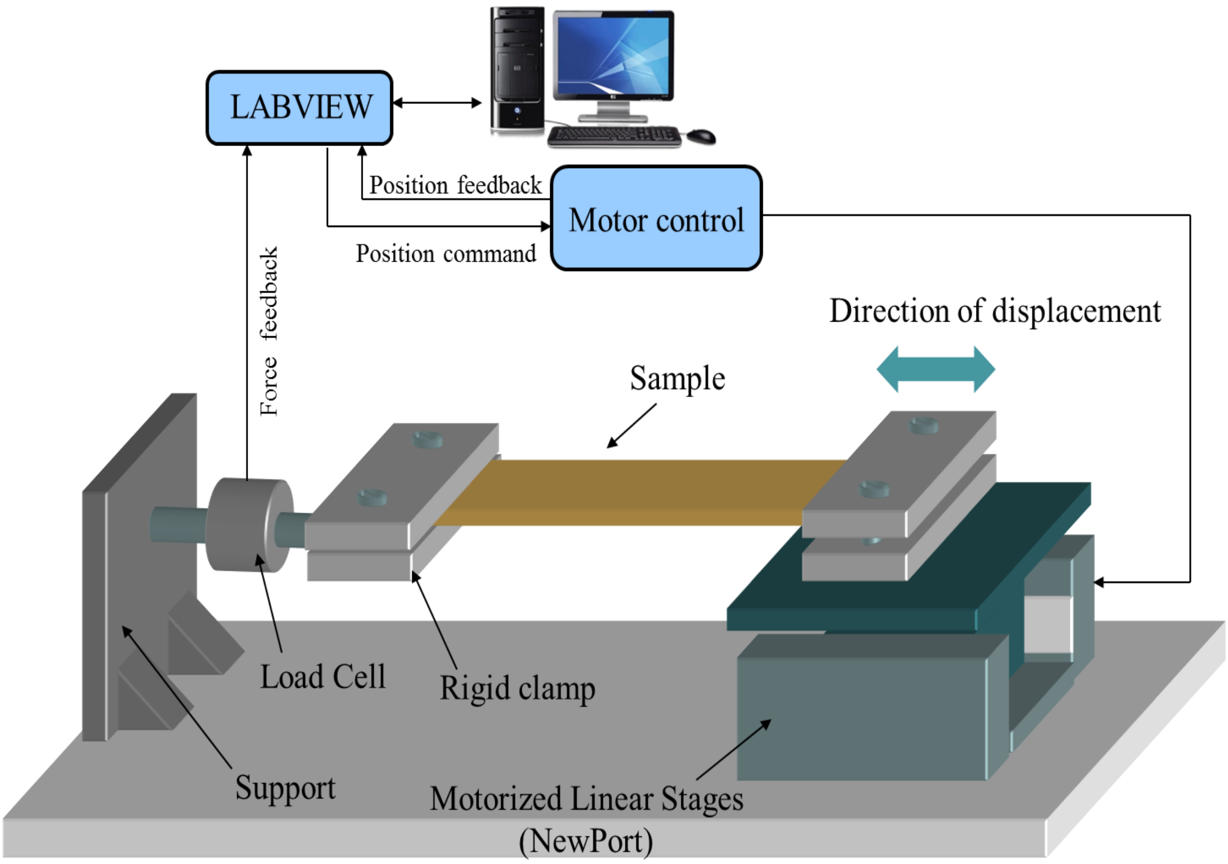

Figure 50. Schematic of the laboratory-built experimental DMA set-up.

III.1.c.iii. Experimental setup of the actuation test

Finally, to evaluate the *electromechanical properties* of the developed films, a dedicated test setup based on a cantilever configuration was performed (Figure 51).

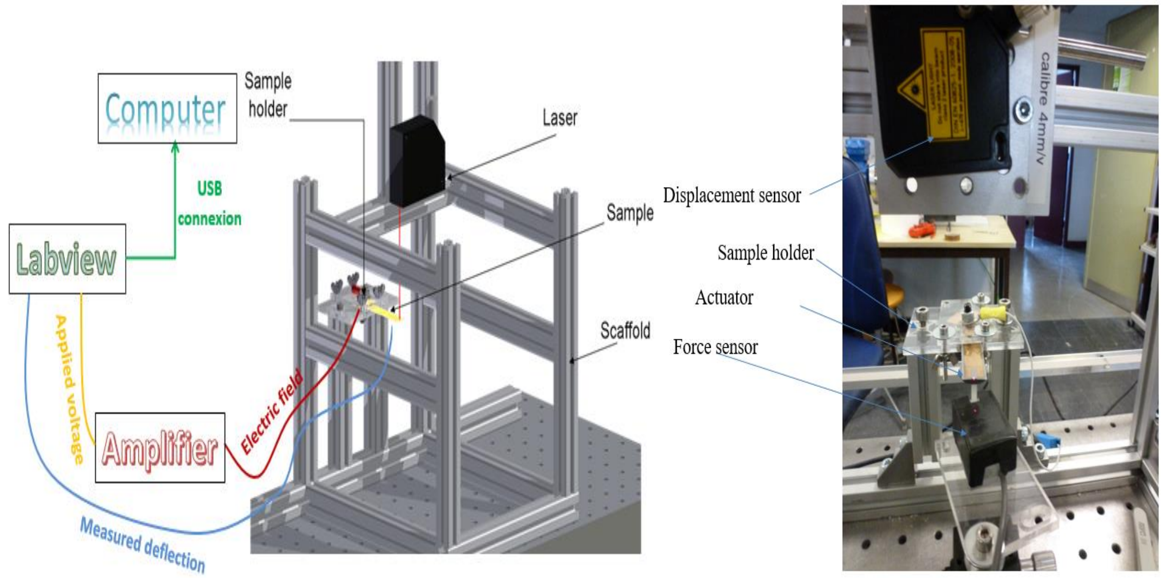

Figure 51. Schematic and photo of the test bench developed to perform the electro-mechanical characterization.

The direction of the applied voltage is illustrated previously in Figure 45.

This section deals with the influence of a measurement apparatus on the results. For complete characterization of the actuator, the displacement, as well as the generated force must be measured.

By definition, "free stroke" is the actuator displacement under zero external load.[130] Measurement of "free stroke" is considered to be the most elementary of the actuation characteristics. However, depending on the boundary conditions, results may greatly vary. Cantilever measurements under no load present no difficulty, but for unimorph actuators, several factors need to be taken into account. Holding the active parts of the actuator or the inactive part will produce slightly different results especially depending on where and how it is held. For instance, it is usually specified that the unimorph should be held with particular distance from the edge of the actuator, as the displacement of an electroactive actuator depends upon the applied voltage, frequency, and force.

Displacement measurement is quite simple. Whether the instrument is a non-contact type such as a laser-based device, or whether it is a contacting type such as an LVDT, the problem is simply to accurately measure the motion of a specified point on the actuator. Transducer accuracy can vary from quite coarse (e.g. mechanical dial gauges with 0.025 mm precision) to extremely fine (e.g. laser interferometers with high resolution in the order of micrometer) and the choice is largely dependent on experimental needs and cost. The instrument must be mounted to limit vibration and minimize interference with actuator motion and environment, but these mechanical limitations are readily overcome. In our case, the system was mounted on top of the Iso-Plate Passive Isolation System to dampen vibrations in the room. The tip displacement was measured using the non-contact laser sensor (Microtrak II; MTI Instrument, Inc.). The contact-type instrument was not employed in our device in order to limit the inertial effects that may distort the measurements. Furthermore, it is difficult to estimate how the developed forces changed with a presence of an extra mass particularly when its amplitude depend on the contact-type and evaluated in function of time. The situation becomes even more complicated when the frequency varied.

Due to its interpretation and variability, the reliable measurement of the blocking force is often controversial. Shankar defines the blocking force as the point where the external load is such that the resulting output displacement is zero.[131] This definition does not address the boundary conditions at which the actuator is subjected, i.e., simply supported or cantilevered, as well as a variety of other operating conditions. The most difficult variable to measure is cantilevered blocked force. Assuming the mounting type is appropriate, several techniques may be employed, e.g. load cells considering being the most commonly used. Accuracy of force measure highly depends on the range and resolution of the load cell as well as its integration on the actuator. For that reason, when selecting an actuator, the manner through which force is measured becomes an issue. The result can be very dissimilar between each configuration of load cell. As a result, condition of force measurement and its experimental setup should be well defined. For instance, a definition of cantilevered blocked force is given as the force observed on a gauge when holding the tip of the actuator during energization.[131]

It is noteworthy that the fact of integrating the load cell may produce the inertial effect on the actuator. In our case, this phenomenon can be discarded as the system is carried out under relatively low frequencies. Actually, the operating frequency range is selected in such a way that the inertial force can be negligible compared to the actuator's force, allowing to simplify the interpretation and the performance analysis. Another difficulty of the force measure devices stems from the fact that it is unable to accurately operate without restricting the motion of the actuator. Indeed, a load cell can only move a very short distance over its full measuring range, e.g. 25.4 µm to 100 µm for the FC-22 load cell. Hence, the device must be able to measure the actuator's force over the full range of displacement without biasing the result with the force needed to move the device itself. In our case, Transducer Techniques GSO-10 10gram load cell with TMO-1 signal conditioner/amplifier was employed as this sensor has high sensitivity and large frequency bandwidth.

Finally, experimental design for force-displacement measurement of an electroactive polymer actuator requiring adequate equipment seems not to be trivial problem. Figure 51 shows essential components of the test bench including the developed actuator, the load cells allowing measuring the blocking force under extremely low displacement of the sample, the displacement transducers fixing to the upper end of the actuator and enabling to measure the motion of the bender. For improving precision of the force measurement, the load cell was mounted to the carriage of a screw-driven slide, making it possible to accurately determine the relative position between the load cells and the polymer based on the slide's scale and the graduated dial. The input voltage was generated from the NI 9263 output analog card and then was amplified by a high voltage amplifier (Treck 609D-6). The signal was applied to the actuator through the set of electrodes mounted to the fixture base. All the data were monitoring via the LabVIEW software, Paris, France.

All data were acquired at a frequency of 0.1Hz.

III. 1.d. Results and discussion concerning the validation of the FOM

A set of experiments were conducted on actuators made from the neat terpolymer P(VDF-TrFE-CTFE) and the one with the plasticizer DEHP. In order to assess the performance of these electrostrictive polymers, the electromechanical response was measured as a function of different stimuli under very low frequency. As mentioned above, the fact of working at low frequency made it possible to enhance the accuracy of force and strain measurements. Another purpose was the extremely high permittivity of the modified terpolymer under such a low bandwidth. For more details about mechanical and dielectric properties of the proposed material as function of frequency, we can refer to [124].

It is noteworthy that in our experiment, the input electric field is limit to around 40-50V/µm which is small enough with respect to the breakdown strength of the terpolymer (see Table 6). As reported on [124], low electric field also enables to fit with the classical Maxwell electrostrictive model and to avoid all non-linearity due to the saturation effect. The following subsections will demonstrate that under such moderate electric fields, high electrostrictive responses in term of force and strain still achieve, confirming excellent actuation characteristics of the proposed materials.

III.1.d.i.Free displacement

In order to highlight the actuation performances of the all-organic composites, several unimorph architectures were investigated. Figure 49 describes the field-induced actuation of a unimorph comprising an active polymer P(VDF-TrFE-CTFE) + 10 wt%DEHP and an inactive PET substrate. To prevent a discharge effect during operation under high voltage, the surface approximately 1.5 mm from the edge of the active layer was not covered with an electrode. Figure 52 shows the actuation behavior of the developed unimorph under electric fields of 0V/µm and 50V/µm electric field. A high deflection response of the modified terpolymer was achieved under a relatively low electric field.

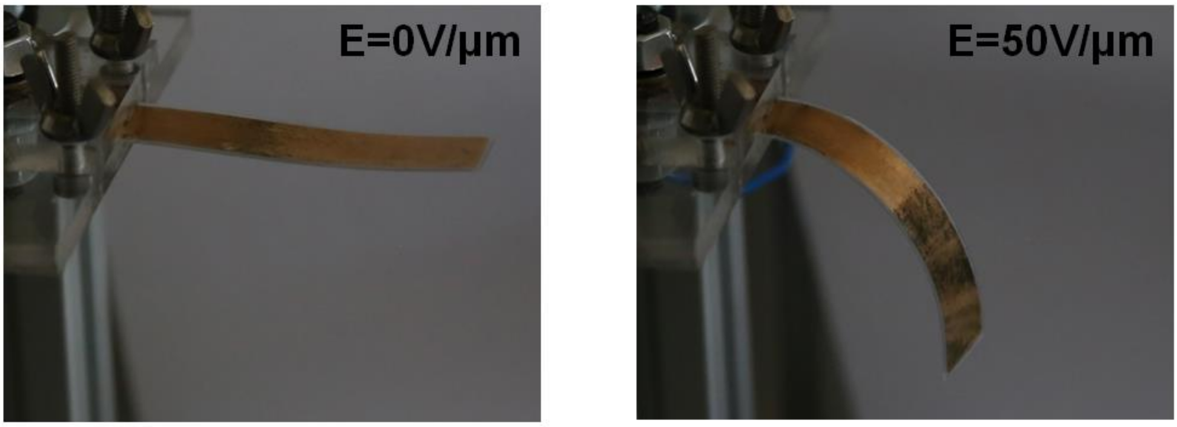

Figure 52. Photographs of the unimorph under different input electric fields

For a unimorph, it has been derived that the tip displacement (δ) depends on the geometry of the device as well as the material properties. Under quasi-static conditions, the transverse strain (S_{31}) of a unimorph can be inferred from the deflection measurements according to the following expression:

$$\delta_0 = \frac{3L^2}{2e} \frac{2AB(1+B)^2}{A^2B^4 + 2AB(2+3B+2B^2)+1} S_{31} \quad (11)$$

where δ_0 is the cantilevered tip deflection, $A = Y_{substrate}/Y_{poly}$ and $B = e_{substrate}/e_{poly}$ with $Y_{substrate}$, Y_{poly}, $e_{substrate}$ and e_{poly} depict the young modulus of the substrate, the Young modulus of the polymer, the substrate thickness, and the polymer thickness respectively; e and L are respectively the sample thickness and the length.

Figure 53 illustrates the empirical quasi-static displacement versus the electric field at 0.1Hz for the pure and modified terpolymers. Under low electric fields below 50V/µm, the induced deflection displayed a quadratic dependence, whereas at higher values, a saturation behavior of the deflection is observed. As expected, a gap between the ascending and the descending branches occurred, representing the hysteresis characteristic of the composite. Similar to other electroactive materials, like magnetic substrates, magnetostrictive, piezoceramics, shape memory alloys, etc., when the electrostrictive actuator partially inherits the piezoelectric property, it exhibits the disadvantages of hysteresis and creep (or drift) behaviors.[132,133] Such comportments may deteriorate the system's performance and lead to oscillation vibration and even instability, especially where very precise positioning is required, for instance in the case of atomic force microscopes or micro-manipulators. On the other hand, compared with shape memory alloys, the hysteresis of our material was much lower under similar electric field cycling.[134,135]

The effect of the DEHP plasticizer on the electrostrictive response of the terpolymer at low frequency is clearly confirmed by Figure 53, with a 2,5-fold enhancement between the modified and neat terpolymers. It has been previously reported that in the case of dielectric polymers, the electrostrictive strain under an electric field can be mainly attributed to Maxwell forces, induced by dipolar orientation within the material.[136] Also, experimental measurements demonstrated exceptional increase in dielectric permittivity as well as somewhat decreased Young's modulus of the plasticized composite, leading to a large enhancement of the electrostrictive coefficient and the figure of merit.

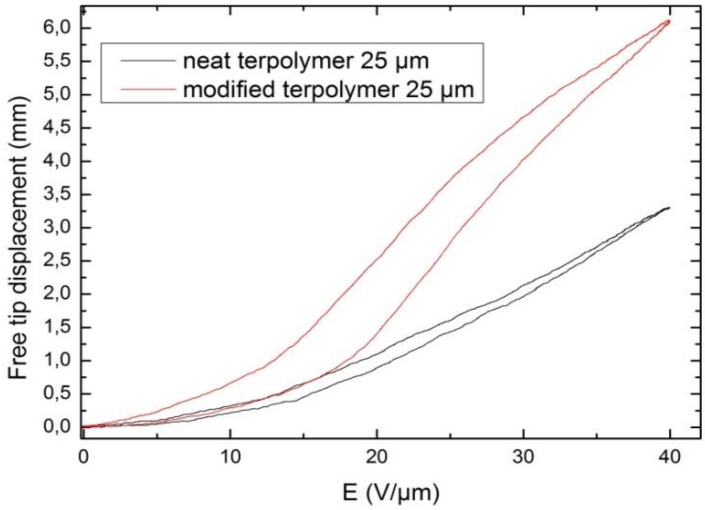

Figure 473. Free displacement versus electric field at 0,1 Hz for two terpolymer compositions

III.1.d.ii.Blocking force

Figure 54 depicts the evaluation of the measured blocking force as a function of the applied electric field for two compositions of terpolymer. A quadratic dependence of the blocking force in terms of the electric field was achieved, confirming good agreement between experiment and theory. A comparison between the conventional and the plasticized terpolymers shows a great enhancement of the blocking force with a 2.5-fold increase under 40V/µm. Such a large improvement can be explained by the fact that the modified material exhibited a higher dielectric permittivity, leading to higher FOM of the blocking force.

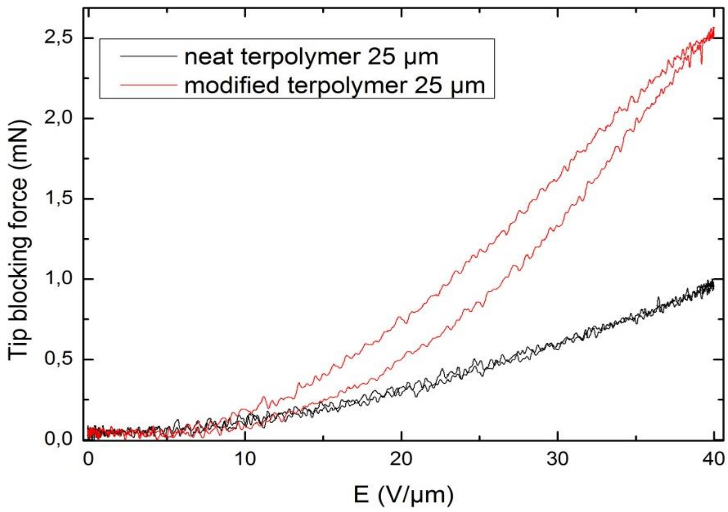

Figure 484. Blocking force versus electric field for two terpolymer compositions.

In conclusion, in order to optimize the force and strain generated by an electrostrictive material, its dielectric permittivity should be increased. This observation is in correlation with the working principles of the electrostrictive materials since the Maxwell electrostatic stress (T_E), induces strain in the material. As a result, an enhancement in force leads to better response in strain and inversely. These two parameters play a key role in the performance of polymer actuation.

III.1.d.iii. Force versus deflection

With electroactive benders, the ability of the actuator to generate force decreases linearly with deflection.[137,138] The experimental force versus the deflection tip were derived as follows : the developed actuator was mounted in a rigid clamp equipped with an electrical contact. The sensing element for the load cell was positioned 1mm to 2mm from the end of the actuator. Also, it was placed at a desired distance from the bender's reference position so that the sample could freely deflect before coming in contact with the load cell. Following excitement from a step electric field, the actuator delivered a force signal whose peak value was recorded by the LabVIEW software. The deflection at which the actuator was unable to exert a measurable force on the load cell was considered the free deflection. Experiments was conducted under 0.1Hz frequency and four electric fields levels comprising 10 V/µm, 20 V/µm, 30V/µm, and 40V/µm.

Figure 55 displays the experimental force as a function of deflection for different input electric fields. As expected, a linear relationship was achieved, representing typical characteristics of the bender actuator. The force at zero deflection is defined as the blocking force corresponding to the maximum force that the actuator can exert upon an electric field. At the opposite of the curve, the deflection at zero force is called the free deflection (δ_0). It is then possible to express the deflection (δ) function of the curve as follows:

$$\delta = \delta_0 - F/K \quad (12)$$

where F is the applied force and K is the stiffness coefficient of the actuator.

Based on the force–deflection curve, it is possible to predict the actuator's displacement as a function of the externally applied load, which is relevant parameter for designing electroactive material applications.

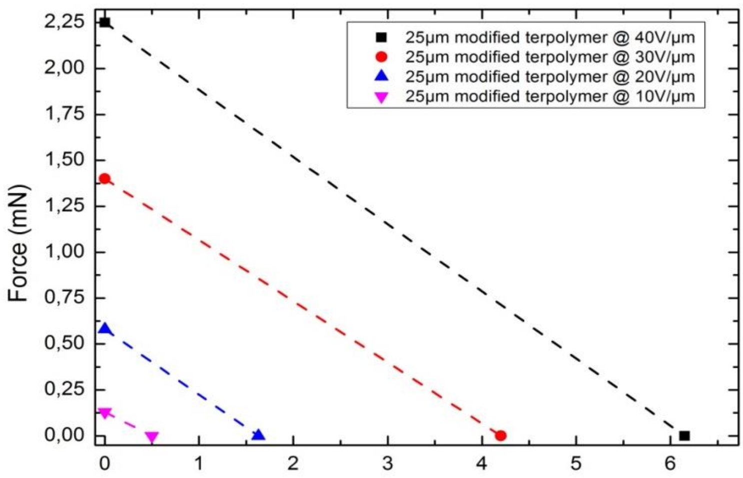

Deflection (mm)

Figure 495. Actuator force versus displacement at 0,1 Hz under different electric fields.

III.1.d.iv.Mechanical energy

The mechanical energy generated by an actuator is also a key parameter reflecting the performance of the electrostrictive polymers. Depending on the position of an object subjected to a conservative force, the mechanical energy is usually defined as the actuator's ability to carry out work. If *F* represents the conservative force and *x* the position, the mechanical energy of the force between the two positions d_1 and d_2 is defined as

$$E_{mechanic} = \int_{d_2}^{d_1} F dx = F.\delta \quad (13)$$

Figure 56 illustrates the mechanical energy generated by two kinds of terpolymer benders as a function of the applied force under a 40V/µm electric field. The result reveals an optimum point where the mechanical energy passes through a maximum, corresponding to the half of the maximum force. It is noteworthy that the mechanical energy of the all-organic plasticized polymer is six-fold that of the neat polymer. These last remarks demonstrate the advantage of using a plasticized composite, since the applied input electric field can be largely reduced to achieve similar electrostrictive properties.

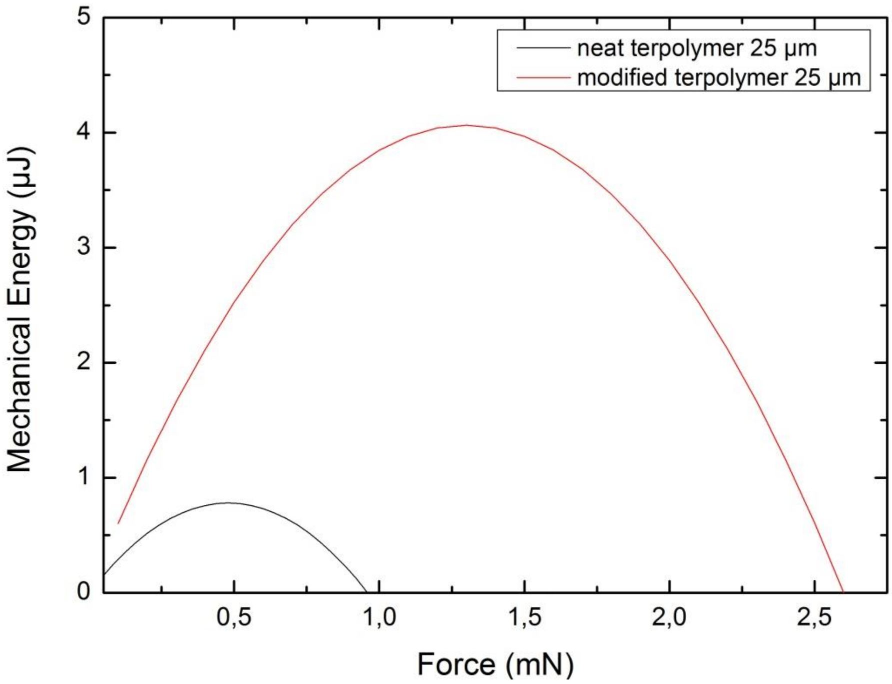

Figure 506. Mechanical energy density as a function of deflection for two compositions of terpolymer for an electric field of 40 V/µm.

The mechanical energy density can be inferred from the relationship or from the calculation of the ratio between the energy $E_{mechanic}$ and the volume. As the volume of the sample is equal to 10^{-8} m^3, the optimal energy density of the pure terpolymer and its plasticized counterpart respectively reach 70 J/m^3 and 400 J/m^3 under a relatively low electric field of 40V/µm. Again, this result demonstrates that the fact of incorporating a plasticizer into the polymer matrix enables a drastic improvement of the actuation properties as well as a reduction in the input voltage, which is currently one of the major drawbacks of electrostrictive materials.

III.1.e. Conclusions

These experiments have proposed new criteria for assessing the electroactive material performance based on the figures of merit of the force, the strain, and the energy density. These characteristic numbers are greatly affected not only by the intrinsic parameters like the permittivity and the Young's modulus of material, but also by the breakdown electric field. The proposed approach is an efficient way to select a polymer matrix with large actuation properties as well as for simplifying a comparison between different kinds of electroactive composites.

These experimental results revealed a large enhancement of the electromechanical activities in terms of free deflection and generated force under relatively low electric field by incorporating a plasticizer into the terpolymer matrix. This phenomenon confirms the high potential of the developed material for real-world actuator applications, especially in multifunctional flexible electroactive devices. However, the plasticizer used for the study is not recommended for the production of medical devices. The next part of the research actions will consist in identifying a plasticizer potentially usable for the application needs.[139,140]

Chapter 2:

Influence of plasticizers on the electromechanical behavior of the terpolymer

This chapter repeats the works published during the thesis in the paper “Influence of Plasticizers on the Electromechanical Behavior of a P(VDF-TrFE-CTFE) Terpolymer: Toward a High Performance of Electrostrictive Blends”, Journal of Polymer Part B; https://doi.org/10.1002/polb.24280, by **N. Della Schiava**, MQ Lê, J. Galineau, A. Millon, F. Domingues Dos Santos , PJ Cottinet et JF Capsal.[141]

III.2.a. Introduction

As explicated in the previous sections, among the polymers with large electromechanical response, P(VDF-TrFE-CTFE) is especially interesting because of their high dielectric permittivity response as well as their low young modulus.[142,143]

To further improve electromechanical properties of this fluorinated terpolymer, Capsal et al lately proposed a simple and efficient solution while applying a low electric field.[144,145] It was revealed that by doping the polymer with the 2-ethylhexyl phtalate plasticizer (DEHP), it was possible to decrease the Young modulus as well as increase the dielectric permittivity, simultaneously. Such a simple chemical modification makes it possible to enhance the electrostrictive strain of the terpolymer at a low electric field that is approximately 5.5 times lower than that of the conventional material. However for the application it is essential to identify a plasticizer different from DEHP, for reasons of biocompatibility.[146]
Based on previous work,[144,145] it is clear that the plasticizer is a key element that strongly affects the electrostrictive behavior of the fluorinated terpolymer. As a result, this chapter consists in providing a complete study on the plasticizer effect by exploiting three types of chemical agents, i.e., DEHP, DINP (diisononyl phthalate, low molecular weight plasticizer), and Palamoll 652 (a polyester based on adipic acid, a polymer plasticizer). This study will thus complement previous work where only DEHP has been explored. Another aspect of this paper involves analyzing the influence of the plasticizer content on the P(VDF-TrFE-CTFE) blends. A comparison of different plasticizers as well as their influence on the electromechanical response was studied in the first section. Next, the effect of the DINP content of the proposed materials, followed by an application in morphing structure was studied.

III.2.b.Comparison of different plasticizers

IIII.2.b.i.Plasticizers selection

The polymer processing was previously described (chapter 1.c.i). Films were made by solution casting. Terpolymer was dissolved in the solvent at 80°C and stirred for 1h to ensure complete dissolution. Then the solution was cooled at room temperature for 2h and in a second step, a plasticizer was added and solutions were kept at 4°C before other steps.

Three plasticizers were evaluated. Two phtalates (DEHP and DINP), and Palamoll 652 were incorporated in the polymer matrix with a weigh fraction of around 15%. The ratio of the plasticizer (i.e., 15%) was chosen so as to fulfill the trade-off between electrostrictive performance and chemical property change. A comparison was performed between the pure polymer sample (namely Terpo-pur), and the three modified ones (namely Terpo-DEHP15, Terpo-DINP15, Terpo-PALA15) corresponding to three terpolymer blends plasticized (with DEHP, DINP, and Palamoll) as indicated in Table 7. DINP and Palamoll 652 have been selected due to their biocompability in medical device.[147-150]

Note that the neat material was provided by Piezotech – Arkema group, whereas the incorporation of the plasticizers into the relaxor polymer matrix was performed in the LGEF laboratory.

III.2.b.ii.DSC characterization

Sample name	Melting peak temperature (°C)	Melting peak Onset (°C)	Half width of the melting peak (°C)	Melting peak enthalpy (J/g)
Terpo-pur	119.0	109.1	9	12.05
Terpo-DEHP15	113.3	103.1	11	12.76
Terpo-DINP15	116.2	105.8	10	12.7
Terpo-PALA15	117.2	104	16	6.76

Table 7. DSC characterizations of a terpolymer with different types of plasticizers

Table 7 summarizes the melting peak temperature, the melting peak onset, the half width of the melting peak, and the melting enthalpy of the pure and the modified terpolymers. Such data were inferred from the DSC measurement.

Based on these results, it is revealed that the DEHP, DINP, and Palamoll plasticizing agent makes it possible to slightly reduce the melting temperature of the crystallites, i.e., from 119° (neat material) to 113°, 116°, and 117°, respectively. Concerning the melting peak enthalpy, it was somewhat increased in case of the DEHP and DINP plasticizers; contrary to Palamoll where the crystallinity dramatically declined to 6.76 J/g, giving rise to a drop of nearly 50%. A similar effect was found for the half width of the melting peak. Indeed, the DEHP and DINP plasticizers gave rise to a moderate increase of around 1–2°C whereas Palamoll led to a significant increase of 7°, i.e., from 9° to 16°. Thus, it was confirmed that Palamoll greatly affected the crystalline phase of the composite and as a result, prevented the crystallization during the annealing process. On the other hand, an increase of the chain mobility in the others plasticizers, i.e., DEHP and DINP, tended to facilitate the crystallization of the terpolymers during this process.

In order to compare the theoretical and experimental melting temperature of the modified blend, the Gordon-Taylor formula (Eq. (1)) was used:[145]

$$\frac{1}{Tg} = \frac{\omega_{polymer}}{Tg_{polymère}} + \frac{\omega_{plasticizer}}{Tg_{plasticizer}} \quad (1)$$

where Tg is the glass transition of the plasticized polymer, ω_{polymer} is the weight fraction of amorphous phase of the polymer, and $\omega_{\text{plasticizer}}$ is the weight fraction of plasticizer within the amorphous phase of the polymer, Tg_{polymer} and $Tg_{\text{plasticizer}}$ are respectively the vitreous transition of the polymer and the plasticizer.

It should be noted that only the phtalate-modified films were chosen as they do not affect the crystalline phase. From the Gordon-Taylor expression, a decrease of the melting temperature was estimated to be equal to 6°C for the DEHP-modified terpolymer and 4°C for the DINP-modified one. These theoretical values are in good agreement with those experimentally measured by the DSC, indicating good miscibility of the phtalate plasticizer within the CTFE-based polymers. As a consequence, it is demonstrated that the chemical modification of the material via DEHP and DINP did not drastically change its chemical and structural properties.[144]

III.2.b.iii.Electrical characterization

Electrical behavior of the neat and modified fluorinated terpolymer have been characterized through the measurement of the dielectric permittivity versus a whole frequency range of [10^{-1} Hz, 10^6 Hz] at a relatively low applied voltage of 1Vrms using a Solartron SI 1296. Figure 57 shows the relative dielectric permittivity of 80µm-thick samples incorporating different plasticizers. The relative dielectric permittivity was found to drastically decrease as a function of the frequency. Compared to the neat polymer, the plasticized samples showed a greatly enhanced dielectric behavior under low frequency but to different extents. As observed, the resulting response of the DEHP and DINP respectively equaled 1200 and 1900 at 0.1 Hz. On the other hand, a much more modest improvement was seen in the case of Palamoll 652, where a dielectric response of 200 was found at a similar frequency.

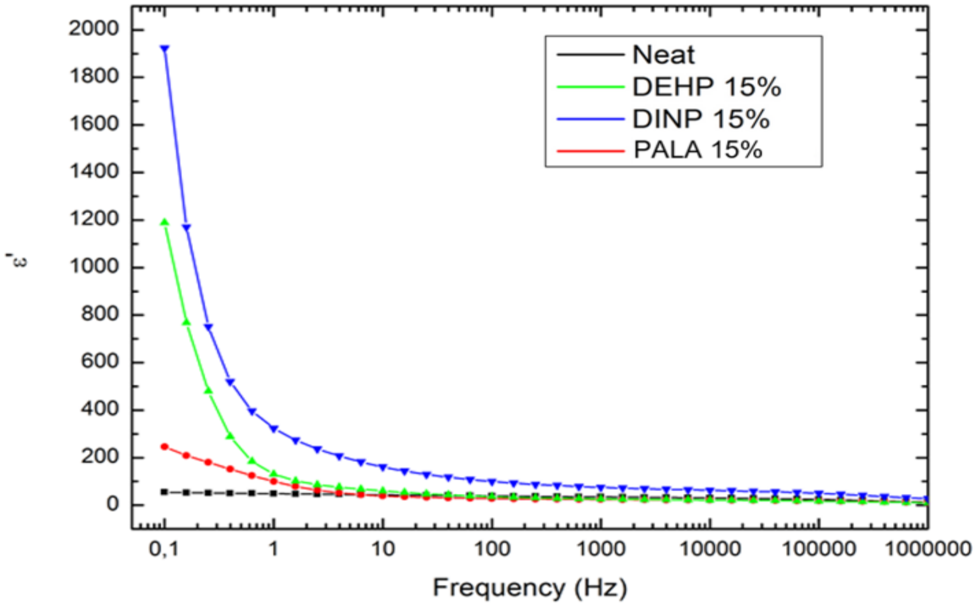

Figure 57. Relative permittivity of a terpolymer with different types of plasticizers.

Based on the above results, it is clear that the terpolymer plasticized with DINP could be considered as the best choice for improving the dielectric response, especially at low frequency. This was probably due to the fact that a greater interaction of the polymers with the DINP plasticizer led to higher polymer chain mobility. Therefore, the Maxwell–Wagner–Sillars (MWS) polarization and the interfacial phenomenon increased, resulting in an enhanced dielectric permittivity.[145]

III.2.b.iv.Mechanical characterization

The mechanical properties of the modified terpolymer blend were assessed based on the evolution of stress versus strain, as illustrated in Figure 58. As expected, the Young modulus of all plasticized terpolymer significantly decreased with respected to the neat one.

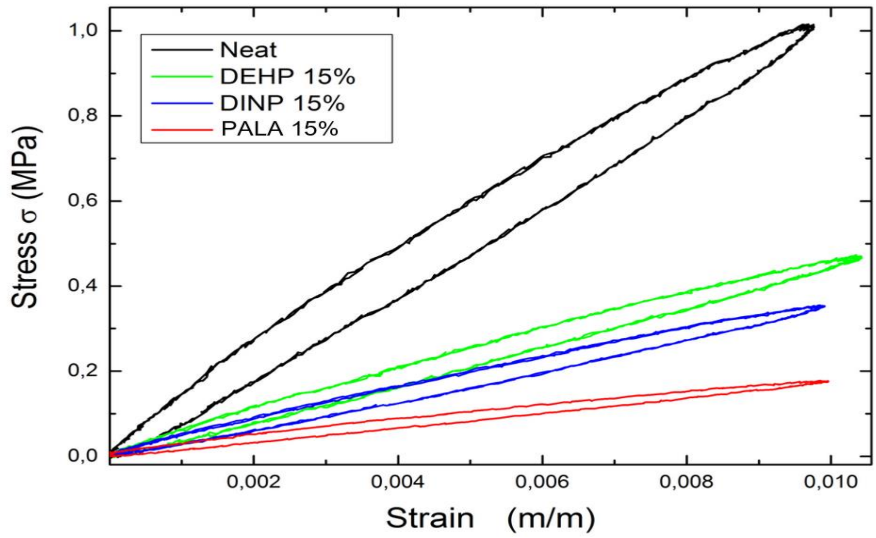

Figure 518. Effect of the plasticizer type on the Young modulus of different terpolymer samples.

It appears that the Palamoll plasticizer gave rise to a much lower Young modulus than its phtalate counterparts, which was consistent with the important decrease of its crystallinity as determined by the previous DSC analysis. Compared to the pure sample whose Young modulus equaled 103 MPa, the Young modulus in the modified samples drastically dropped to 17 MPa, 35 MPa, and 45 MPa, corresponding respectively to the case of Palamoll, DINP, and DEHP.

It is interesting to note that for the phtalate-modified polymers, the evolution of the Young modulus with the plasticizer did not match the change in melting temperature. Actually, since the melting temperature of DEHP was lower than the one of DINP, the plasticizing effect should be more efficient and the Young modulus, as a result, should be superior for DINP as opposed to DEHP. To explain this effect, it seems easier to exploit the dielectric data. The result makes it possible to conclude that the dielectric response and the interfacial phenomena-MWS at low frequency were more apparent in the DINP sample than in the DEHP one. Moreover, under high frequency range, it was believed that the dipolar DINP interacted more actively with the CTFE- terpolymer matrix, involving higher molecular chain mobility, and thus a greater plasticizing effect.

According to the mechanical and electrical characterizations and from the values of permittivity and Young modulus, it was therefore expected that DINP would exhibit a superior mechanical strain to DEHP and Palamoll 652.

III.2.b.v.Electromechanical characterization

The influence of different plasticizers on the electrostrictive response of the developed blend at low frequency (i.e., 0.1 Hz) was characterized through transverse strain S_{31} under an electric field and experimental data were achieved as illustrated in Figure 59.

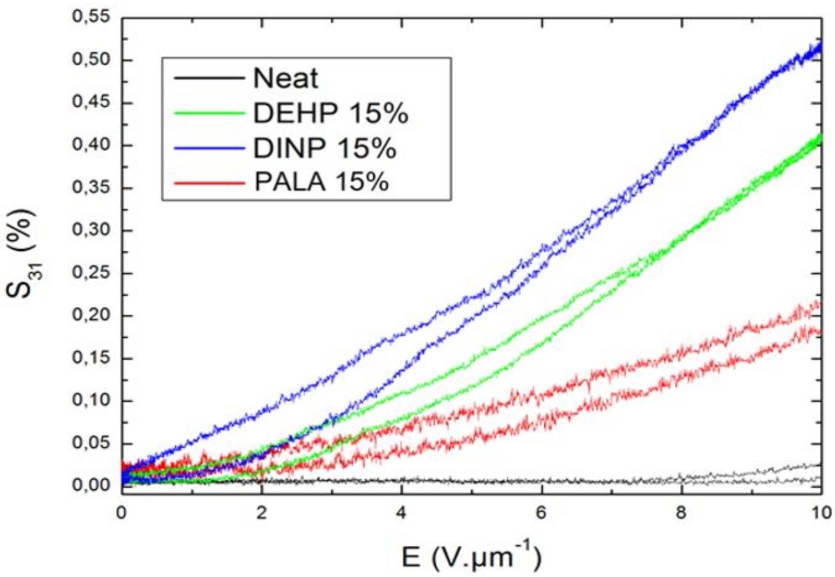

Figure 529. Transverse strain S_{31} versus electrical field applied to terpolymer samples.

It has been previously shown that in the case of dielectric polymers, the electrostrictive strain under an electric field can be mainly attributed to Maxwell forces induced by dipolar orientation within the material.[145] In the thickness direction, the transvers strain S_{31} under the electric field E is given by

$$S_{31} = M_{31}.E^2 \quad (2)$$

where M_{31} is the electrostrictive coefficient that can be expressed as

$$M_{ij} \propto \frac{\varepsilon_0.\varepsilon_r}{Y} \quad (3)$$

where ε_r, ε_0, and Y respectively depicted the relative permittivity of the polymer, permittivity of vacuum, and the Young modulus of the polymer.

According to Eqs. (2)–(3), in order to enhance the resulting strain without increasing the electric field, one can either increase the permittivity, decrease the Young modulus or both. As illustrated in Figure 59, the transvers strain S_{31} of the neat terpolymer was extremely low and difficult to empirically achieve, particularly under an electric field below 10V.µm^{-1}. At such an excited input, the plasticized films, on the other hand, made it possible to considerably enhance the influence of the defect in the polymer chains, leading to a significantly increased strain by a factor of 8, 16 and 20 for Palamoll 652, DEHP and DINP, respectively. Accordingly, the DINP plasticizer gave the best electromechanical response, which was expected from its highest dielectric permittivity compared to the other plasticizers.

Nevertheless, the electrostrictive strain response of the polymer was not the only key issue that needed to be studied. Another alternative parameter permitting to assess the actuation performance of the electroactive material was the transverse mechanical energy density W_{m31} given by the following expression:

$$W_{m31} = \frac{1}{2} Y.S_{31}^2 \quad (4)$$

Combining Equations (2)–(4) yields:

$$W_{m31} = \frac{1}{2} \frac{\left(\varepsilon_0 .\varepsilon_r\right)^2}{Y} E^4 \quad (5)$$

For practical applications in electroactive devices, the strain response and the mechanical energy density under a low electric field must be simultaneously enhanced through the proposed plasticizer modification. It has been previously demonstrated that significant electrostrictive strains (few percent) can be achieved by reducing the Young modulus and/or increasing the dielectric permittivity of the polymer. The fact of the decreased Young modulus may, however, deteriorate the mechanical energy density (Eq. (5)), especially for low frequency actuator applications. In order to enhance the energy density, the increase in strain must thus be more significant than the decrease in the elasticity modulus of the material.[145] The mechanical energy density of the neat and modified CTFE-based terpolymers was calculated from (Eq. (4)) and plotted in Figure 60, under low electric field of 10V/µm. It is interesting to note that an excellent improvement of both strain and mechanical energy density was obtained for the modified films. For instance, the Palamoll-based terpolymer offered a 10-fold increase in mechanical energy density as well as an 8-fold increase in transverse strain as compared to those of the pure polymer. Moreover, the phtalate-based terpolymers, especially the DINP blend, achieved the best responses with an almost 170-fold increase in mechanical energy density and an almost 20-fold increase in transverse strain as compared to their neat counterpart. Such a remarkable enhancement certainly came from the considerable increase in dielectric permittivity as described previously.

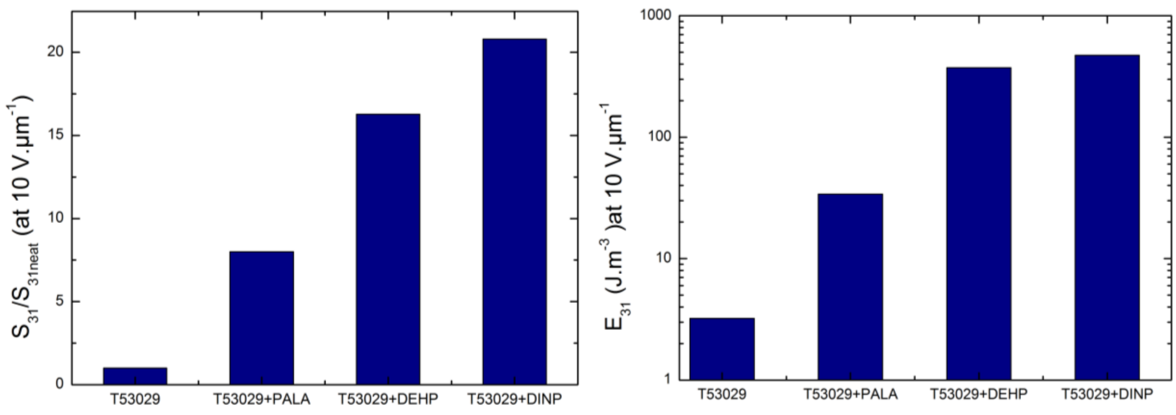

Figure 60. Normalized strain S_{31} for a terpolymer under 10V/µm (left) and the corresponding mechanical energy density (right).

The above results confirm that the DINP-plasticized material offered further advantages in terms of strain and mechanical energy density under a small electric field. Hence, the next section aims at providing a detailed study of the effect of the DINP content on the electrostrictive performance of the plasticized terpolymers.

III.2.c.Influence of the DINP plasticizer content

In order to evaluate the influence of the DINP agent on the actuation performances of the composite, several modified composites with different weight fractions of plasticizer were employed. The various DINP compositions used in this study were equal [2%, 4%, 6%, 8%, 10%, 12%, 14%, 16%]. A DINP weight ratio above 16% was not of interest due to the large seepage of plasticizer when incorporated in high quantity in the polymer matrix.

Similar to the procedure described previously, the next parts focus on analyzing the thermodynamical, mechanical, electrical, and electromechnical properties of this new material based on different DINP contents.

III.2.c.i.DSC measurements

Table 8 summarizes the thermodynamic behavior of the proposed blend based on the melting peak temperature, melting peak onset, half width of the melting peak, and melting enthalpy that were directly inferred from the DCS characterizations. It is noteworthy that all samples were recrystallized at the onset of the endothermic fusion peaks.

Sample name	Plasticizer content (%)	Melting peak temperature (°C)	Melting peak Onset (°C)	Half width of the melting peak (°C)	Melting peak enthalpy (J/g)
Terpo-pur	0	120	109.1	9	12.1
Terpo-DINP2	2	119.7	106.9	10	11.2
Terpo-DINP4	4	119.6	107	11	11.1
Terpo-DINP6	6	118.8	105.7	12	12.1
Terpo-DINP8	8	117	104.5	12	12.7
Terpo-DINP10	10	115.6	104.8	12	12.9
Terpo-DINP12	12	118.2	106.5	11	13.1
Terpo-DINP14	14	116.1	105.0	11	13.3
Terpo-DINP16	16	115.9	105.0	12	13.5

Table 8. DSC characterizations of a terpolymer with different weight fractions of DINP

As shown in Figure 61, the melting peak temperature progressively decreased as a function of the DINP content, which is coherent with a diminution of the crystallinity when introducing the defects into the polymer chains. The melting temperature dropped somewhat from 120°C for the neat sample to 116°C for the sample with 16% DINP.

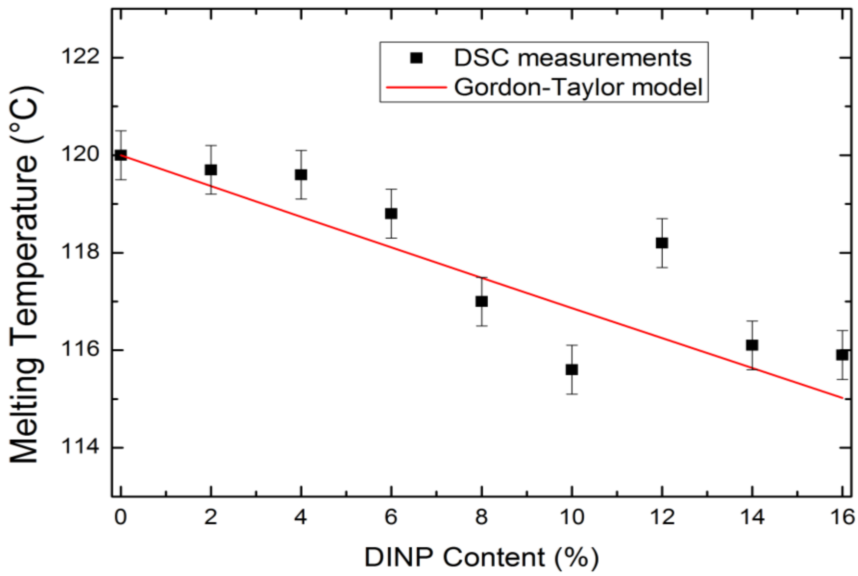

Figure 61. Experimental and theoretical melting peak temperature of a terpolymer as a function of the DINP content.

Based on the assumption that the melting transition temperature is affected in the same proportion of the vitreous transition temperature, it is possible to use the Gordon-Taylor formula of Eq. (1) to predict the effect of a miscible plasticizer on the melting temperature of a polymer matrix. As expected, in Figure 61, the quasi-linear decrease of the melting temperature with the DINP content was in good agreement with theory based on the Gordon Taylor equation. Thus, it seems that regardless of the DINP fraction ($\leq$ 16%), the plasticizer was miscible with the CTFE terpolymer chains.

Figure 62 (left) displays the melting enthalpy versus DINP content, which is a direct reflection of the polymer crystallinity. At the first DINP weight fractions (*i.e.*, 2% and 4 %), the crystallinity declined and then rapidly increased at 4% and 8%. Such an increase continued after 8% but in a more moderate linear way. It can be assumed that once the polymers had reached a certain plasticization (*i.e.*, around 6% to 8%), the chains could move more freely and could therefore crystallize more easily.

A homogeneity of the size of the crystallites can be deduced from the half peak width of the melting peak as displayed in Figure 62 (right). The half peak width slightly increased until a 6% DINP content before reaching a steady state. As a result, regardless of the plasticizer weight fraction, the homogeneity of the crystallites was not disrupted.

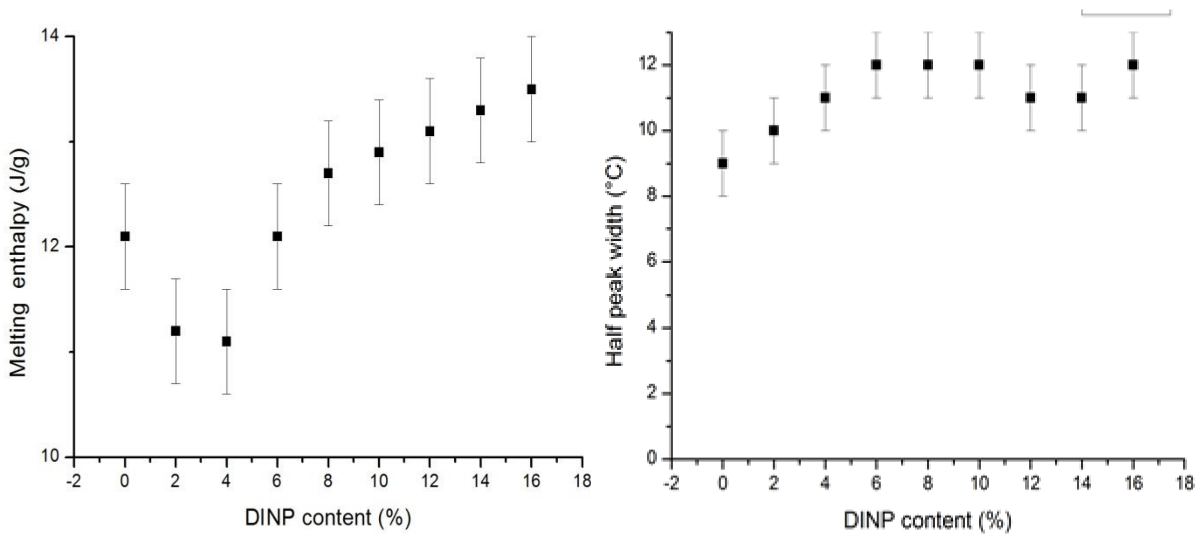

Figure 62. Melting peak enthalpy (left) and half width of the melting peak (right) of s terpolymer as a function of the DINP content.

III.2.c.ii.Mechanical behavior

The influence of the DINP plasticizer on the Young modulus is depicted in Figure 63. As observed, the experimental Young modulus considerably decreased when increasing the DINP quantity: the value went from 103 MPa for the pure material to 55 MPa by only injecting 2% DINP; in other words the value was practically cut in half. Such a huge decrease in the Young modulus was believed to mainly stem from the molecular mobility increase of the polymer chain.

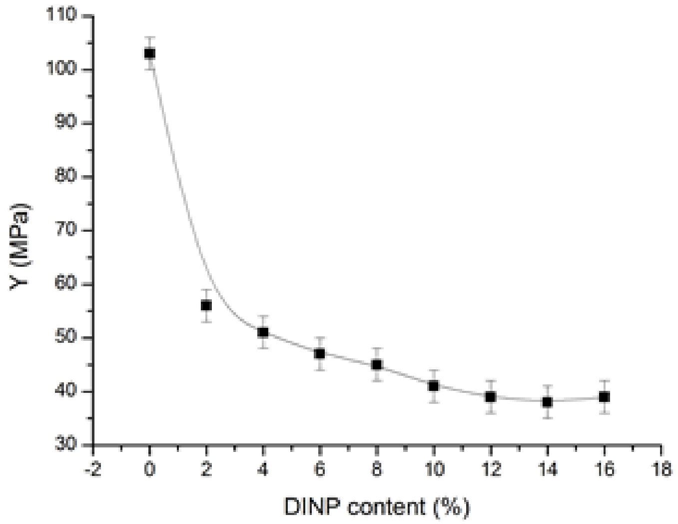

Figure 533. Young modulus of a terpolymer as a function of the DINP content.

Above 2% DINP content, a slight decrease of the Young modulus versus the plasticizer content was recorded, before reaching a plateau of 39 MPa for a DINP fraction greater than 10%. The saturation of the Young modulus when augmenting the plasticizer quantity was the result of two opposed effects. The first effect is related to an enhancement in molecular mobility particularly with more than 4% of DINP, leading to decrease Young modulus of the fluorinated polymer. On the contrary, the second effect is due to an increase of the melting enthalpy as a function of the plasticizer ratio (> 4%wt) obtained from the DSC analysis (Figure 62). Such a phenomenon tends to improve the crystallinity phase of the polymer matrix and as a result, making the Young modulus increase. Accordingly, these two effects compete with each other and lead to a saturation of the Young modulus for a DINP content above 10%.

III.2.c.iii.Electrical behavior

In order to assess the electrical behavior of the proposed electrostrictive polymer, experimental measures of the dielectric permittivity in terms of frequency were performed. As depicted in Figure 64 (left), the dielectric trend of the developed material differed significantly depending on whether the bandwidth range was low or high.

For instance, at a low frequency of 0.1 Hz, the permittivity increased exponentially as a function of the DINP weigh fraction, based on the result of Figure 64 (right). Indeed, the dielectric permittivity was 8-fold higher for the 16%DINP sample as compared to the 2%DINP terpolymer. From seepage observations and permittivity measurements, it was found that a large increase of permittivity occurred when excess plasticizer was present within the material. At high frequency, e.g. at 10kHz before the dielectric relaxation associated with the glass transition, the dielectric permittivity decreased until a DINP content of 8% and then became saturated.

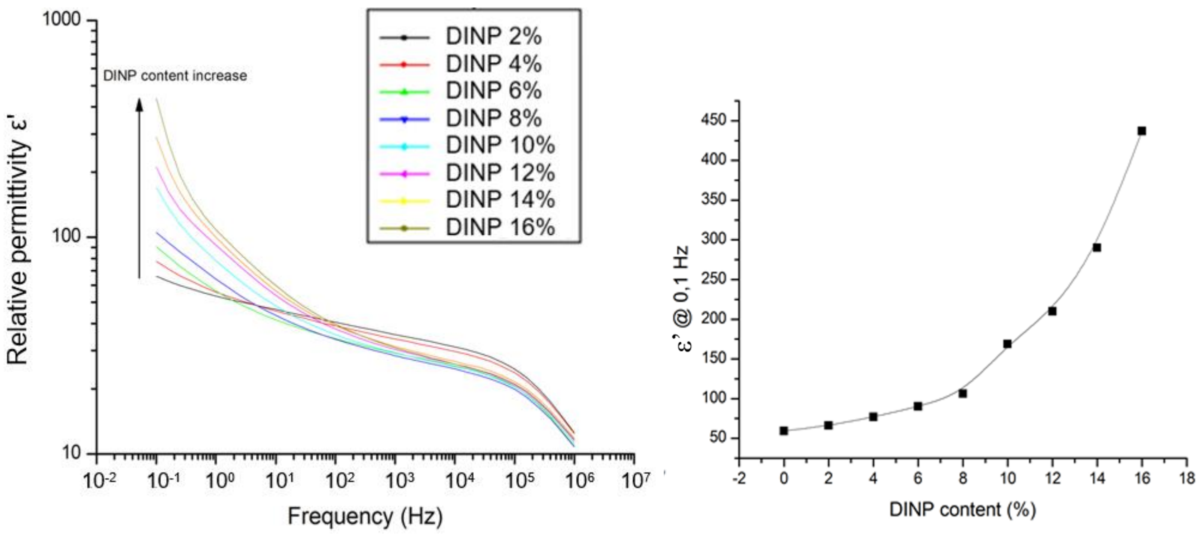

Figure 544. Relative permittivity of a terpolymer with varying DINP contents : versus frequency (left) and at 0,1 Hz (right).

This fact was caused by two opposite phenomena comprising a reduction of the number of dipoles and an increase in crystalline phase. Indeed, above 8%wt plasticizer, the ratio of dipole number in the polymer matrix decreases as the DINP content increases, leading to decrease dielectric permittivity. On the other hand, due to an increase in melting enthalpy versus the DINP content (Figure 62), the crystallinity effect improves, making an increase of the dielectric permittivity. These two effects tended to mutually compensate each other, resulting in saturated dielectric behaviors under high frequency ranges.

With the aim of evaluating the influence of the DINP content on the dielectric relaxation of the dipolar entities of the polymer matrix, the tanδ formalism (Eq. (6)) of the dielectric measurements was used:

$$\tan\delta = \frac{\varepsilon''}{\varepsilon'} \quad (6)$$

Here, ε'' and ε' are respectively the imaginary part and real part of the dielectric permittivity. The ionic conduction of polymers above their glass transition temperature makes it possible to increase the measured dielectric losses, according to the following expression:

$$\varepsilon'' = \varepsilon_{dipol} + \varepsilon_{conductivity} \quad (7)$$

Since the response is a summation of the dipolar relaxation losses as well as the ionic conductivity, it is difficult to extract the frequency dependence of dielectric relaxations in semi-crystalline polymers from the direct measurements. Since the ionic conductivity does not affect the real part of the dielectric permittivity at very low frequency, an easy way to discard this parameter is to use the mathematical Kramer-Kronig transform [151] presented in Eq. (8):

$$\varepsilon'' = -\frac{\pi}{2}\frac{d\varepsilon'}{d\ln(2\pi f)} \quad (8)$$

where f is the excited frequency.

Figure 65 illustrates the dielectric losses of a 16%DINP-based terpolymer measured by experiment, and calculated from the real part of the dielectric permittivity based on Eq. (8). For the direct measurements, two relaxations are clearly distinguishable. The high-frequency relaxation, considered to be a dipolar relaxation, describes the dielectric manifestation of the glass transition of a constrained amorphous phase with less molecular mobility affecting the ferroelectric relaxor of the fluorinated terpolymer. The low-frequency relaxation, on the other hand, corresponds to the ionic conduction, and the interfacial phenomena (MWS) originating from the charges trapped in the heterogeneities of the semi-crystalline polymer.

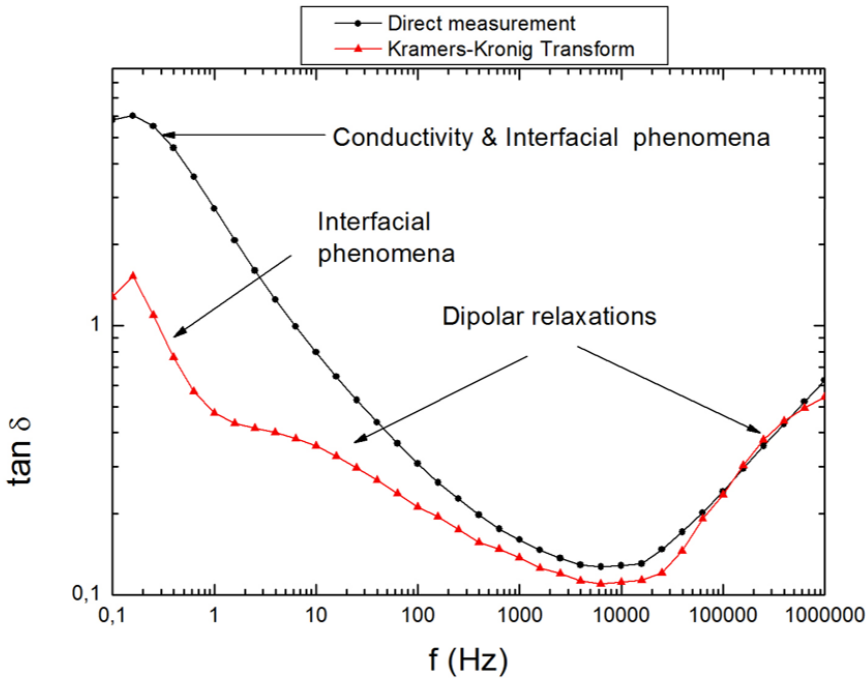

Figure 555. Dielectric losses versus frequency of a terpolymer with 16% DINP: experimental measurements (black) and calculated from the real part of the dielectric permittivity (red).

It can be seen in Figure 65 that the experimental and theoretical dielectric losses were quite different at low bandwidth whereas they remained almost the same at high frequencies. This can be explained by a simplification of the Kramer-Kronig model where only an interfacial phenomenon is involved at relatively low frequencies, contrary to the real measure comprising both conductivity ionic and interfacial effect. A significant variation between the theoretical and experimental responses, particularly at a low bandwidth, leads to the conclusion that the ionic conductivity was not negligible in the developed material. Such a variation was substantial up to 10Hz, and was then progressively reduced until the two curves approached each other at higher frequencies. In this case, a gradual suppression of the ionic conductivity occurred, leading to a place of dipolar relaxation. Consequently, it was demonstrated that the Kramer-Kronig transform is a powerful tool for studying molecular dynamics in plasticizer-based materials.

Figure 66 presents the dielectric losses estimated from the Kramer-Kronig transform [151] for various DINP weight fraction. As expected, the resulting responses of different samples were very similar at high frequency (i.e., α mode). Indeed, the dipolar relaxation did not depend on the plasticizer quantity, inversely to the interfacial phenomenon that occurred at low frequency (i.e., α’ mode).

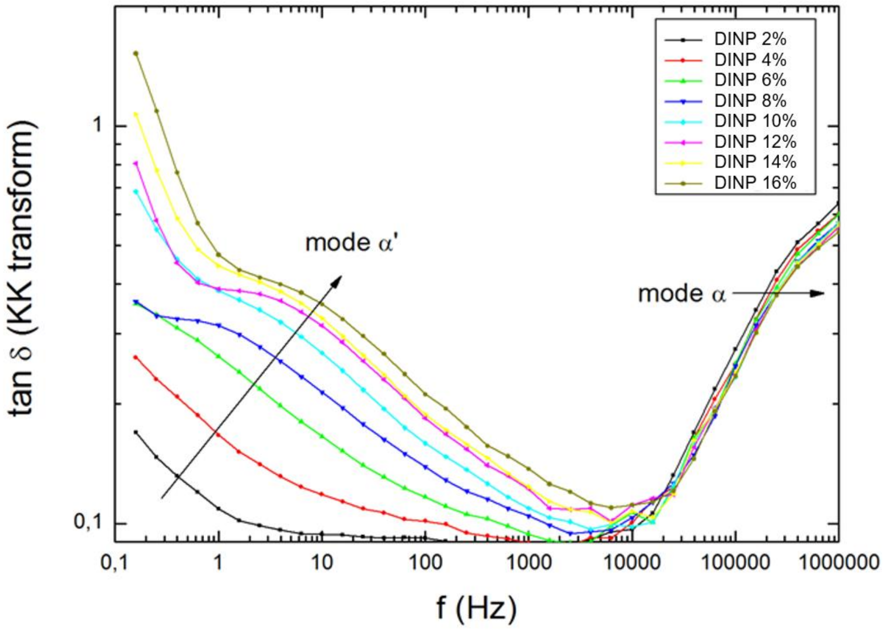

Figure 566. Dielectric losses calculated from the Kramer-Kronig transform of a terpolymer with varying DINP contents.

In reality, the α' mode relates to the constrained amorphous phase greatly affected by the plasticizer content, as a large increase was found between the 2%DINP sample and its 16% counterpart. As reported previously, the plasticizer tends to improve the molecular mobility of the dipolar entities. For the pure sample or with a low content of DINP, the molecular mobility within the constrained amorphous phase remained too slow to enable the charges to migrate within the phase. This was contrary to blends with a high content of DINP, whose charges were able to migrate freely, resulting in enhanced molecular mobility and easier movement of free carriers within the polymer matrix. As the MWS relaxation is related to the charges trapped at the boundaries between the amorphous and crystalline phases, a change in the molecular mobility can be considered to disturb the MWS polarization. Indeed, when the charges tend to accumulate at the interfaces, they lead to a significant MWS effect. Such a phenomenon is strongly dependent on the dielectric permittivity gradient and the conductivities between the two phases that are governed by the DINP content injected in the polymer chains.

III.2.c.iv.Current versus electric field

Figure 67 displays the current versus the electric field at 0.1 Hz for several composites with different plasticizer ratios. For low DINP contents, the current had a capacitive behavior with low losses and the Ohmic conductivity could be derived from the slope of *I*(*E*) data. The losses went up with an increase in DINP content up to the 12%DINP sample. Above this plasticizer weight fraction, the losses seemed to decrease. This behavior was in agreement with the low frequency dielectric losses obtained from the direct measurements where tan(δ) values followed the same behavior.

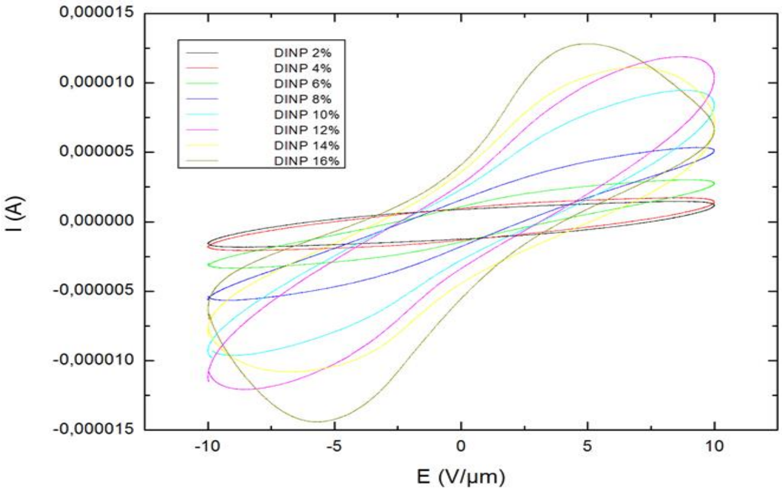

Figure 577. Experimental current versus electric field at 0,1 Hz.

The dielectric displacement (*D*) excited at a 0.1 Hz frequency and a 10V/µm electric field was computed from the *I*(*E*) curves after subtraction of the linear model of the Ohmic conduction (Figure 68). It was found that *D* increased slightly up to 8% DINP. This tendency became more obvious and reached 37mC/m² in the case of 16% DINP. The evolution of *D*with respect to the DINP fraction was good match to the influence of the plasticizer quantity on the dielectric permittivity.

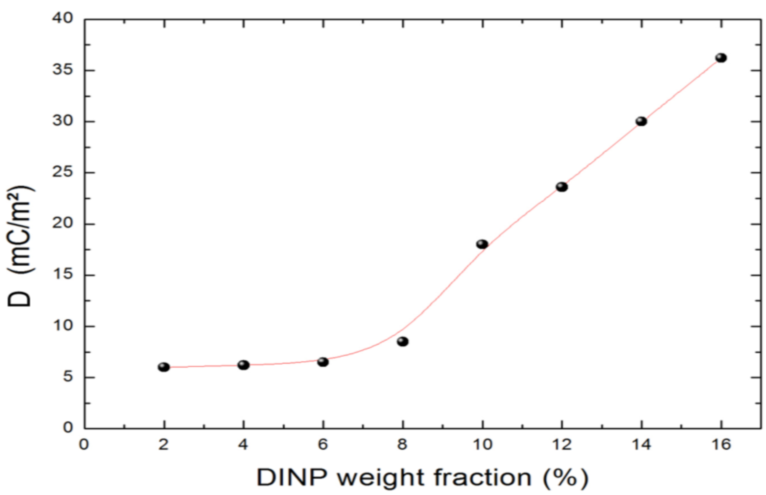

Figure 588. Dielectric displacement calculated at 10V/µm versus the DINP weight fraction.

At high DINP contents, the behavior of the *I*(*E*) curves looked like the current of a ferroelectric material. Nonetheless, it should be kept in mind that in this work, we only used a linear model to illustrate the Ohmic conduction of the plasticized terpolymers. A study of the nonlinear conductive behavior in plasticized ferroelectric relaxor blends needs to be studied more deeply since it governs the MWS polarization and thus the electromechanical response of the polymer.

III.2.c.v.Electromechanical conversion

An evaluation of the experimental transverse strains as a function of the electric field was performed and the results are presented in Figure 69 (left). It is noteworthy that all the data are given at a low electric field of 10 V/µm so that no cantilever tip displacements exceed 3 mm. They are thus within the linear range. As shown in Figure 69 (left), an increase of the electrostrictive response of the polymers versus the DINP content was achieved, but the intensity was not the same. Actually, from 2% to 8% DINP, a slight augmentation of the mechanical strain S31 was expected, which was caused by the moderate decrease in the Young modulus demonstrated in the above section. Beyond 8%, a larger increase of the electromechanical response was obtained, principally due to a large increase of the permittivity, as the Young modulus was relatively stable in this configuration. It is also noteworthy that a significant increase in permittivity occurred when seepage of the plasticizer occurred in the films.

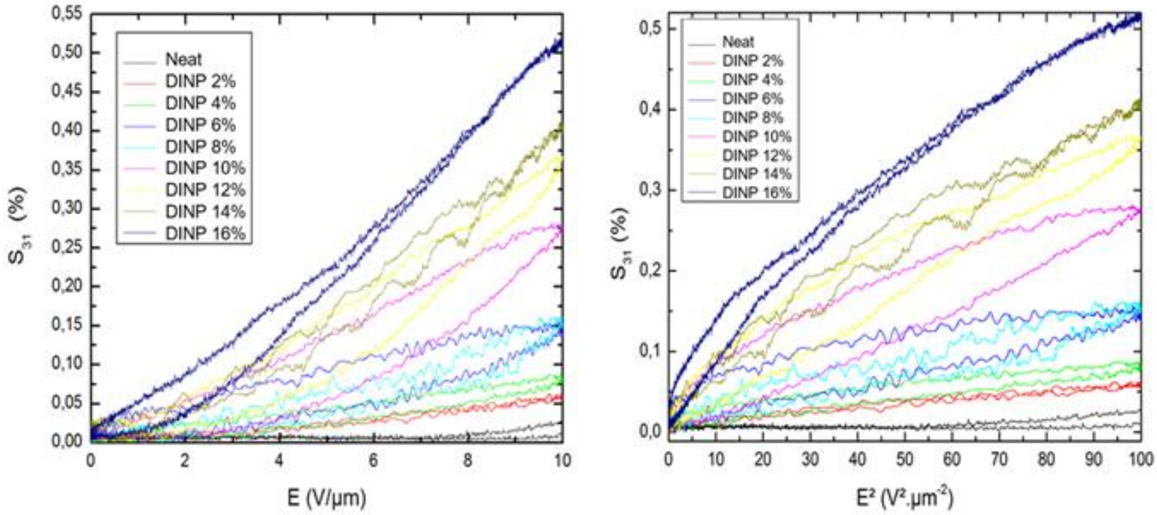

Figure 599. Transverse strain of DINP-based terpolymers versus electric field (left), and versus the square of the electric field (right).

The area of each curve in Figure 69 is an image of the losses, including both electrical and mechanical losses. It can be seen that the losses increased as the DINP content was raised up to 10-12% and then decreased with higher plasticizer concentrations. Such an effect is consistent with the evolution of the dielectric losses associated with ionic conductivity found in the dielectric and electrical measurements. At a frequency of 0.1Hz, it seemed that the electromechanical losses were mainly affected by the electrical losses.

Transverse strains as a function of the square of the electric field are displayed in order to verify the quadratic dependence as well as a constant dielectric permittivity. As depicted in Figure 69 (right), up to 4% plasticizer, the evolution of the transverse strain S31 was linear to the electric field square, reflecting a quadratic dependence of the electrostrictive strain on the electric field whose value did not exceed 10V.µm-1. Hence, excited under such an input electric field range, the terpolymers with less than 4% DINP showed an almost constant dielectric permittivity. When the plasticizer content exceeded 4%, the non-quadratic behavior of the electrostrictive strain became more pronounced. This behavior reveals that a low electric field saturation of the dipolar entities involved in the MWS process can lead to a decrease of the dielectric permittivity.

The electrostrictive strain measured at an applied electric field of 10V.µm^{-1} has been plotted in Figure 70 as a function of the DINP content. These values were then compared to the theoretically predicted strain calculated from the dielectric permittivity or the dielectric displacement. In spite of several differences, both models give a good description of the evolution of S_{31} as the DINP content is increased. However, the model from the dielectric displacement appeared more accurate than the other, especially at high DINP contents.

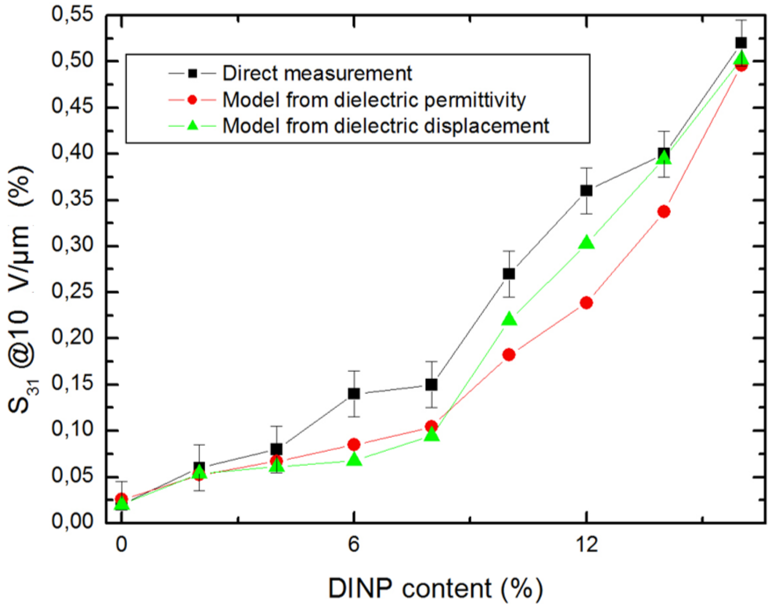

Figure 70. Transverse strain at 10V/µm as a function of the DINP content from direct measurements and from models.

It is demonstrated in Figure 71 that the mechanical energy density increased exponentially with the DINP content, according to the physical and the electromechanical properties of the modified material. Moreover, it is interesting to note that for the terpolymer with 6% DINP, no seepage of plasticizer was observed. Furthermore, the strain was enhanced 6-fold and the mechanical energy density was increased by one decade. As a result, it can be conclude that even at low DINP content, the modification of the polymer chains caused by the plasticizer was highly effective.

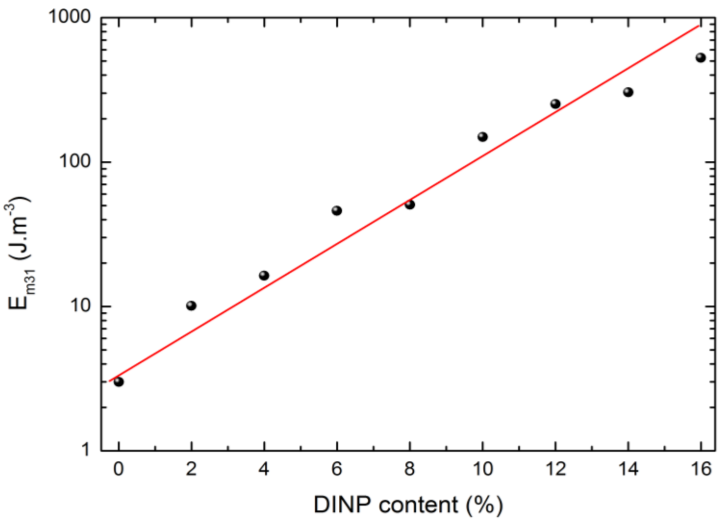

Figure 71. Mechanical energy density at 10V/µm as a function of the DINP content.

Such an improvement in the electrostrictive performance of these DINP-modified polymers can also be expressed in terms of electromechanical coupling using the coupling coefficient k_{31} of the proposed material, defined as the square root of the mechanical energy over the total energy (without losses) :

$$k_{31} = \sqrt{\frac{E_m}{E_m + E_s}} = \sqrt{\frac{YS_{31}^{\ 2}}{YS_{31}^{\ 2} + \varepsilon_{33}E^2}} \tag{9}$$

Here, S_{31}, Y and ε_{33} are the transverse strain, the Young modulus, and the dielectric permittivity, respectively. As shown in Figure 72, linear increase behavior between the coupling factor k and the DINP content was observed. It was found that the 16% DINP sample made it possible to achieve more than 5.5% under a 10 V.µm^{-1} electric field, which is 5 times greater than for the neat material. This confirms an excellent electromechanical property of our proposed novel polymer, merely by employing a simple and cheap approach.

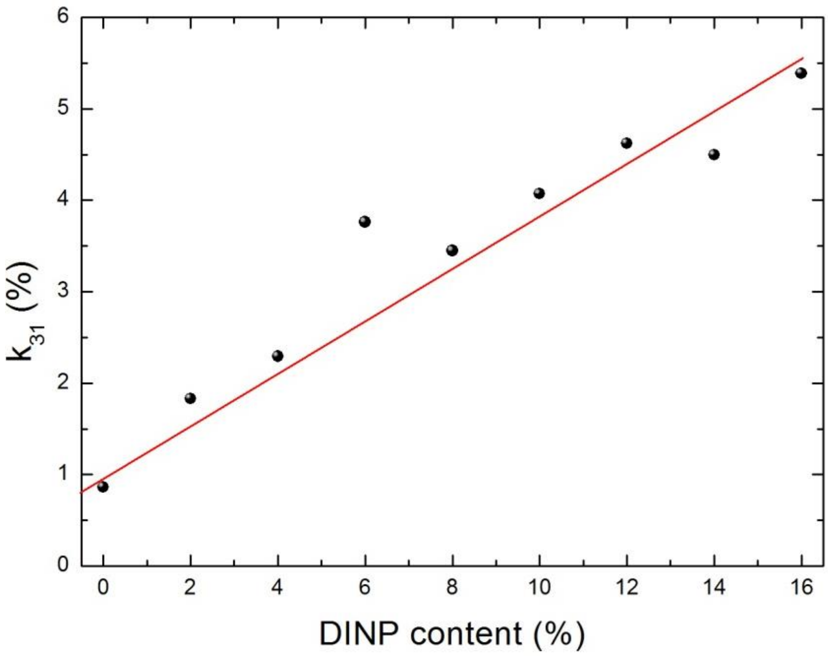

Figure 72. Coupling coefficient k at 10V/µm as a function of the DINP content from direct measurements (dotted line) and from linear modeling (solid line).

III.2.d. Applications to the morphing structure

To better evaluate the potential of the proposed approach, an application as morphing structure for the developed actuator is performed. As it has been known, morphing can provide a means of overcoming the geometric constraints of structures. Hard components have usually been employed to create morphing structures in previous works.[152] Their body parts are normally constructed of hard or high-stiffness materials, while a motor combined with a pneumatic or hydraulic actuator is used to improve flexibility.[153] However, only morphing structures with very limited magnitudes of deformation can be achieved with this method.

To implement soft morphing or large structural deformations, the body material and actuator must be soft or have a low stiffness.[154,155] By embedding the actuators in the morphing structure, the overall structure can be made very simple and lightweight. Based on this idea, we performed in this part the developed novel electrostrictive polymer. The concept of the proposed structure was illustrated in Figure 73, containing a sandwich of polyethylene substrate where the organic composite is glued using double tape adhesive.

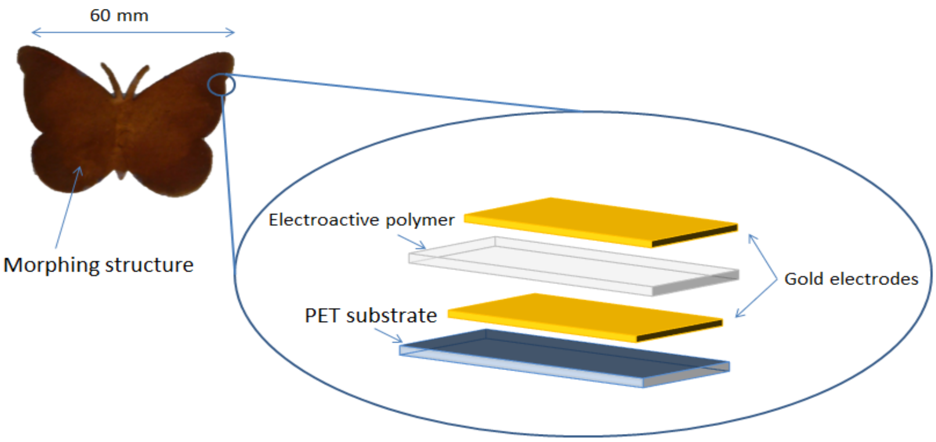

Figure 73. Concept of morphing structure using electroactive polymer.

The results of the actuator were depicted in Figure 74, for an electric field of 10V/µm. As expected, the achievable curvature is higher when the applied electric field is maximal. This behavior is in agreement to the previous analysis where the generated strain proportionally increases to the square of the electric field. In addition, the proposed design corresponds to the typical properties required for a mini-UAV (i.e., Unmanned Aerial Vehicle or mini-aircraft without a human pilot aboard) with a displacement of 16 mm at tip wing of the butterfly.[156,157] Good results of the electromechanical morphing clearly confirms that only devices combining high strain under low electric excitation can be exploited in practical applications like change shape of structure, with further advantages like being flexible, lightweight, easy integration, and simple fabrication process.

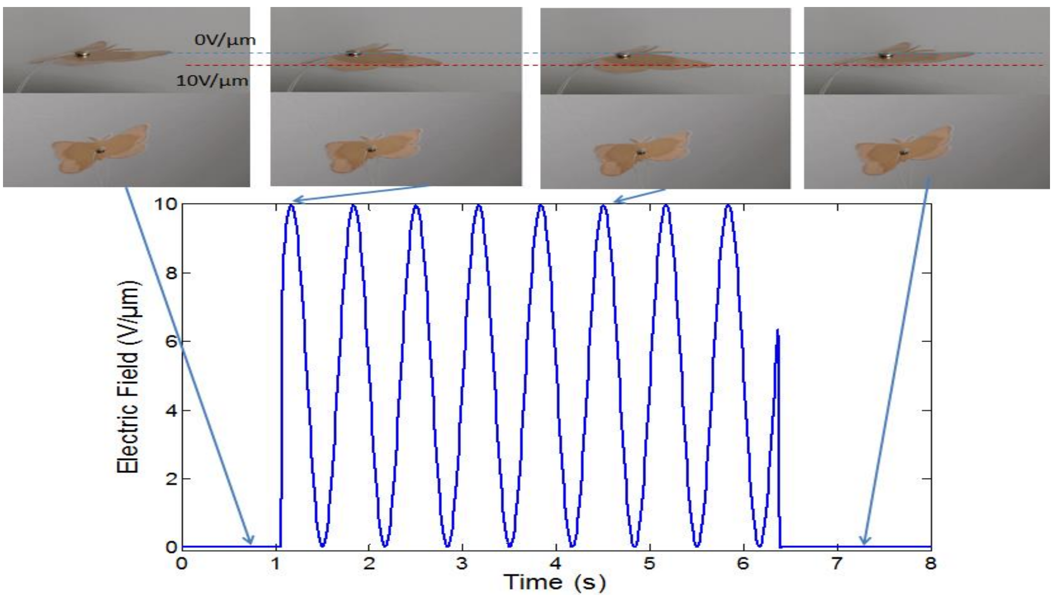

Figure 74. Performance of modified terpolymer with 10wt% of DINP

III.2.e. Conclusions

This work has reported the effect of plasticizers on the electrostrictive behavior of terpolymer blends. The study was based on three types of plasticizing agents, i.e., DINP, DEHP, and Palamoll 652. The fact of incorporating a plasticizer into the polymer matrix was clearly an easy and cheap way to dramatically reduce the applied electric field while maintaining the electrostrictive strain performance. It was concluded in this study that DINP led to the best performance in terms of electrical and mechanical properties, involving in excellent electrostrictive strain response as well as mechanical energy density. This material will certainly be considered as one of the most appropriate candidates allowing us to overcome several limitations of the existing electroactive polymer, such as high input voltage, low strain and limited energy density.

Experimental results showed considerable improvements in the electrostrictive properties of the proposed novel materials as opposed to conventional terpolymers. For instance, an 8-fold increase in strain was seen for the Palamoll blend and a 20-fold enhancement was achieved for the DINP blend. Similar improvements were also obtained in terms of the mechanical energy density with an extremely high factor equal to 10 (with Palamoll) and 170 (with DINP) between the pure and modified films.

With the aim of evaluating the effect of the DINP content on the terpolymer actuation performance, a series of characterizations based on different plasticizer weight fractions were carried out. It appeared that the transverse strain under a defined electric field increased as a function of the DINP quantity. As expected, a 16wt% DINP content gave rise to a remarkably improved electromechanical response, but this quantity was limited due to the seepage phenomenon.

Accordingly, the novel material developed in this study was validated by a simple and efficient demonstration of the morphing structure. Excellent electromechanical behavior was obtained, confirming high potential application of the proposed approach in flexible electronic field especially for medical instrumentation like smart guidewire, haptic system, etc.

Future work will involve dielectric spectroscopy over a large temperature range in order to obtain a better understanding of the physical interactions of a plasticizer in a polymer matrix as well as the molecular mobility and charge transport in plasticized blends. Another focus will be on the physical origin of the low frequency relaxation process, e.g., electrode polarization or bulk MWS polarization.

Chapter 3:

Toward a medical use of the terpolymer

This chapter repeats the works published during the thesis in the paper "Effect of beta-based sterilization on P(VDF-TrFE-CFE) terpolymer for medical applications", Scientific reports 2020,10 (8805) https://doi.org/10.1038/s41598-020-65893-2, by **N. Della Schiava**, F. Pedroli K. Thetpraphi, A. Flocchini, MQ. Le, P. Lermusiaux, JF. Capsal et PJ. Cottinet.[158]

The final desired application is a guide wire for intravascular navigation and catheterism. So it is a medical device which is intra-arterial so invasive, even if non implantable. For use this guide on humans, we can first obtain CE marking. (see appendix 1 page 171)

As for each medical invasive medical device used in a surgery room, sterilization is mandatory.

Biocompatibility and no cellular and tissues toxicity may be also demonstrated.

III.3.a.The Terpolymer and its resistance to sterilization

III.3.a.i.Introduction

Sterilization is mandatory for all invasive medical devices to avoid infections in patients. Among several methods of sterilization for surgery devices, irradiation with γ/β rays and autoclaving with steam are the most used. For autoclave sterilization, the necessary temperature is high, approximately 120°C to 135°C, which is not compatible with the terpolymer because it has a melting point of around 120°C. Conversely, radiation-based sterilization is a cold method with no heat dependence and treatment can be efficient event at ambient temperature or sub-zero temperatures. Thus, this technique is well compatible with many polymers that are sensitive to high temperature such as pharmaceuticals and biological samples. Moreover, γ/β radiation offers numerous advantages over traditional heat-based sterilization. In reality, only a single variable relating to the exposure dose/time must be monitored, making radiation sterilization simple and easy to control. Another benefit stems from the flexibility of this technique which can sterilize any material with variable density, size or thickness, and homogeneous or heterogeneous systems, regardless of temperature and pressure conditions.

Both beta and γ-rays are suitable for medical sterilization. The main differences between them are their depths of penetration and their dose rates. Beta-ray limited penetration is given at a high dose rate where a sterilization dose can be given within a few seconds or minutes. However, with gamma-ray deep penetration is traded for a low dose rate that may take several hours or even days to accumulate at a high dose. As in our study all samples are very thin (i.e. few hundred of micrometers), the use of β-radiation seems to be more suitable based on the best compromise between penetration and time consumption. Although radiation sterilization technologies have been extensively developed for medical applications, their effects on polymer characteristics have been poorly studied or published.[159] Irradiation destroys microorganisms and also changes material properties. These changes often depend on the radiation dose. Following radiation sterilization, application-specific tests should be carefully investigated to confirm which polymer is optimally suited to an individual application. Yang *et al*. studied the effects of e-beam ionizing radiation based γ-rays on P(VDF-TrFE-CFE) terpolymer and P(VDF-TrFE) copolymer.[160] To the best of our knowledge, a similar investigation dedicated to β-based sterilization has not been reported yet in the literatures. The main objective of the following experiments involves evaluating the β-radiation effect on the morphology and electromechanical properties of the terpolymer in order to determine if sterilization of our proposed material is possible for medical use.

III.3.a.ii.Methods

The terpolymer film fabrication was depicted in the previous sections. Methods to modify polymeric films realized by blending P(VDF-TrFE- CFE) terpolymer with 10%wt. of a phthalate plasticizer was also described in the previous section. The pure and modified EAPs were then subjected to high-energy β-irradiation at 50 Mrad which is standard sterilization dose for medical instrument (according to industrial process of IONISOS). A comparison between the pristine and the sterilized samples in terms of thermal/electrical/electromechanical performance will be investigated in following sections.

III.3.a.ii.1.Thermal analysis

In order to determine any possible morphological changes in the crystalline structure induced by the radiative sterilization treatment, *Differential Scan Calorimetry* (DSC) measurements are performed on all post-annealed and post-sterilized films.

The post-annealed and post-sterilized polymeric films were heated from room temperature to 180°C at a heating rate of 10 K/min. Crystallinity degree (or X_c) is then calculated as the integral of the melting peak divided by the melting enthalpy of a hypothetic 100% crystalline terpolymer (42 J/g).[161]

The second melting DSC ramp (10 K/min) that was performed on as-received terpolymer powder was implemented to identify the optimal annealing temperature.

III.3.a.ii.2.Electrical characterization

Broadband dielectric spectroscopy (BDS) was performed using a Solartron 1260 impedance-analyzer. Ambient temperature dielectric spectra are acquired under an alternative voltage of $1V_{peak\text{-}peak}$ amplitude at a frequency range of 10^{-1} – 10^{6} Hz.

The dielectric strength of the selected materials was determined by applying a DC voltage linear ramp at a slew rate of 500V/s. For each polymeric film, several breakdown events were recorded to show the probability distribution of electrical failures.

III.3.a.ii.3.Electromechanical performances

To efficiently assessing the electromechanical actuation of the sterilized samples via beta radiation, a dedicated set-up based cantilever structure was built.[162] Firstly, 50x10 mm² terpolymer film specimens were coated on both sides using 20nm-thick gold electrodes. Secondly, by mean of an adhesive energy transfer tape, the electroded terpolymer was attached on a 100µm-PET inactive substrate. Finally, the three-layer cantilever was laminated at room temperature under high vacuum for 15mn to cure the adhesion of each layer. The multilayer cantilever was clamped on one end, while the other end was free and its deflection (the so-called unimorph tip displacement) was measured using a laser sensor (Baumer CH8501). A full description of the experimental setup was detailed in our previous sections.[163] One of the most relevant parameter characterizing the electromechanical performance of The transversal strain S_{31} can be deduced from the deflection measurements of an unimorph under quasi-static conditions according to the following expression: [164]

$$\delta_0 = \frac{3L^2}{2e}\frac{2AB(1+B)^2}{A^2B^4+2AB(2+3B+2B^2)+1}S_{31} \quad (1)$$

where δ_0 is the cantilevered tip deflection, $A=Y_{substrate}/Y_{poly}$ and $B=e_{substrate}/e_{poly}$ with $Y_{substrate}$, Y_{poly}, $e_{substrate}$ and e_{poly} depict the Young modulus of the substrate, the Young modulus of the polymer, the substrate thickness, and the polymer thickness, respectively; e and L are respectively the sample thickness and length. It is noteworthy that the model based on Eq. (1) is only available for relatively small deflections. Consequently, all materials explored in this study will be excited under electric fields where the tip deflection of the unimorph does not exceed 3 mm (corresponding to a strain less than 1%).

III.3.a.iii.Results and discussion

III.3.a.iii.1.Thermal analysis

Figure 75 shows the DSC thermal analysis results of the pure and 10% DINP plasticized terpolymers with/without the β-irradiation process. Similar to our previous works,[163] the plasticized terpolymer lightly decreased the melting peak temperature (i.e. 122.3°C) compared to the pure terpolymer (i.e. 125.8°C). On the other hand, the melting peak enthalpy was slightly higher, increasing from 18.6 J/g for the neat sample to 20.1 J/g for the modified sample. This phenomenon is probably caused by increase molecular chain mobility as well as large Maxwell Wagner Sillars interfacial polarization effects which facilitate the polymer crystallization especially when being doped with a plasticizing substance.[163]

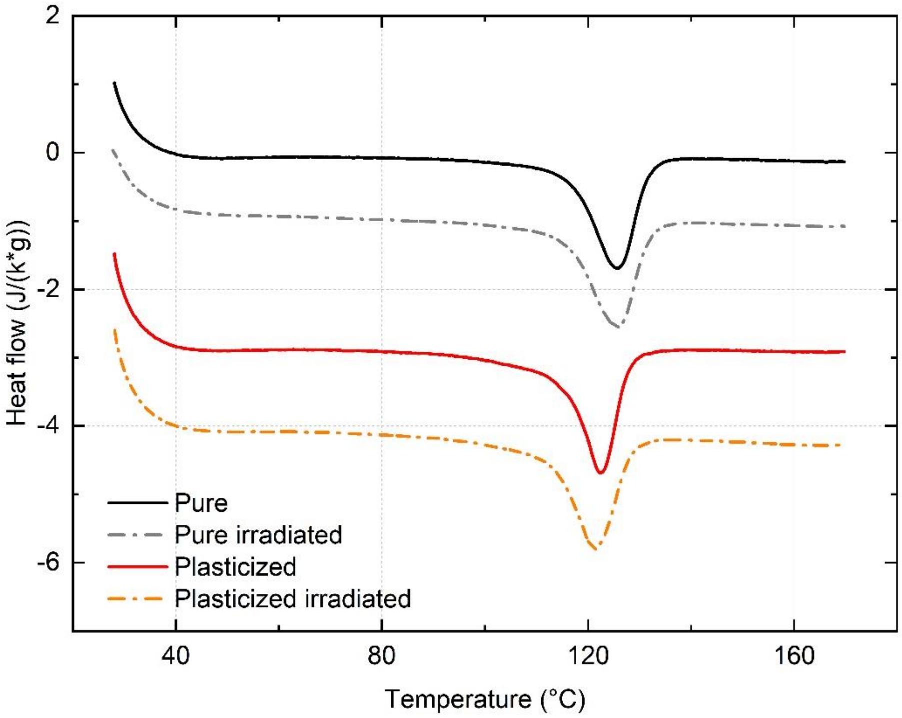

Figure 605. DSC thermographs of the pristine and irradiated neat and plasticized terpolymers.

To better understand the influence of β-radiation on EAP morphology, analysis of the melting peak together with the thermographs in Figure 75 are summarized in Table 9, which contains complete information about quality and distribution size of crystal domains. Similar results were obtained for both with- and without- sterilized samples, confirming that β-based sterilization does not alter the morphology of the crystalline phase or the thermal behavior of the fabricated EAPs.

	$T_{melting}$ (°C)	$\Delta H_{melting}$ (J/g)	FWHM (°C)	X_c (%)
Pure	125.8	18.6	9.4	44.3
Pure irradiated	126.2	18.8	10.0	44.7
Modified	122.3	20.1	8.3	47.8
Modified irradiated	121.8	19.7	9.3	46.9

Table 9. DSC thermograph analysis results

III.3.a.iii.2.Dielectric spectroscopy

In this subsection, broadband dielectric spectroscopy was investigated to further assess the β-radiation effect on the dielectric behavior of the pure and plasticized terpolymers.

Figure 616a illustrates the real part of relative permittivity of the four samples over a wide frequency range of $10^{-1}-10^{6}$ Hz. As expected, the pure materials (i.e. black and gray curves) showed the typical dielectric behavior of a polar polymer above its glass transition temperature. In other words, at high frequencies (greater than 1kHz), it is possible to observe the contribution of dipole polarization whereas at low frequencies, the dielectric permittivity remains almost constant. For the modified terpolymer (red and orange curves), its permittivity values considerably increased at low frequencies because of boosted interfacial phenomena that typically occur for this material structure.[165] Actually, the interfacial polarization is largely improved by ions conduction and molecular mobility in plasticized samples thanks to the augmented free volume in the polymer amorphous phase. This effect can be seen in Figure 76b where under low frequencies, the related dielectric losses of the modified EAP are definitively more significant than the neat one, regardless of the radiative procedure.

It has been also seen in Figure 616b that the radiative treatments gives rise to dramatically increase permittivity imaginary (ε”) at a very low frequency for the pure terpolymer, increasing from 4 (before sterilizing) to 70 (after sterilizing). Such a huge increase dielectric losses of the neat material may stem from the higher mobility of the intrinsic molecular chains after being treated with β-radiation, resulting in expanding inter-chain distance of the polymer’s internal chemical crosslinks. This phenomenon, nonetheless, is not the same as the plasticized EAP where the dielectric losses of both irradiated and pristine samples are almost the same, having negligible discrepancies under the whole frequency range. Because the plasticized terpolymer demonstrated extremely high molecular mobility,[166,167] some ruptured molecular chains from β-radiation processing probably only slightly influenced the polymer structure.[168,169]

In conclusion, these results demonstrated that the β-radiation led to a variation in dielectric performances of the neat P(VDF-TrFE-CFE) terpolymer while there was no major change in the plasticized sample. To some extents, the sterilization procedure may affect the morphological modification of EAP, specifically favoring its interfacial polarization related to the molecular mobility.[170,171]

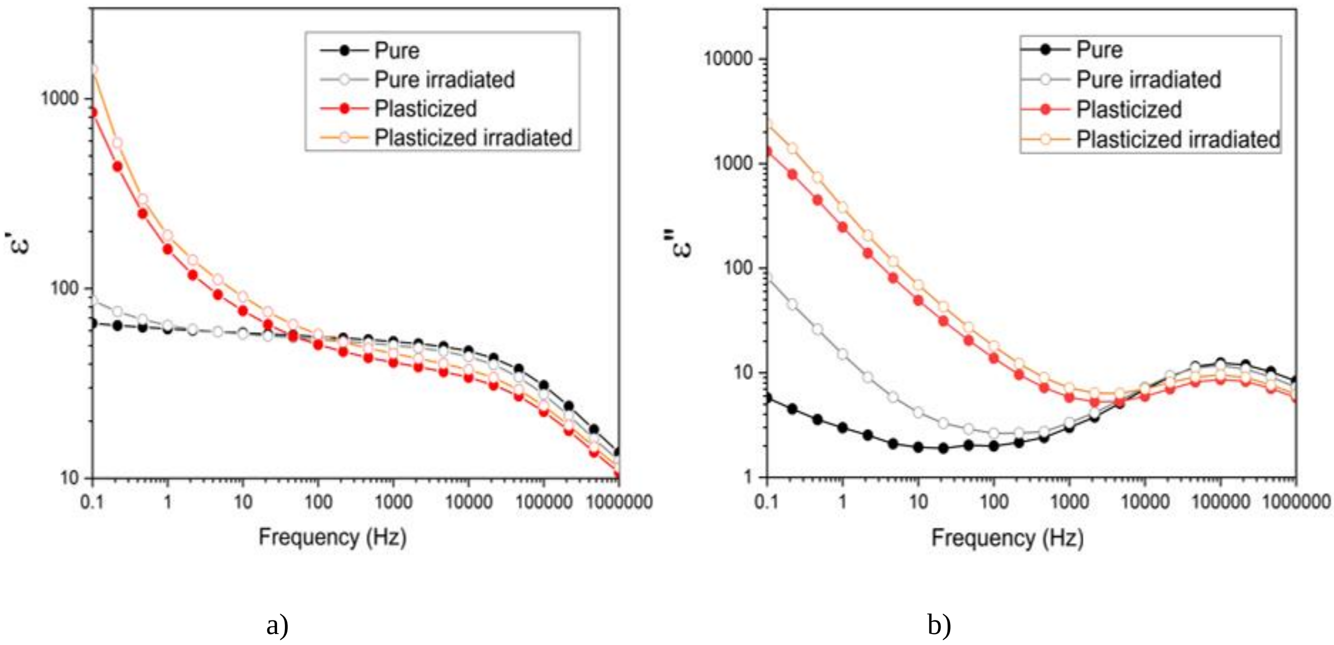

Figure 616. BDS spectra for the pristine and irradiated material: a) real part of relative permittivity, and b) imaginary part of relative permittivity.

III.3.a.iii.3.Electrical breakdown

Figure 627 illustrated the experimental breakdown probability $P(E)$ versus electric field for the four different polymeric films (neat/modified and with/without β-radiation) based on the following Weibull model:

$$P(E) = 1 - \exp\left[-\left(\frac{E}{E_{BD}}\right)^k\right] \quad (2)$$

where $P(E)$ is the breakdown probability at a given electric field E, E_{BD} is the parameter corresponding to the breakdown electric field for a failure probability of 63.2%, and k is the shape factor defining the distribution spread.[172] These parameters of the four samples determined from the Weibull model are summarized in Table 10.

	E_{BD} (V/µm)	k
Pure	267	4.7
Pure irradiated	271	4.4
Modified	119	3.3
Modified irradiated	116	3.1

Table 10. DC breakdown electric field from Weibull analysis

The results clearly highlights that for a given failure probability, the EAP filled with DINP plasticizer performed lower electrical breakdown strength, e.g. 119 V/µm for the modified terpolymer as opposed to 276 V/µm (2-fold greater) for the pure one. As a consequence of some defections in modified terpolymer, adding excessively plasticizer content can limit the operating voltage which will strongly affect to the strain production. Nonetheless, in our application where low electric field is employed (i.e. less than 50V/µm), the breakdown probability for the terpolymers is extremely low, event for those filled with 10% DINP plasticizer content. It is noteworthy that the electrical strength of either pure or modified sample was totally conserved after a β-radiation treatment.

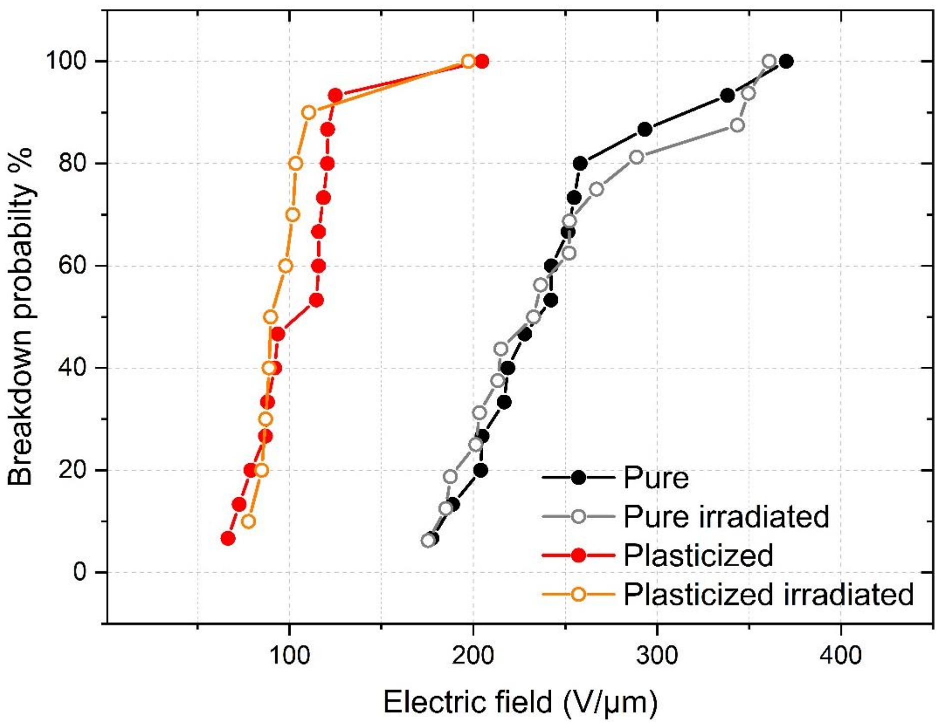

Figure 627. Experimental DC breakdown electric field distribution

III.3.a.iii.4.Electromechanical performance

To evaluate the electromechanical performances of the pristine and irradiated materials, actuation characterization based on tip displacement measurements are carried out thanks to unimorph cantilevers as described in previous section.

Figure 638 displayed the experimental transversal strain S_{31} for the pure and plasticized EAPs before and after sterilization. It has been observed that the radiative treatment did not alter the electromechanical activity of the plasticized terpolymers. As also confirmed by the above dielectric spectroscopy, β-radiation could not further expand the already large molecular mobility of the polymer amorphous phase, leading to unchanged actuation behavior. Concerning the pure terpolymers, on the other hand, its transversal strain S_{31} exhibits superior electromechanical response in the case of the sterilized sample. The enhanced electromechanical conversion for the irradiated pure terpolymer can be justified by its higher dielectric permittivity as shown in Figure 76.

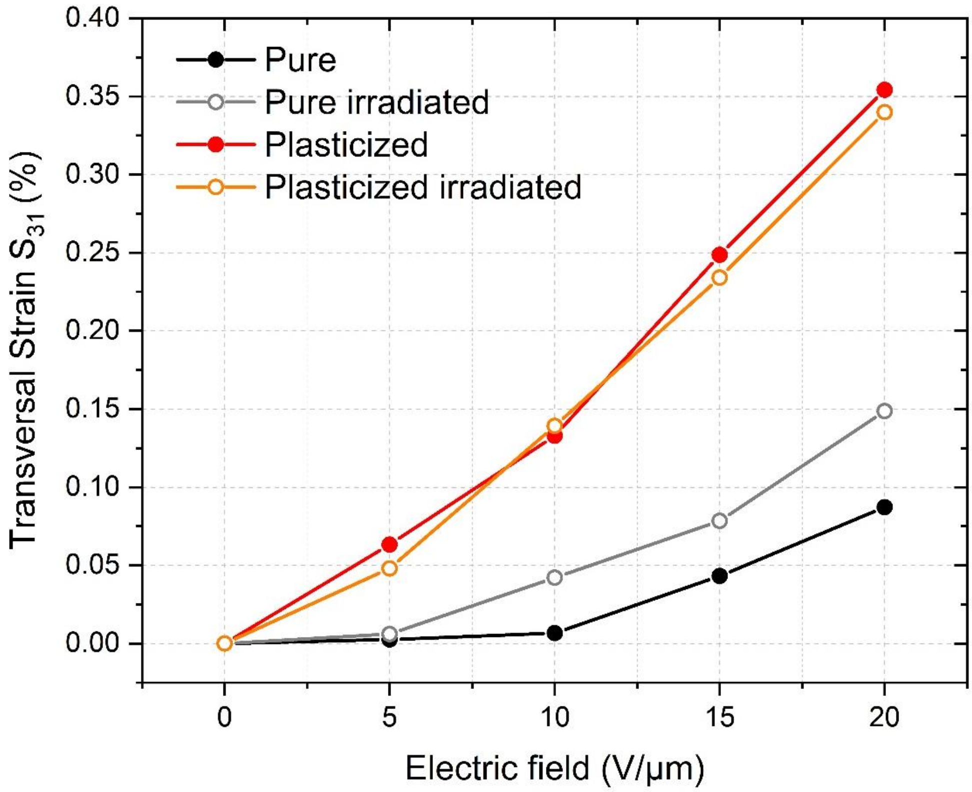

Figure 638. Transversal strain of pure and plasticized terpolymers with/without β-irradiation treatment as a function of applied electric field

III.3.a.iv.Conclusions

This work confirmed a reliability of our novel material that was based on 10% DINP plasticized terpolymer for a new generation of ultra-flexible active bending system that can be used as a steerable guidewire tip in endovascular surgery. Sterilization of all medical devices is required to reduce the contamination risk for the patient. As a result of extensive investigations into the bactericidal effects of radiation and continuing improvements in irradiation technology, ionizing radiation is increasingly being used in this field. However, radiation based sterilization is an extremely sensitive, critical step because biomedical devices should maintain their chemical and physical properties through different stages of processing including terminal sterilization. Our study revealed that the ionizing β-ray did not significantly alter the intrinsic properties of the neat/plasticized terpolymers, causing non change in its electromechnical activities as well as its thermal and electrical characteristics. These results are extremely interesting, suggesting the possibility of using EAP as biocompatible and sterilizable material that can be implemented in future smart guidewire for endovascular surgery.

III.3.b. The terpolymer and its cellular compatibility

III.3.b.i.Introduction

Even though the terpolymer will not be directly in contact with human cells and tissues, it is necessary to prove that the terpolymer is not toxic for the human cells. The terpolymer could release chemical products in the blood through the surrounding hydrophilic coating of the guide wire. The modified terpolymer with the plastifiant agent must also be evaluated because the plasticizer agent may have its own cytotoxicity.

This step is absolutely mandatory in order to can obtain the CE marking (appendix) and to use the new device.

Biocompatibility tests are performed for all the polymers used for medical applications.[173-175] Polypyrrole is the electroactive polymer the most studied about cytotoxicity.

To the best of our knowledge, there is no study of the biocompatibility of the terpolymer P(VDF-TrFE-CTFE). However, there are studies about biocompatibility of copolymer P(VDF-TrFE). This copolymer seems to be not cytotoxic. Some studies even show that the copolymer could enhance the proliferation of some cellular lineage under external stimulation.[176-178]

In the following section, we will present our results about cytotoxicity and cellular proliferation for the neat and the modified terpolymer.

III.3.b.ii.Methods

We have made 2 types of experiments on human cells in contact with the terpolymer. With the first experiment we want to evaluate the cytotoxicity and with the second experiment the influence on cell proliferation.

For each experiment, we have tested the neat and the modified terpolymer.

For cytotoxicity as well as for cell proliferation, we use human cells named MG-63. It is cells quite undifferentiated, from osteoblasts lineage.

For the cytotoxicity test, we use cell culture plate with 24 wells. We seeded 5000 cells on each well. A suspension of 5000 cells in 50 µL was placed on the terpolymer film. The film of terpolymer was cut into 1 cm diameter disc to be compatible with well's size.

For the cells proliferation test, we use the Prestoblue® Technique. The PrestoBlue® reagents contain resazurin and a propriety buffering system. When added into the plate, the reagents are rapidly taken up by cells. The reducing environment within viable cells converts the non-toxic resazurin, which is blue and no fluorescent, in resorufine a red-fluorescent dye. We can detect this change by measuring fluorescence. For this measure, we used a fluorometer INFINITE PRO 200 with following parameters: excitation at 535 nm/emission at 610 nm/gain at 40.

We evaluate the fluorescence after 3, 6 and 10 days. During this time, cells incubated in a 37°C oven, with 5 % CO2 in a wet atmosphere. Then 10 % prestoBlue reagents were added into each well and cells incubated 1h30 with the same conditions. For reading, we waved the plates and we transferred the cell culture into black-bottomed plates.

The neat terpolymer was named 1-TP 4 pure.

The modified terpolymer was named 1-TP 2D10%

There is a control group with the same cells without any polymer.

We performed the fluorescence measurement 3 times for each sample and we performed complete cellular tests 3 times. We calculated the average of the 3 fluorescence measures for the 3 tests.

III.3.b.iii. Results

Figure 79 shows the average cell proliferation of each sample. The control group validates the test. We see a comparable proliferation between the 2 samples with terpolymer and the control group that means a good biocompatibility of the terpolymer and of the plasticizer. On the third day, we note a better cell proliferation with the modified terpolymer but this effect disappears on the 6^{th} and 10^{th} days.

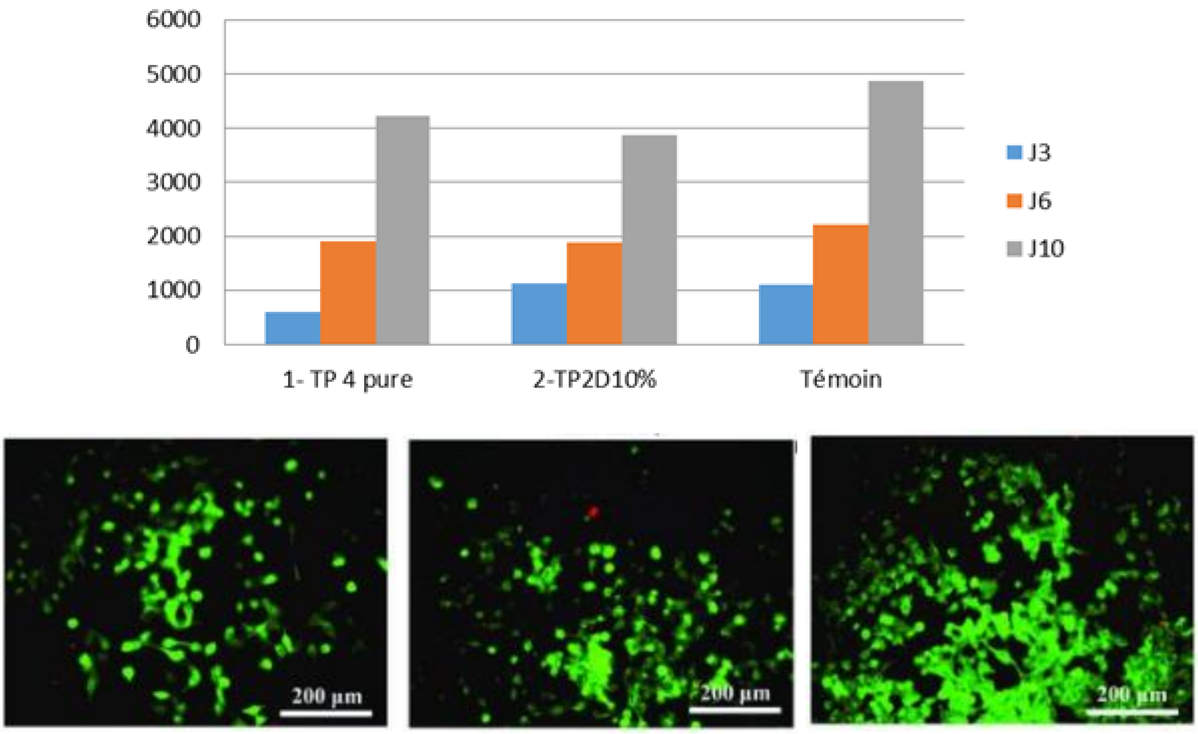

Figure 649. The average cell proliferation evaluate with the PrestoBlue technique at day 3, 6 and 10.

The following tables detailed each measure for the 3 tests.

Gain 40- J3	test 1					
Quantité cellulaire	Fluorescence 1	Fluorescence 2	Fluorescence 3	Moyenne Fluo	Fluo - Blanc	Ecart-type
Blanc	2536	2697	2673	2635,3	0,0	86,9
1- TP 4 pure	3091	3582	2770	3147,8	512,4	408,8
2-TP2D10%	3718	3845	3617	3726,9	1091,6	114,1
Témoin	3394	3343	5902	4212,9	1577,6	1462,6

Gain 40 - J3	test 2					
Quantité cellulaire	Fluorescence 1	Fluorescence 2	Fluorescence 3	Moyenne Fluo	Fluo - Blanc	Ecart-type
Blanc	2589	2717	2702	2669,3	0,0	70,0
1- TP 4 pure	3110	3226	3275	3203,4	534,1	84,9
2-TP2D10%	3500	3605	3814	3639,4	970,1	160,0
Témoin	3170	3243	3241	3218,2	548,9	41,5

Gain 40 - J3	test 3					
Quantité cellulaire	Fluorescence 1	Fluorescence 2	Fluorescence 3	Moyenne Fluo	Fluo - Blanc	Ecart-type
Blanc	2554	2608	2598	2586,7	0,0	28,7
1- TP 4 pure	3354	3329	3457	3379,8	793,1	68,0
2-TP2D10%	3810	3946	4001	3919,1	1332,4	98,7
Témoin	3438	3822	4093	3784,4	1197,8	328,9

Figure 80. Results of the 3 tests on the third day

Gain 40 - J6 test 1

Quantité cellulaire	Fluorescence 1	Fluorescence 2	Fluorescence 3	Moyenne Fluo	Fluo - Blanc	Ecart-type
Blanc	2522	2473	2617	2537,3	0,0	73,2
1-TP 4 pure	3096	3782	3665	3514,1	976,8	367,1
2-TP2D10%	3736	3706	4162	3868,0	1330,7	255,1
Témoin	4008	4160	4628	4265,4	1728,1	323,0

Gain 48 - J6 test 2

Quantité cellulaire	Fluorescence 1	Fluorescence 2	Fluorescence 3	Moyenne Fluo	Fluo - Blanc	Ecart-type
Blanc	2508	2486	2496	2496,7	0,0	11,0
1-TP 4 pure	4387	4726	3646	4253,0	1756,3	552,0
2-TP2D10%	4457	5473	3804	4578,3	2081,7	841,1
Témoin	4850	4620	4507	4659,2	2162,6	174,9

Gain 40 - J6 test 3

Quantité cellulaire	Fluorescence 1	Fluorescence 2	Fluorescence 3	Moyenne Fluo	Fluo - Blanc	Ecart-type
Blanc	2537	2497	2511	2515,0	0,0	20,3
1-TP 4 pure	6054	5539	4914	5502,3	2987,3	570,7
2-TP2D10%	4362		5184	4772,8	2257,8	581,5
Témoin	4584	5561	5575	5239,7	2724,7	568,2

Figure 81. Results of the 3 tests on the 6th day

Gain 40 - J10 test 1

Quantité cellulaire	Fluorescence 1	Fluorescence 2	Fluorescence 3	Moyenne Fluo	Fluo - Blanc	Ecart-type
Blanc	2543	2598	2605	2582,0	0,0	34,0
1-TP 4 pure	8276	7292	7700	7755,9	5173,9	494,2
2-TP2D10%	6962	7254	8027	7414,3	4832,3	550,6
Témoin	7035	8242	7811	7696,1	5114,1	611,7

Gain 40 - J10 test 2

Quantité cellulaire	Fluorescence 1	Fluorescence 2	Fluorescence 3	Moyenne Fluo	Fluo - Blanc	Ecart-type
Blanc	2275	2310	2311	2298,7	0,0	20,5
TA6VELi	5512	5130	5834	5491,8	3193,1	352,4
TiZrCuPdSn	5529	6317	6309	6051,8	3753,1	452,8
Témoin	6156	6235	7155	6515,4	4216,8	555,6

Gain 40 - J10 test 3

Quantité cellulaire	Fluorescence 1	Fluorescence 2	Fluorescence 3	Moyenne Fluo	Fluo - Blanc	Ecart-type
Blanc	2363	2332	2349	2348,0	0,0	15,5
1-TP 4 pure	7118	6683	6079	6626,7	4278,7	522,1
2-TP2D10%	4467	4589	7007	5354,3	3006,3	1432,3
Témoin	6882	7739	8222	7614,1	5266,1	678,6

Figure 82. Results of the 3 tests on the 10th day

III.3.b.iv.Conclusions

These experiments confirm the biocompatibility of the terpolymer for in vitro conditions. Without external stimulation, there is no enhancement of cell proliferation. This biocompatibility must be confirmed also in an in vivo model with cells and tissues studies. We can also test the cell proliferation with externally stimulated terpolymer.

Chapter 4:
Modeling of the structure and design of the smart guide wire based P(VFD-TrFE-CTFE) driven by an electric field

III.4.a.Introduction

In previous sections, we described in detail the fabrication and the optimization of the electromechanical performance of the terpolymer. We have also begun to check its biocompatibility and the possibility of sterilizing it without altering its properties.
The final desired application is the development of a smart steerable guide wire to navigate into angulated vessels. The following section describe the modeling of the possible structure and design of this smart guide wire based P(VDF-TrFE-CTFE) driven by an electric field.

III.4.b.Methods

The requirements for actuators to be used for "smart" guide wires can be very broad. However, the main performances to take into account when designing remotely steerable guide wires are the bending angles achievable by the guide wire, the time to obtain bending, the degree of rotation that can be achieved and the capacity of miniaturization of the design.[179] The choice of material (the terpolymer) determines the level of pushability, torque and flexibility. This can be also manipulated along the all length of the guide wire to achieve the desired effects.
But this is the design of the guide wire shaft which is a significant factor in determining the formation of curves, the angles of deflection and the levels of steerability.
As mentioned and described in Chapter 1.a, the overriding constraints were related to typical angle in human vessels and time response of human.[125,127]
Figure 83 illustrates the "smart" guide wire application.

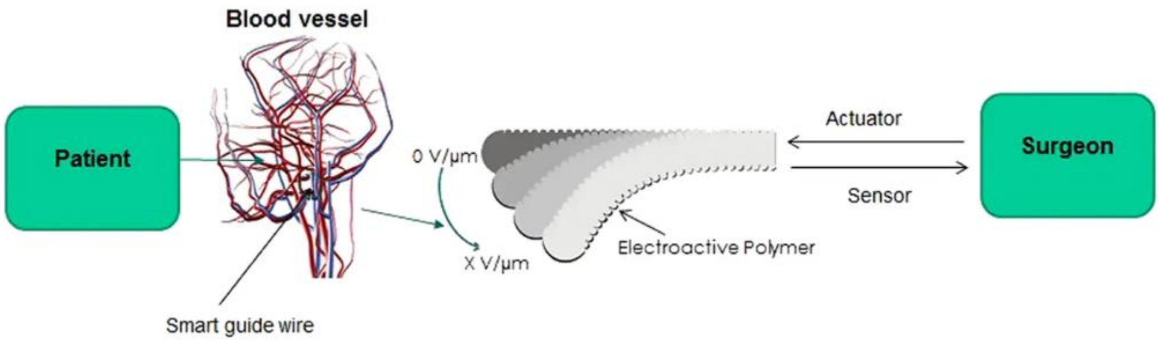

Figure 653. Schematic illustration of the "smart" guide wire application.

Figure 714 illustrates the working principal of the developed smart guide wire. The architecture of the steerable guide wire is composed of a conductive electric wire surrounded by a two degrees of freedom (DOF) electrostrictive terpolymer. Such 2-DOF functionality was achieved based on two electrodes sputtered on the surface of a cylindrical EAP, enabling the smart guide wire bending in both directions. In fact, a quadratic relationship between the strain and the electrical field makes the generated displacement independent of the sign of the input voltage excitation. If an electrical field is applied between the central electrode and electrode 1, the polymer is, due to the electrostatic force, compressed in the thickness direction, causing a bending structure on the up direction. On the other hand, in case of the electrical field is applied between the central electrode and electrode 2, the smart catheter bends in the down direction. Therefore, by alternatively activate the electrodes 1 and 2, it is possible to easily control the movement of the EAP.

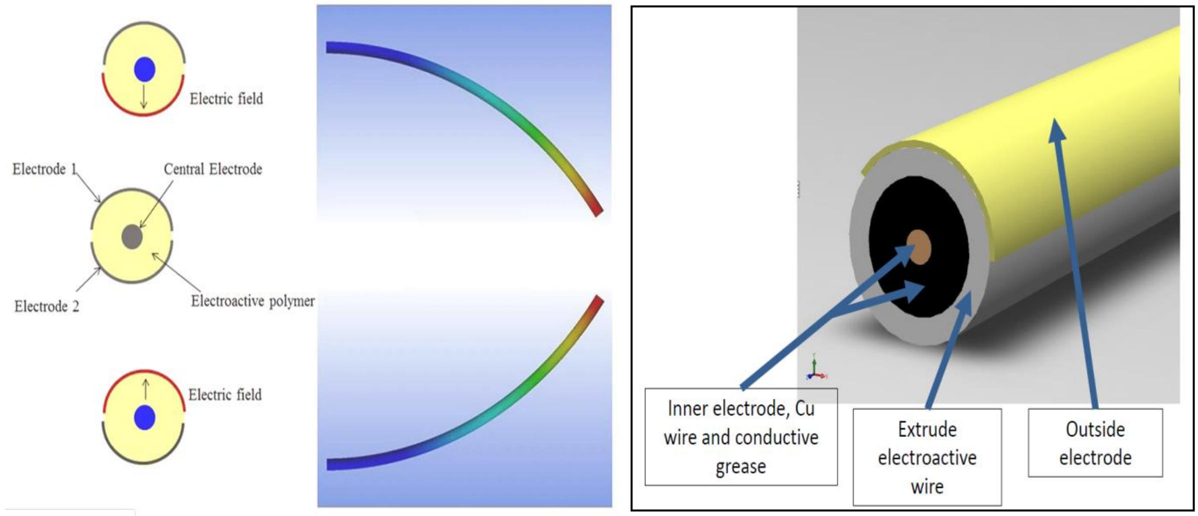

Figure 664. Principal of a "smart" guide wire with 2 degrees of freedom.

In view of the architecture of the actuator, an analytical approach was deemed too complex for modeling the electromechanical behavior of the "smart" guide wire. Therefore, finite element modeling was chosen. The multi-physics finite element model was developed using Ansys. This tool is used to model the basic physics occurring within an electrostrictive polymer. The models are developed to track the geometric variation of the electroactive polymer in the presence of an electric field. These variations of geometrics are then correlated to a mechanical generated stress.[180] To produce this model, the geometry of the smart guide wire was idealized as a perfect circle with constant electrode shapes. These geometries were created using the built-in Ansys tools. The use of these built-in geometry tools made it possible to input the dimensions as Ansys parameters and easily adjust them throughout the modeling process. To create the three-dimensional shape, a two-dimensional electroactive polymer cross-section was drawn and then extruded to create the length of the guide wire. The mesh was defined on the face of the EAP and then extended along the length of the EAP. It was designed to be fine near the electrode polymer interface which was accomplished using a distribution boundary condition. This condition guaranteed that the number of elements in this critical region remained constant even when the whole size in the middle was varied. The region was considered critical since it was where the largest changes in concentration were seen.

To perform the simulation, two physics packages were simultaneously used: electro-statics and solid mechanics.[180] The electro-statics analysis focuses on the input of the electrical field to the EAP, and this physics package is governed by Poisson's law. The last physics package used in the simulation was the structural mechanics model. The bending in the tube-type EAP was modeled using a linear elastic model. The simulation parameters can be seen in Table 11. The neat and the plasticized terpolymer were used: the data were extracted from the literature and is presented in table 12.[141,144]

Name	Value	Description
D_{outer}	1.4 mm	Outer diameters
D_{inner}	1 mm	Inner diameters
L	60 mm	Extrusion Length
E	30 V/µm	Electric field

Table 11. Ansys parameters and variables

Type	Y (MPa)	ε_r at 0.1Hz and E = 20 V/µm	M_{31} (m^2/V^2)
P(VDF-TrFE-CTFE)	100	30	3.10^{-18}
P(VDF-TrFE-CTFE) + 15wt%DEHP	30	400	38.10^{-18}

Table 12. Electromechanical properties of electroactive polymers at room temperature.

For the first simulation, an electrical field of 30 V/µm was applied between electrode 1 and the central electrode.

The second set of simulations that were realized concerned the electromechanical activities of the smart guide wire. A comparison between the different compositions of the terpolymer under a constant electrical field of 30 V/µm was made.

Then we made simulation with an electric excitation applied to electrode 1 or 2 and for different electrical fields.

To test in quasi-real conditions, we made a prototype. The architecture of the smart guide wire can be described as a tube, and can thus be realized by extrusion. Initially, the tubings were extruded through a Laboratory Mixing Extruder (LME, Dynisco, Inc.) with a 0,476 cm outer die head and a 0,3175 cm mandrel tip at a mandrel temperature of 150 °C and a die temperature of 130°C at 180 revolutions per minute (RPM). Next the tube was cut into the desired length and recrystallized in an oven at the onset of the melting peak determined by a Setaram EVO 131 DSC. Figure 85 shows a picture of an extruded tube of P(VDF-TrFE-CTFE) with plasticizer.

Figure 675. Extruded tube of plasticized P(VDF-TrFE-CTFE).

To evaluate the steerable properties of the tube, a dedicated test setup was built. On one side of the tube, a gold electrode was deposited by sputtering (Cressington 208 HR) through a mask. This made it possible to realize electrode 1 and 2. The inner electrode was created with the help of conductive grease. The sample was then connected to a commercially usual guide wire. The electric contact between the guide wire and the tube was assured with conductive glue. The setup developed for characterizing the transverse vibration response is shown schematically in figure 86. As seen in this figure, the prototype to be tested was clamped in one end at a solid base near the electric contact whereas the other end was free. When the prototype was subjected to an electrical field, its expansion and contraction caused the free end of the tube to move and the movement was detected using an optical technique. In the current setup, a high resolution camera was used to monitor the deflection (Canon 6D). The electrical field application was performed with the Agilent 33220A Function Generator and Treck power amplifier. All measurements were recorded in an open air environment (22 °C).

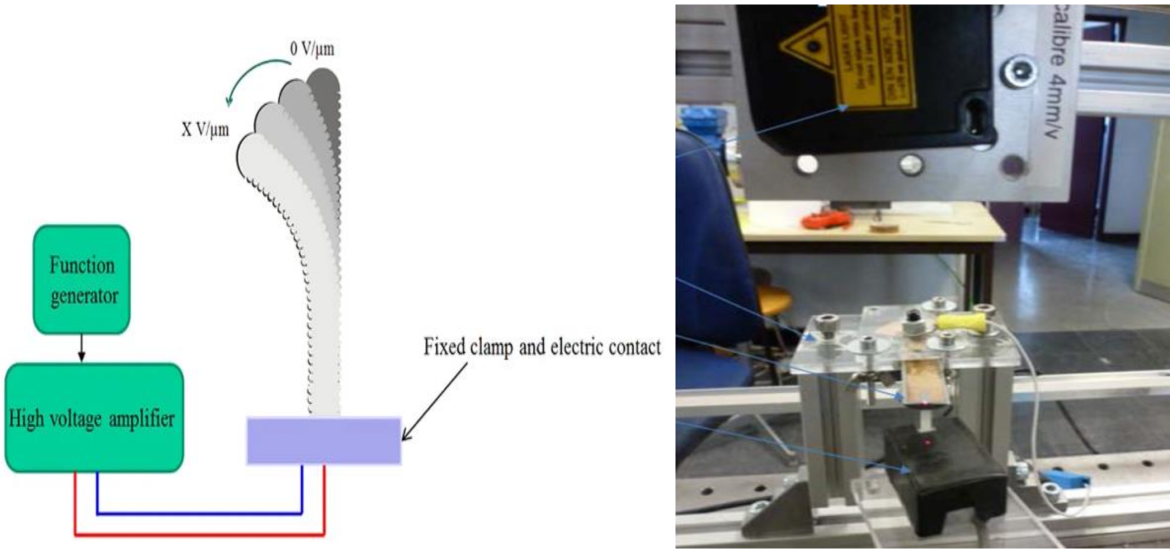

Figure 686. Schematic of the electromechanical characterization test setup of the prototype

Several tube actuators were fabricated with different ratios between their length and outside diameter.

III.4.c.Results

For the first simulation, the electric potential in the cross-section of the EAP is shown in Figure 87. The electrical field spread across the EAP in a symmetric manner between the central electrode and the electrode 1. Due to geometric inconsistencies in the real sample, this is not always the case. The electrical field between electrode 2 and the central electrode appeared to be null, which was logical since no electrical field was applied. This electrode configuration allows a sectoring of the electrical field distribution in the structure. This was necessary for the development of a steerable guide wire.

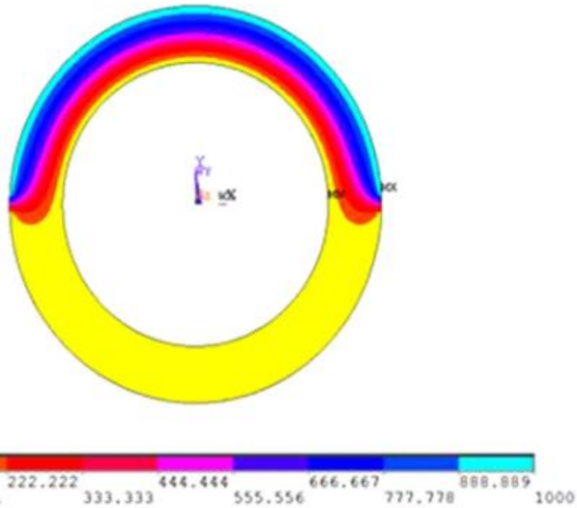

Figure 697. Electrostatic reparation in the cross-section view.

In the second set of simulations, we showed that the strain occurring mainly in the section near the base of the electrical field was the highest, and therefore corresponded to the electrostatic force. This result is presented in figure 88.

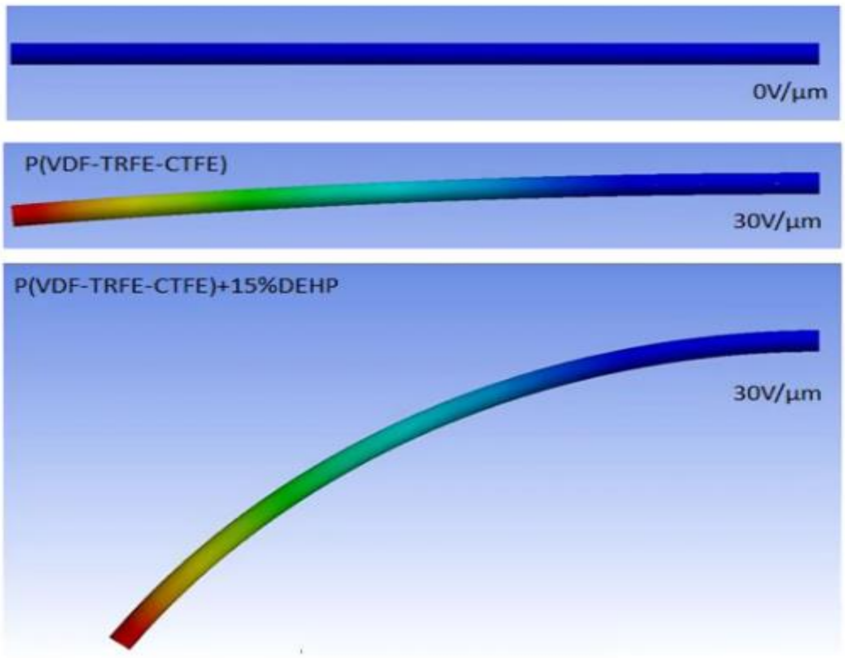

Figure 708. Bending displacement of the neat and the plasticized terpolymer under a constant electrical field of 30 V/µm.

An electrical field six times higher will be needed to obtain the same strain for a pure polymer, which corresponds to the dielectric breakdown of the material.[141]

Figure 89 described the modeled electromechanical behavior based Comsol finite element method for a 10%wt. DINP plasticized terpolymer under different level of input voltage excitation. It can be seen in Figure 90 that experimental results is in agreement to the theoretical model where discrepancy is less than 10%. The displacement response of the proposed actuator has been practically demonstrated to be sufficient to lift a rigid guide wire tip.

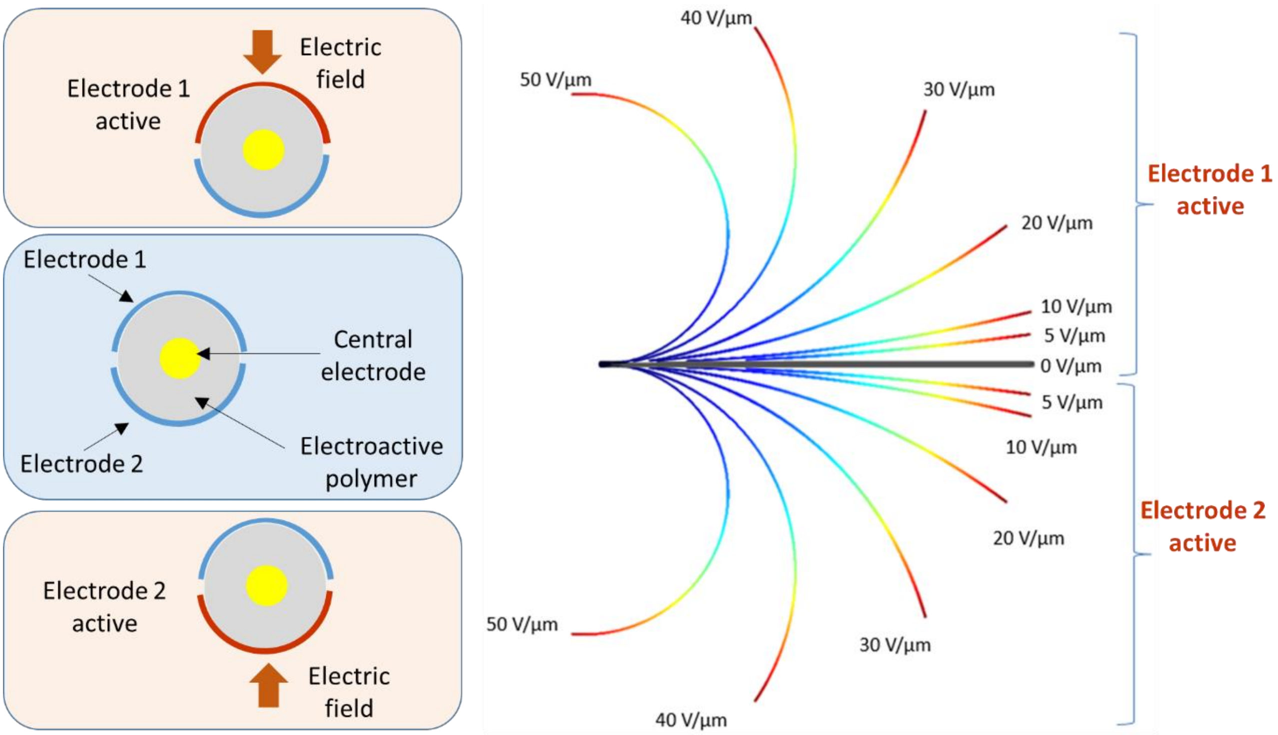

Figure 719. a) Architecture of smart guidewire based EAP driven by an electric field alternatively applied on 2 electrodes; b) Electromechnical deformation of the irradiated plasticized terpolymer under different electric field excitation.

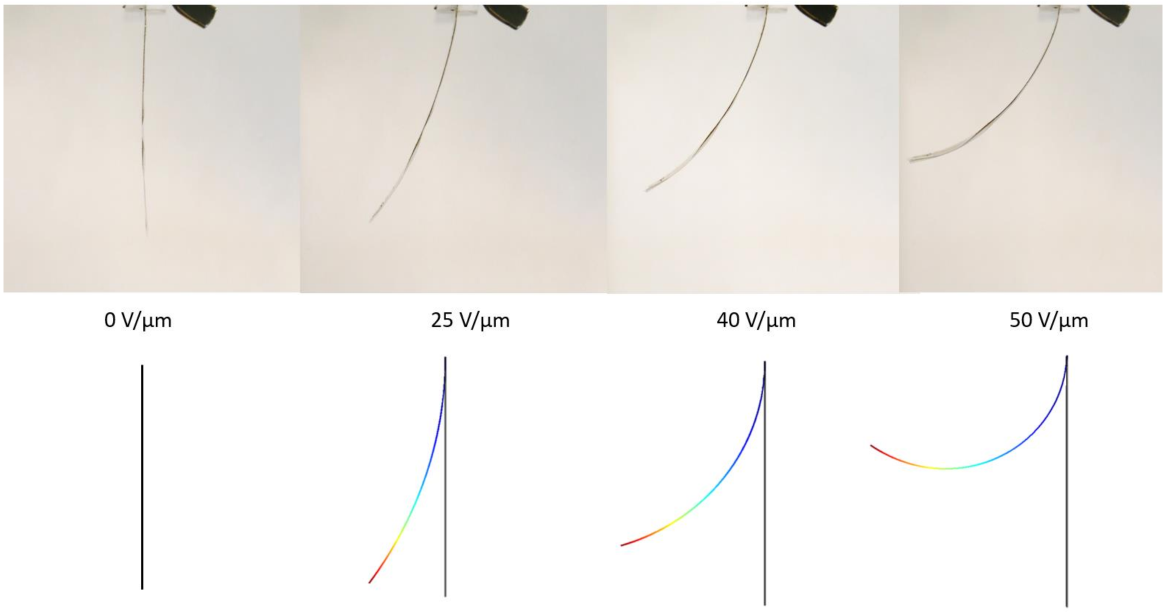

Figure 90. Experimental results of smart guide wire obtain on plasticized and irradiated prototype

Figure 91 shows the measured curvature for an electrical field of 25 V/µm as a function of the length (L)/outer dimater (D_{outer}) ratio of the tube. It is antersting to note that theachievable curvature for a constant electrical field was higher when the L/D_{outer} ratio was maximal.This dependence was logical since the global stiffness of the structure was lower when the ratio was high.[181]

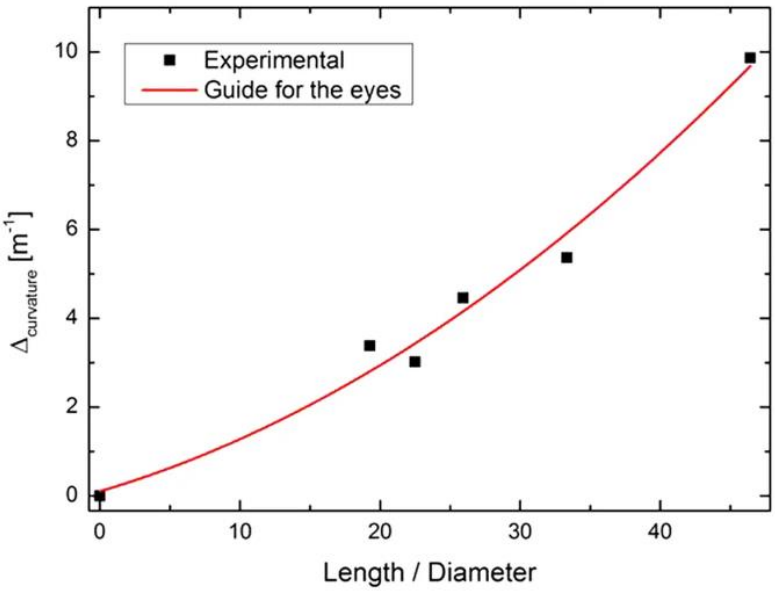

Figure 91. Experimental bending angles as a function of the electrical field.

Figure 92 shows the bending angles generated as a function of a static electrical field at room temperature for a sample with a length of 65 mm, an inner diameter of 1 mm and a outer diameter of 1,4 mm. A quadratic dependence between the bending angles and the electrical field can be noted. This observation corresponds to the theory that shows such a dependence between the strain and the electrical field in electrostrictive materials.[182,183] Moreover, the bending angle produced by the proposed design corresponds to the typical angle available in the human body,[125] making it possible to navigate through the blood vessels.

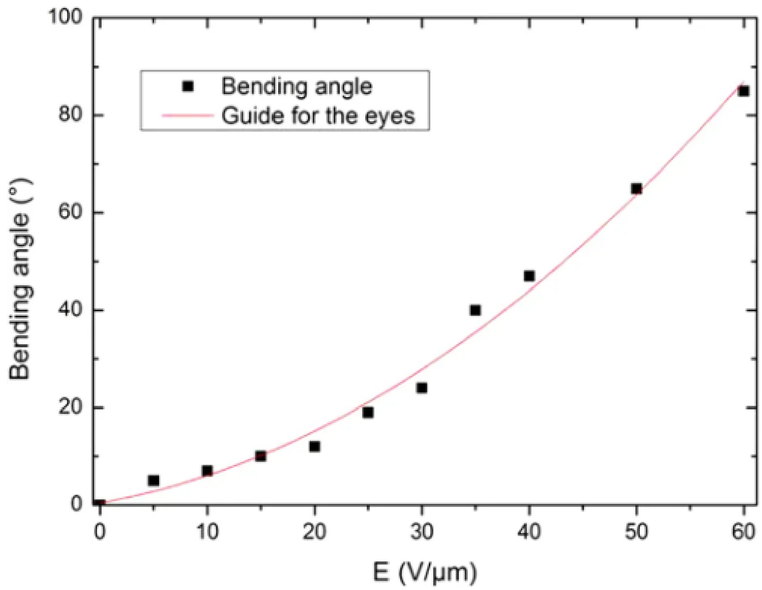

Figure 92. Smart guide wire for two electrical fields.

In order to significantly reduce the needing voltage, it is necessary to reduce the thickness of the electrostrictive material. This can be achieved based on a multilayer structure consisting several thin electrostrictive polymers sandwiched between the electrodes. For this structure, we work with Zeus Company which is capable to extrude the polymer in very thin layers. Figure 93 shows the new tubes fabricated by Zeus Company.

Figure 723. Tubes of terpolymer fabricated by Zeus Company.

III.4.d.Conclusions

This section presents the modeling and development of a terpolymer tube for the steering of a guide wire. This prototype seems to be an efficient device to easily navigate into human angulated vessels.

Further empirical tests in *in vitro* and *in vivo* conditions should be investigated in future work for better assess the new device performance.

Part IV:

Conclusions

and

Perspectives

IV.1. Conclusions

Since the last decade, endovascular techniques are the first line treatment for most of the cardiovascular diseases. For all endovascular procedures, a guide wire is needed to navigate into the arterial circulation and to support the endoprosthesis and the stents. They are many angulations in the human arterial tree and commercially usual guide wires are straight. To entry in angulated arteries, angulated catheters are needed. A steerable guide wire could be a very interesting device to reduce arterial complications and procedural costs.

EAPs which can realize the conversion between electrical and mechanical energy in both ways, have been emerging as one of the most interesting smart materials in the past two decades and many applications are possible. P(VDF-TrFE-CTFE) is particularly interesting because of excellent electromechanical performances. Its main drawback is the great voltage necessary to obtain the desired deformation.

In this work, after having explained, in the Chapter 1.a, the reasons why this terpolymer was chosen, we elaborate it into films and we characterize it in detail in Chapter 1.c.

In the Chapter 1.b, we studied the figures of merit of polymers to achieve a method to enhance performances of polymers. Then we studied the FOM of the neat and the modified terpolymer. The experimental results revealed a large enhancement of the electromechanical activities in terms of free deflection and generated force under relatively low electric field on the modified terpolymer with DEHP. These results confirm the high potential of the developed material for real-world actuator applications, especially in multifunctional flexible electroactive devices.

In the Chapter 2, we reported the effect of plasticizers on the electrostrictive behavior of terpolymer blends. The fact of incorporating a plasticizer into the polymer matrix was clearly an easy and cheap way to dramatically reduce the applied electric field while maintaining the electrostrictive strain performance. It was concluded in this study that DINP led to the best performance in terms of electrical and mechanical properties, involving in excellent electrostrictive strain response as well as mechanical energy density. It appeared that the transverse strain increased as a function of the DINP quantity.

This improved terpolymer will certainly be considered as one of the most appropriate candidates allowing us to overcome several limitations of the existing electroactive polymer, such as high input voltage, low strain and limited energy density.

Accordingly, the novel material developed was validated by a simple and efficient demonstration of the morphing structure confirming its possible use for medical flexible device as steerable guide wire in the Chapter 2.d.

In the Chapter 3, we focus on demonstrating that the polymer could be used for medical invasive device that means it could resist to sterilization and it could be biocompatible with vascular cells. So, in the chapter 3.a, we submit the terpolymer to beta-radiations to sterilize it. Sterilization of all medical devices is required to reduce the contamination risk for the patient. Our study revealed that the ionizing β-ray did not significantly alter the intrinsic properties of the neat/plasticized terpolymers, causing no change in its electromechanical activities as well as its thermal and electrical characteristics. These results are extremely interesting, suggesting the possibility of using EAP as biocompatible and sterilizable material that can be implemented in future smart guidewire for endovascular surgery.

In the Chapter 3.b, we evaluate the cellular compatibility of the neat and the modified terpolymer. These experiments show that the terpolymer and the plasticizer are not cytotoxic. They don't alter cell proliferation.

In the Chapter 4, we work on the modeling of the structure and design of the smart guide wire and we realize a first tubular prototype. We tested the bending of this prototype. These experiments confirm that this prototype seems to be an efficient device to easily navigate into human angulated vessels.

As we can see on the figure 94, our work has reached the level 4 in the Technology Readiness Level. We will see in the following sections the future work envisaged in order to reach the TRL 9.

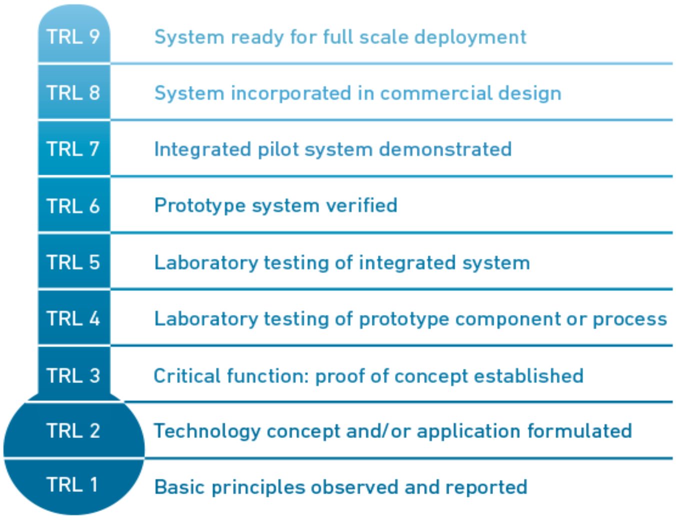

Figure 734. The Technology Readiness Level (TRL)

IV.2. Futures experiments and perspectives

The next step will consist to finalize the prototype in order to test it in an in vitro model of intra-arterial navigation. We will create this in vitro model with a silicon circuit with arterial angulation. We will create an abdominal aortic silicon phantom with left and right renal arteries with two different angulations. Then we will penetrate in the circuit with the prototype and we will apply various electrical fields in order to obtain the angulation needing to entry in the renal arteries. We will use a camera to film this step.

When we obtain good and reproducible results in this in vitro model, we will begin an in vivo model. We have chosen the pig for this in vivo model. The pig seems to be the better model because of its arterial anatomy truly comparable to that of human. It is necessary that arterial diameter and branch angulations are close to those of human so that the results are the most relevant to humans. Moreover, femoral artery puncture is not difficult.

This in vivo study will permit to validate the technical efficacy of the prototype by catheterize several angulated arteries. This model will also permit to verify the security of the prototype particularly because of the electrical field. We have already started writing the experimental protocol. The animal experiments will take place at the CERMEP Laboratory. We obtained their agreement for this protocol. All the surgical and anesthetic materials are available in this laboratory particularly the brightness amplifier to do the surgery under radioscopy. A radio-opaque marker will be added at the end of the smart guide wire to be able to follow it on the screen.

In order to respect the ethics for animals and the rule of 3R for animal experimentation (Reduce, Refine, Replace) we will use pigs already used for another protocol. It's a protocol studying cardiac transplantation needing the heart harvesting. We will make our experiments and then the other team will make them experiments.

After these in vitro and in vivo studies, if technical efficacy is validated with the prototype, we will contact companies which fabricate guide wires to see if they could be interested by our new possible device in order to move from the prototype to the final device usable in humans.

This in vivo study will not permit to verify the absence of toxicity of the terpolymer on animal cells and tissues. So we will perform at the same time another in vivo study on mice. The goal of this study is to analyze the effects of the terpolymer on cells and tissues. We will surgically introduce a piece of terpolymer film subcutaneously on mice and let it during several days. After this delay, we will euthanize the mice and analyze their tissues and cells in contact with the terpolymer. With histologic colorations, we will particularly analyze if the terpolymer induce inflammation.

In parallel, we will perform other cellular studies to analyze the adhesion of the cells on the material in scanning microscopy. We will evaluate this phenomenon without any external stimulation but also with the application of an electrical field. We will reproduce works realized about copolymer and osteogenesis. We will see if the terpolymer induces a modification of the adhesion, the orientation and the proliferation of the cells. For this study, we will use endothelial cells.

The goal of all these new experiments is to obtain the CE marking for this new invasive but non implantable device.

Finally, for the instance, we worked only on the terpolymer as actuator. But this terpolymer can be used also as sensor. We plan to work on this sensor function as well. Indeed, this function of the same material could permit us to measure the intra-arterial blood pressure before and after a stenotic lesion to evaluate if this lesion is hemodynamically significant. In interventional cardiology, it exists a guide wire with a sensor function. This technology is named FFR for fractional flow reserve. Our device could combine the 2 functions.

It will be a very smart device which can be very interesting for vascular surgeons but also for cardiologists, radiologists… for public health by the costs reduction and for the patients by the reduction of complications. It could be commercialized and sold in thousands copies every day.

References

1. Roth GA, Johnson C, Abajobir A, Abd-Allah F, Abera SF, Abyu G, et al. Global, Regional, and National Burden of Cardiovascular Diseases for 10 Causes, 1990 to 2015. J Am Coll Cardiol. 4 juill 2017;70(1):1‑25.

2. Song P, Rudan D, Zhu Y, Fowkes FJI, Rahimi K, Fowkes FGR, et al. Global, regional, and national prevalence and risk factors for peripheral artery disease in 2015: an updated systematic review and analysis. Lancet Glob Health. août 2019;7(8):e1020‑30.

3. Reimerink JJ, van der Laan MJ, Koelemay MJ, Balm R, Legemate DA. Systematic review and meta-analysis of population-based mortality from ruptured abdominal aortic aneurysm. Br J Surg. oct 2013;100(11):1405‑13.

4. Cervin A, Ravn H, Björck M. Ruptured popliteal artery aneurysm. Br J Surg. 2018;105(13):1753‑8.

5. Leake AE, Avgerinos ED, Chaer RA, Singh MJ, Makaroun MS, Marone LK. Contemporary outcomes of open and endovascular popliteal artery aneurysm repair. J Vasc Surg. janv 2016;63(1):70‑6.

6. Aboyans V, Ricco J-B, Bartelink M-LEL, Björck M, Brodmann M, Cohnert T, et al. 2017 ESC Guidelines on the Diagnosis and Treatment of Peripheral Arterial Diseases, in collaboration with the European Society for Vascular Surgery (ESVS): Document covering atherosclerotic disease of extracranial carotid and vertebral, mesenteric, renal, upper and lower extremity arteriesEndorsed by: the European Stroke Organization (ESO)The Task Force for the Diagnosis and Treatment of Peripheral Arterial Diseases of the European Society of Cardiology (ESC) and of the European Society for Vascular Surgery (ESVS). Eur Heart J. 01 2018;39(9):763‑816.

7. Mascarenhas JV, Albayati MA, Shearman CP, Jude EB. Peripheral arterial disease. Endocrinol Metab Clin North Am. mars 2014;43(1):149‑66.

8. Norgren L, Hiatt WR, Dormandy JA, Nehler MR, Harris KA, Fowkes FGR, et al. Inter-Society Consensus for the Management of Peripheral Arterial Disease (TASC II). J Vasc Surg. janv 2007;45 Suppl S:S5-67.

9. Marso SP, Hiatt WR. Peripheral arterial disease in patients with diabetes. J Am Coll Cardiol. 7 mars 2006;47(5):921‑9.

10. Stather PW, Sidloff D, Dattani N, Choke E, Bown MJ, Sayers RD. Systematic review and meta-analysis of the early and late outcomes of open and endovascular repair of abdominal aortic aneurysm. Br J Surg. juin 2013;100(7):863‑72.

11. de Ruiter QMB, Moll FL, van Herwaarden JA. Current state in tracking and robotic navigation systems for application in endovascular aortic aneurysm repair. J Vasc Surg. janv 2015;61(1):256‑64.

12. Rafii-Tari H, Payne CJ, Yang G-Z. Current and emerging robot-assisted endovascular catheterization technologies: a review. Ann Biomed Eng. avr 2014;42(4):697‑715.

13. Schwein A, Kramer B, Chinnadurai P, Walker S, O'Malley M, Lumsden A, et al. Flexible robotics with electromagnetic tracking improves safety and efficiency during in vitro endovascular navigation. J Vasc Surg. 2017;65(2):530‑7.

14. Schwein A, Kramer B, Chinnadurai P, Virmani N, Walker S, O'Malley M, et al. Electromagnetic tracking of flexible robotic catheters enables « assisted navigation » and brings automation to endovascular navigation in an in vitro study. J Vasc Surg. 2018;67(4):1274‑81.

15. Manstad-Hulaas F, Ommedal S, Tangen GA, Aadahl P, Hernes TN. Side-branched AAA stent graft insertion using navigation technology: a phantom study. Eur Surg Res Eur Chir Forsch Rech Chir Eur. 2007;39(6):364‑71.

16. Abi-Jaoudeh N, Glossop N, Dake M, Pritchard WF, Chiesa A, Dreher MR, et al. Electromagnetic navigation for thoracic aortic stent-graft deployment: a pilot study in swine. J Vasc Interv Radiol JVIR. juin 2010;21(6):888‑95.

17. Manstad-Hulaas F, Tangen GA, Gruionu LG, Aadahl P, Hernes TAN. Three-dimensional endovascular navigation with electromagnetic tracking: ex vivo and in vivo accuracy. J Endovasc Ther Off J Int Soc Endovasc Spec. avr 2011;18:230‑40.

18. Kim Y, Parada GA, Liu S, Zhao X. Ferromagnetic soft continuum robots.Science Robotics.2019.4.

19. L. Lebrun, D. Guyomar, B. Guiffard, PJ. Cottinet, C. Putson. Sensors and actuators A 153 (2009) 251-257.

20. P. Colombo. Polymer-derived ceramics : 40 years of research and innovation in advanced ceramics. J. Am. Ceram. Soc.2010;93:1805-1837.

21. Raghu Das. Electroactive polymers and devices 2013-2018: forecasts, technologies, players dielectric elastomers, electronic and ionic EAPs and their applications.

22. W.C Roentgen. About the changes in shape and volume of dielectrics causes by electricity. Section III in G. Wiedemann (Ed.), Annual Physics and chemistry series.1880;11:771-786.

23. M.P. Sacerdote. Strains in polymers due to electricity. J. Phys. Ser.1899;3(8):282.

24. M. Eguchi. On the permanent electret. Philosophical Magazine.1925;49:178.

25. A. Katchalsky. Rapid swelling and deswelling of reversible gels of polymeric acids by inization.Cellular and molecular Life science.1949.

26. H. Kawai. The piezoelectricity of poly(vinylidene fluoride). Japanese Journal of Applied physics.1969;8(7):975-976.

27. J.C. Bergman. Pyroelectricity and optical second harmonic generation in polyvinylidene fluoride films. Applied physics letters.1971;18(5):203-205.

28. M. Tamura, K. Ogasawara, N. Ono, S. Hagiwara. Piezoelectrocity in uniaxially stretched poly(vinylidene fluoride). journal of appllied physics.1974;45(9):3768-3771.

29. A.M. Glass, J.H. Mcfee, J.C Bergman Jr. Pyroelectricity properties of polyvinyidene fluoride and its use for intrared detection. Journal of applied physics.1971;42(13):5219-5222.

30. T. Yamada, T. Ueda, T. Kitayama. Ferroelectric-to-paraelectric phase transition of vinylidene fluoride-trifluoroethylene copolymer. Journal of applied physics.1981;52(2):948-952.

31. H.Ohigashi, K. Koga. Ferroelectric copolymers of vinylidenefluoride and trifluoroethylene with a large electromechanical coupling factor. Japanese journal of applied physics.1982;21(8A):L455.

32. H. Ohigashi. Electromechanical properties of polarized polyvinylidene fluoride films as studied by the piezoelectric resonance method. Journal of applied physics.1976;47(3):949-955.

33. M. Oshiki, E. Fukada. Inverse piezoelectric effect and electrostrictive effect in polarized poly(vinylidene fluoride) films. Journal of materials science.1975;10(1):1-6.

34. T. Furukawa, G.E Johnson, H.E. Bair, Y. Tajitsu, A. Chiba, E. Fukada. Ferroelectric phase transition in a copolymer of vinylidene fluoride and trifluoroethylene. Ferroelectrics.1981;32(1):61-67.

35. H. Shirikawa, L. Edwin,A.G Macdiarmid, C.K. Chiang, A.J.Heeger. Synthesis of electrically conducting organic polymers : halogen derivatives of polyacetylene. Journal of the chemical society.1977;16:578-580.

36. A.J. Lovinger. Ferroelectric polymers. Science.1983;220:1115-1121.

37. T. Furukawa. Ferroelectric properties of vinylidene fluoride copolymers. Phase transition, A multinational journal.1989;18:143-211.

38. K. Oguro, Y. Kawami, H. Takenaka. Bending of a ion-conducting polymer film-electrode composite by an electric stimulus at low voltage. Journal of micromachine society.1992;5:27-30.

39. Q.M. Zhang, V. Bharti, G. Kavarnos, M. Schwartz. Poly(vinylidene fluoride (PD+VDF) and its copolymers. Encyclopedia of smart materials.1,2:807-825.

40. R.H. Baugman, et al. Carbon nanotube actuators. Science.1999;284(5418):1340-1344.

41. Y. Bar-Cohen. Electroactive polymers: current capabilities and challenges. Proceedings of the SPIED Smart Structures and Materials Symposium, EAPAD, 1999. Paper 4695-02.

42. Y. Bar-Cohen. Biomimetics: biologically inspired technollogies. CRC Press, 2006.

43. M. Shahinpoor, Y. Bar-Cohen, T. Xue, J.O Simpson, J.Smith. ionic polymer-metal composites as biomimetics sensors, actuators and artificial muscles. A review.Smart Materials and Structures.1998;7(6):R15.

44. T. Hirai, T. Ueki, M. Takasaki. Electrical actuation of textile polymer materials. Journal of fiber bioengineering and informatics.2008.

45. H. Takenaka, E. Torikai, Y. Kawami, N. Wababayashi. Solid polymer electrolyte water electrolysis. International journal of hydrogen Energy.1982;7(5):397-403.

46. P. Millet, M. Pineri, R. Durand. New solid polymer electrolyte composites for water electrolysis. Journal of applied electrochemistry.1989.19(2):162-166.

47. K.J. Kim, M. Shahinpoor. Ionic polymer metal composites: II. Manufacturing techniques. Smart materials and structures.2003;12(1):65.

48. S. Nemat-Nasser, J.Y. Li. Electromechanical response of ionic polymer metal composites. Journal of applied physics.2000;87(7):3321-3331.

49. S. Nemat-Nasser. Micromechanics of actuation of ionic polymer-metal composites. Journal of applied physics.2002;92(5):2899-2915.

50. K.J. Kim, M. Shahinpoor. A novel method of manufacturing three-dimensional ionic polymer metal composites biomimetic sensors, actuators and artificials muscles.Polymers.2002;43:797-802.

51. Y. Bar-Cohen, T. Xue, M. Shahinpoor, J.O Simpson, J.Smith. Flexible, low mass robotic ar actuated by electroactive polymers. Proceedings of SPIE's 5th annual international symposium on smart structures and materials.San Diego.1998.

52. Y.Tong, Z. Xue, X. Zhou, X. Xie, C.Y. Tang. Novel sulfonated polysulfone ion exchange membranes for ionic polymer-metal composite actuators. Sensors and actuators B: Chemical.2014;202(0):11664-1174.

53. Y. Tang, C. Chen, Y.S. ye, Z. Xue, X. Zhou, X. Xie. The enhanced actuation response of an ionic polymer-metal composite actuator based on sulfonated polyphenylsulfone. Polymer chemical.2014;5:6097-6107.

54. C. Jo, D. Pugal, I.K. Oh, K.J. Kim, K. Asaka. Recent advances in ionic polymer-metal composite actuators and their modeling and applications. Progress in polymer science.2013;38(7):1037-1066.

55. S.W. Yeom, I.K. Oh. A biomimetic jellyfish robot based on ionic polymer metal composite actuators. Smart materials and structures.2009;18(8).

56. H. Tamagawa, M. Taya. A theoretical prediction of the ions distribution in an amphoteric polymer gel. Materials science and engineering A.2000;285:314-325.

57. Y. Osada, J.P. Gong. Soft and wet materials: polymer gels. Advanced materials.1998;10:827-837.

58. P. Brochu, Q. Pei. Advances in dielectric elastomers for actuators and artificial muscles. Macromolecular rapid communications.2010;31(1):10-36.

59.T. Mirfakhrai, J.D.W. Madden, R.H. Baughmann. Polymer artificial muscles. Materials today.2007;10(4):30-38.

60. E.W.H Jager, E. Smela, O. Inganas. Microfabricating conjugated polymer actuators. Science.2000;290(5496):1540-1545.

61. S. Hara, T. Zama, W. Takashima, K. Kaneto. Tris(trifluoromethylsulfonyl)methide doped polypyrrole as a conducting polymer actuator with large electromechanical strain. Synthetic metals.2006;156(2-4):351-355.

62. R.H. Baughmann. Conducting polymer artificial muscles. Synthetic metals. 1996;78(3):339-353.

63. E. Smela. Conjugated polymer actuators for biomedical applications. Advanced materials. 2003;15(6):481-494.

64. S. Iijima. Helical microtubules of graphitic carbon.Nature.1991;354(6348):56-58.

65. S.Iijima, T. Ichihashi. Single-shell carbon nanotubes of 1 nm diamter. Nature.1993;363(6430):603-605.

66. G. Gao, T. Cagin, W.A. goddard III. Energetics, structure, mechanical and vibrational properties of single-walled carbon nanotubes. Nanotechnology.1998;9(3):184.

67. U. Vohrer, I. Kolaric, M.H. Haque, S. Roth, U. Detlaff-Weglikowska. Carbon nanotube sheets for the use as artificial muscles. Carbon.2004;42(5-6):1159-1164.

68. M. Hughes, G.M. Spinks. Multiwalled carbon nanotube actuators. Advanced materials.2005;17(4):443-446.

69. R.H. Baughmann, A.A. Zakhidov, W.A. de Heer. Carbon nanotube-the route toward applications. Science.2002.297(5582):787-792.

70. D. Li, W.F. Paxton, R.H. Baughmann, T.J. Huang, J.F. Stoddart, P.S. Weiss. Molecular supramolecular, and macromolecular motors and artificial muscles. MRS Bulletin.2009;34:671-681.

71.M. Zhang, K.R. Atkinson, R.H. Baughmann. Multifunctional carbon nanotube yarns by downsizing an ancient technollogy. Science.2004;306(5700):1358-1361.

72. A.M. Fennimore, T.D. Yuzvinsky, W.Q. Han, M.S. Fuhrer, J. Cumings, A. Zettl. Rotational actuators based on carbon nanotubes. Nature. 2003;424(6947):408-410.

73. J. Foroughi, et al. Torsional carbon nanotube artificial muscles. Science. 2011;334(6055):494-497.

74. M.D. Lima, et al. Electrically, chemically, and photonically powered torsional and tensile actuation of hybrid carbon nanotube yarn muscles. Science.2012;338(6109):928-932.

75. J.A Lee, et al. All-solid-state carbon nanotube torsional and tensile artificial muscles. Nano letters.2014;14(5):2664-2669.

76. R.E. Pelrine, R.D. Kornbluh, J. R. Heydi, Q. Pei, S. Chiba. High-field deformation of elastomeric dielectrics for actuators. Materials science and engineering C.2000;11:89-100.

77. M. Zhenyi, J.I. Scheinbeim, J.W. Lee, B.A. Newman. High field electrostrictive response of polymers. Journal of polymer science Part B: Polymer physics.1994;32(16):2721-2731.

78. R.E. Pelrine, R.D. Kornbluh, J.P. Joseph. Eleectrosctriction of polymer dielectrics with compliant electrodes as a means of actuation. Sensors and actuators A: Physical.1998;64(1):77-85.

79. J.S. Plante, S. Dubowsky. large-scale failure modes of dielectric elastomer actuators. International journal of solids and structures. 2006;43(25-26):7727-7751.

80. R.E. Pelrine, R.D. Kornbluh, Q. Pei, J. Joseph. High-speed electrically actuated elastomers with strain greater than 100 %. Science.2000;287(5454):836-839.

81. R.E. Pelrine, R.D. Kornbluh, G. Kofod. High-strain actuators materials based on dielectric elastomers. Advanced materials.2000;12:1223-1225.

82. R.D. Kornbluh, et al. Electroelastomers: Applications of dielectric elastomers transducers for actuation, generation, and smart structures. Proc. SPIE.2002;4698:254-270.

83. J. Biggs, et al. Electroactive polymers: developments of and perspectives for dielectric elastomers. Angewandte Chemie international edition.2013;52(36):9409-9421.

84. R. Shankar, T.K. Ghosh, R.J. Spontak. Dielectric elastomers as next generation polymeric actuators.Soft Matter.2007;3:1116-1129.

85. M. Watanabe, T.H.M. Suzuki, Y. Amaike. Electric conduction in bending electrostriction of polyurethanes. Appl. Phys. Letter.1999;74:217.

86. Guiffard B, et al. Enhanced electroactive properties of polyurethane films loaded with carbon -coated SiC nanowires. Journal of physics D, applied physics.2009;42:3722-3727.

87. Q. Pei, R.E. Pelrine, M.A. Rosenthal, S. Standford, H. Prahlad, R.D. Kornbluh. Recent progress on electroelastomer artificial muscles and their applications for biomimetic robots.Proc. SPIE.2004;5385:41-50.

88. P. Brochu, X. Niu, Q. Pei. Acrylic interpenetrating polymer network dielectric elastomers for energy harvesting. Electroactive polymer actuators and devices. 2011;7976:797606.

89. S.M. Ha, et al. High electromechanical performance of electroelastomers based on interpenetrating polymer networks.Proc. SPIE.2008;6927:69272C-9.

90. C. Hunag, Q.M. Zhang, G. deBotton, K. Bhattacharya. All-organic dielectric percolative-three-component composite materials with high electromechanical response.Applied physics letters.2004;84(22):4391-4393.

91. F. Carpi, D.D. Rossi. Improvement of electromechanical actuating performances of a silicone dielectric elastomer by dispersion of titanium dioxide powder.IEEE transactions on dielectrics and electrical insulations.2005;12(4):835-843.

92. B. Kussmaul, et al. Enhancement of dielectric permittivity and electromechanical response in silicone elastomers: molecular grafting of organic dipoles to the macromolecular network. Advanced Functional Materials.2011;21(23):4589-4594.

93. S. Rosset, H.R. Shea. Flexible and stretchable electrodes for dielectric elastomer actuators.Applied physics A.2013;110(2):281-307.

94. J. Su, J.S. Harrison, T.L. Clair, Y. Bar-cohen, S. Leary. Electrostrictive graft elastomers ans applications.MRS symposium: FF:Electroactive polymers.Boston.1999.

95. Y. Wang, C. Sun, E. Zhou, J. Su. Deformation mechanisms of electrostrictive graft elastomer. Smart materials and structures.2004;13:1407-1413.

96. P.G. de Gennes, T.C. Chung. Réflexions sur un type de polymères nématiques.Seances Acad. sci. ser.B.1975;281:101.

97. C. Ohm, M. Brehmer, R. Zentel. Liquid crystalline elastomers as actuators and sensors. Advanced materials.2010;22(31):3366-3387.

98. D.L. Thomsen, et al.Liquid crystal elastomers with mechanical properties of a muscle. Macromolecules.2001;34(17):5868-5875.

99. M. Kondo, Y. Yu, T. Ikeda. How does the initial alignment of mesogens affect the photo-induced bending behavior of liquid-crystalline elastomers ?Angewandte chemie.2006;118(9):1406-1410.

100. Y. Yu, T. Ikeda. Soft actuators based on liquid-crystalline elastomers. Angewandte chemie international edition.2006;45(33):5416-5418.

101. M. Chambers, H. Finkelmann, M. Remskar, A. Sanchez-ferrer, B. Zalar, S. Zumer. Liquid-crystal elastomer nanoparticle systems for actuation. J. mater. chem. 2009;19:1524-1531.

102. C. Huang, Q.M. Zhang, A. Jakli. Nematic anisotropic liquid-crystal gels self-assembled nanocomposites with high electromechanical response. Advanced functional materials.2003;13(7):525-529.

103. W. Lehmann, et al. Giant lateral electrostriction in ferroelectric liquid-crystalline elastomers. Nature.2001;410(6827):447-450.

104.H. Yang, et al. Micron-sized main-chain liquid crystalline elastomer actuators with ultralarge amplitude contractions. Journal of the american chemical society.2009;131(41):15000-15004.

105. A. M. Vinogradov, V.H. Schmidt, G.F. Tuthill, G.W. Bohannan. Damping and electromechanical energy losses in the piezoelectric polymer PVDF. Mechanics of materials.2004;36:1007-1016.

106. L. Zhu, Q. Wang. Novel ferroelectric polymers for high energy density and low loss dielectrics. Macromolecules.2012;45(7):2937-2954.

107. T. Yagi, M. Tatemoto, J. Sako. Transition behavior and dielectric properties in trifluoroethylene and vinylidene fluoride copolymers.Polymer journal.1980;12(4):209:223.

108. A.J. Lovinger, T. Furukawa, G.T. Davis, M.G. Broadhurst. Curie transitions in copolymers of vinylidene fluoride. Ferroelectrics.1983;50(1):227-236.

109. S. Khan, et al. Flexible tactile sensors using screen-printed P(VDF-TrFE) and MWCNT/PDMS composites. IEEE sensors journal.2015;15(6):3146-3155.

110. F. Guan, et al. Crystal orientation effect on electric energy storage in poly(vinylidene-fluoride-co-hexafluoropropylene) copolymers. Macromolecules. 2009;43(1):384-392.

111. Q.M. Zhang, V. Bharti, X. Zhao. Giant electrostriction and relaxor ferroelectric behavior in electron-irradiated poly(vinylidene fluoride-trifluoroethylene) copolymer. Science.1998;280(5372):2101-2104.

112. X.Z. Zhao, V. Bharti, Q.M. Zhang, T. Romotowski, F. Tito, R. Ting. Electromechanical properties of elecrostrictive poly(vinylidene fluoride trifluoroethylene) copolymer. Appllied physics letters.1998;73(14):2054-2056.

113. Z.Y. Cheng, V. Bharti, T.B. Xu, H. Xu, T. Mai, Q.M. Zhang. Electrostrictive poly(vinylidene fluoride trifluoroethylene) copolymers.Sensors and actuators A: Physical.2001;90(1-2):138-147.

114. F. Bauer. relaxor fluorinated polymers: novel applications and recent developments. IEEE Transactions on dielectrics and electrical insulation.2010;17(4):1106-1112.

115. H. Xu, Z.Y. Cheng, D. Olson, T. Mai, Q.M. Zhang, G. Kavarnos. Ferroelectric and electromechanical properties of poly(vinylidene-fluoride-trifluoroethylene-chlorotrifluoroethylene) terpolymer. Applied physics letters.2001;78(16):2360-2362.

116. F. Xia, et al. High electromechanical responses in a poly(vinylidene-fluoride-trifluoroethylene-chlorotrifluoroethylene) terpolymer. Advanced materials.2002;14(21):1574-1577.

117. Q.M. Zhang, et al. An all-organic composite actuator material with a high dielectric constant. Nature.2002;419(6904):284-287.

118. X. Yin, JF Capsal, D. Guyomar. A comprehensive investigation of poly(vinylidene-fluoride-trifluoroethylene-chlorofluoroethylene) terpolymer nanocomposites with carbon-black for electrostrictive applications. Applied physics letters.2014;104(5):p.052913

119. S.H. Bae, et al. Graphene-P (VDF-TrFE) multilayer film for flexible applications. ACS nano.2013;7(4):p.3130-3138.

120. C. Huang, M.Q. Zhang. Enhanced dielectric and electromechanical responses in high dielectric constant all-polymer percolative composites.Advanced functional materials.2004;14(5):501-506.

121. S. Zhang, N. Zhang, C. Huang, K. Ren, Q.M. Zhang. Microstructure and electromechanical properties of carbon nanotube/poly(vinylidene-fluoride-trifluoroethylene-chlorotrifluoroethylene) composites.Advanced materials.2005;17(15):1897-1901.

122. F. Bauer, E. Fousson, Q.M. Zhang. Recent advances in highly electrostrictive P(VDF-TrFE-CTFE) terpolymers. IEEE transactions on dielectrics and electrical insulation.2006;13(5):1149-1154.

123.J.D.W. Madden. Artificial muscle technology: physical principles and naval prospects.IEEE journal of oceanic engineering.2004;29(3):706-728.

124. N. Della Schiava, K. Thetpraphi, M.Q. Le, P. Lermusiaux, A. Millon, J.F. Capsal, P.J. Cottinet. Enhanced Figures of Merit for a high-performing actuator in electrostrictive materials. Polymers.2018;10(3):263.

125. G.M. Hutchins, M.M. Miner, J.K. Boitnott. Vessel caliber and branch-angle of human coronary artery branch points.Circ. Res.1976;38:572-576.

126. G. Liegeon, N. Della Schiava. Marquage CE d'un fil guide intelligent. Mémoire de stage école ISIFC génie biomédical. 2018.

127. D.G. Wiley. Measuring reaction time.Phys. Teach.1985;23:314.

128. Bauer, F.; Fousson, E.; Zhang, Q. M. Recent Advances in Highly Electrostrictive P(VDF-TrFE-CFE) Terpolymers. *IEEE Trans. Dielectr. Electr. Insul.* 2006;*13*(5):1149–1154.

129. Klein, R. J.; Xia, F.; Zhang, Q. M.; Bauer, F. Influence of Composition on Relaxor Ferroelectric and Electromechanical Properties of Poly(vinylidene Fluoride-Trifluoroethylene-Chlorofluoroethylene). *J. Appl. Phys.*2005 ;*97*(9) :094105.

130. Wise S A. Displacement properties of RAINBOW and THUNDER piezoelectric actuators Sens. Actuators Phys.1998;69:33–8.

131. Shankar R, Ghosh T K and Spontak R J.Mechanical and actuation behavior of electroactive nanostructured polymers Sens. Actuators Phys.2009;151:46–52.

132. Bar-Cohen Y, Sherrit S, Lih SS. Characterization of the electromechanical properties of EAP. Materials.2001;4329:319-327

133. Cottinet PJ, Le MQ, Degraff J, Souders C, Liang Z, Wang B, Zhang C. Strain phenomenon in carbon nanotube buckpaper actuator.Experiments and modeling Sens. Actuators Phys.2013; 194:252–258.

134. De Tommasi D, Puglisi G and Zurlo G. Hysteresis in electroactive polymers Eur. J. Mech. – A Solids.2014;48:16–22.

135. Watanabe M, Suzuki M, Hirako Y, Shirai H and Hirai T. Hysteresis in bending electrostriction of polyurethane films J. Appl. Polym. Sci.2001;79:1121–6.

136. Le M Q, Capsal J-F, Galineau J, Ganet F, Yin X, Yang M (Dawn), Chateaux J-F, Renaud L, Malhaire C, Cottinet P-J and Liang R. All-organic electrostrictive polymer composites with low driving electrical voltages for micro-fluidic pump applications. Sci. Rep.2015;5.

137. Wang Q-M and Eric Cross L. Constitutive equations of symmetrical triple layer piezoelectric benders IEEE Trans. Ultrason. Ferroelectr. Freq. Control.1999;46:1343–51.

138. Moskalik A J and Brei D. Force-deflection behavior of piezoelectric C-block actuator arrays Smart Mater. Struct.1999;8:531.

139. E.D.S Van Vliet, E.M. Reitano, J.S. Chhabra, G.P. Bergen, R.M. Whyatt. A review of alternatives to di (2-ethylhexyl) phthalate-containing medical devices in the neonatal intensive care unit.J Perinatol.2011;31(8):551-560.

140. SCENIHR (Scientific Committee on Emerging and Newly-Identified Health Risks). Scientific opinion on the safety of medical devices containing DEHP-plasticized PVC or other plasticizers on neonates and other groups possibly at risk, 6 February 2008.

141. Della Schiava N, Le M.Q, Galineau J, Domingues Dos Santos F, Cottinet P.J, Capsal J.F. Influence of plasticizers on the electromechanical behavior of a P(VDF-TrFE-CTFE) terpolymer: toward a high performance of electrostrictive blends. Journal of polymer science, Part B :polymer physics.2017;55:355-369.

142. Nalwa, H. S. Ferroelectric Polymers: Chemistry: Physics, and Applications. CRC Press. 1995; 28.

143. Lovinger, A. J. Ferroelectric Polymers. Science. 1983;220(4602):1115–1121.

144. Capsal, J.-F.; Galineau, J.; Lallart, M.; Cottinet, P.-J.; Guyomar, D. Plasticized Relaxor Ferroelectric Terpolymer: Toward Giant Electrostriction, High Mechanical Energy and Low Electric Field Actuators. Sens. Actuators Phys.2014 ;207:25–31.

145. Capsal, J.-F.; Galineau, J.; Le, M.-Q.; Domingues Dos Santos, F.; Cottinet, P.-J. Enhanced Electrostriction Based on Plasticized Relaxor Ferroelectric P(VDF-TrFE-CFE/CTFE) Blends. J. Polym. Sci. Part B Polym. Phys. 2015;53(19):1368–1379.

146. https://www.theguardian.com/lifeandstyle/2015/feb/10/phthalates-plastics-chemicals-research-analysis

147. https://view.joomag.com/dinp-plasticizer-global-market-dinp-plasticizer-global-market/0711093001455866711?page=2

148. https://www.plasticisers.org/plasticiser/ortho-phthalates/

149. European commission concludes DINP and DIDP safe for use in consumer applications. Additives for polymers.2014;4:11.

150. P.J. Lioy, C. Gennings, R. Hauser, H.M. Koch, A. Kortenkamp. Changing trends in phthalate exposures.Environ Health perspec.2014;122(10):A264.

151. Barsoukov, E.; Macdonald, J. R. Impedance Spectroscopy: Theory, Experiment, and Applications; John Wiley & Sons, 2005.

152. Kuder, I. K.; Arrieta, A. F.; Raither, W. E.; Ermanni, P. Variable Stiffness Material and Structural Concepts for Morphing Applications. Prog. Aerosp. Sci. 2013;63:33–55.

153. Nguyen, V. Q.; Ahmed, A. S.; Ramanujan, R. V. Morphing Soft Magnetic Composites. Adv. Mater. 2012;24(30):4041–4054.

154. Rossiter, J.; Walters, P.; Stoimenov, B. Printing 3D Dielectric Elastomer Actuators for Soft Robotics.2009;7287:72870H–72870H–10.

155. Kempaiah, R.; Nie, Z. From Nature to Synthetic Systems: Shape Transformation in Soft Materials. J. Mater. Chem. B.2014;2(17):2357–2368.

156. Abdulrahim, M.; Garcia, H.; Lind, R. Flight Characteristics of Shaping the Membrane Wing of a Micro Air Vehicle. J. Aircr. 2005;42(1):131–137.

157. Uh, K.; Yoon, B.; Lee, C. W.; Kim, J.-M. An Electrolyte-Free Conducting Polymer Actuator That Displays Electrothermal Bending and Flapping Wing Motions under a Magnetic Field. ACS Appl. Mater. Interfaces 2016;8(2):1289–1296.

158. N. Della Schiava, F. Pedroli K. Thetpraphi, A. Flocchini, M.Q. Le, P. Lermu.siaux, J.F. Capsal, P.J. Cottinet. Effect of beta-based sterilization on P(VDF-TrFE-CFE) terpolymer for medical applications.Sci Rep.2020,10 (8805).

159. Tipnis NP, Burgess DJ. Sterilization of implantable polymer-based medical devices: A review. Int J Pharm. 2018;544(2):455‑60.

160. Yang L, Li X, Allahyarov E, Taylor PL, Zhang QM, Zhu L. Novel polymer ferroelectric behavior via crystal isomorphism and the nanoconfinement effect. Polymer. 2013;54:1709-1728.

161. R.J. Klein, J. Runt, Q.M. Zhang. Influence of Crystallization Conditions on the Microstructure and Electromechanical Properties of Poly(vinylidene fluoride−Trifluoroethylene−chlorofluoroethylene) Terpolymers. Macromolecules.2003;36 :7220–7226.

162. F. Ganet, M.-Q. Le, J.F. Capsal, J.F. Gérard, S. Pruvost, J. Duchet, S. Livi, P. Lermusiaux, A. Millon, P.-J. Cottinet. Haptic feedback using an all-organic electroactive polymer composite, Sens. Actuators B Chem.2015;220:1120–1130.

163. F. Pedroli, A. Marrani, M.-Q. Le, C. Froidefond, P.-J. Cottinet, J.-F. Capsal. Processing optimization: A way to improve the ionic conductivity and dielectric loss of electroactive polymers. J. Polym. Sci. Part B: Polym. Phys. 2018;56:1164–1173.

164. Q.-M. Wang, L.E. Cross, Performance analysis of piezoelectric cantilever bending actuators. Ferroelectrics. 1998;215 :187–213.

165. J.-F. Capsal, J. Galineau, M.-Q. Le, F. Domingues Dos Santos, P.-J. Cottinet. Enhanced electrostriction based on plasticized relaxor ferroelectric P(VDF-TrFE-CFE/CTFE) blends. J. Polym. Sci. Part B: Polym. Phys. 2015;53:1368–1379.

166. K. Thetpraphi, M.Q. Le, A. Houachtia, P.-J. Cottinet, L. Petit, D. Audigier, J. Kuhn, G. Moretto, J.-F. Capsal. Surface Correction Control Based on Plasticized Multilayer P(VDF-TrFE-CFE) Actuator—Live Mirror. Adv. Opt. Mater. 2019 ;7.

167. M.Q. Le, J.-F. Capsal, J. Galineau, F. Ganet, X. Yin, M. (Dawn) Yang, J.-F. Chateaux, L. Renaud, C. Malhaire, P.-J. Cottinet, R. Liang. All-organic electrostrictive polymer composites

with low driving electrical voltages for micro-fluidic pump applications. Sci. Rep. 2015;5:11814.

168. H. Otaguro, L.F.C.P. de Lima, D.F. Parra, A.B. Lugão, M.A. Chinelatto, S.V. Canevarolo. High-energy radiation forming chain scission and branching in polypropylene. Radiat. Phys. Chem. 2010;79:318–324.

169. Gahleitner Markus, Johannes Wolfschwenger, Joachim Fiebig, Karl Dobianer, Christa Hametner. Sterilization Effects on Polypropylene. Technology and Polymer Type Effects.2003: 12–14.

170. J.L. Williams, T.S. Dunn, V.T. Stannett. Mobility as a mechanism for radiation stabilization of polypropylene. Radiat. Phys. Chem.1982;19:291–296.

171. X. Yin, M. Lallart, P.-J. Cottinet, D. Guyomar, J.-F. Capsal. Mechanical energy harvesting via a plasticizer-modified electrostrictive polymer. Appl. Phys. Lett.2016;108:042901.

172. X. Zhou, X. Zhao, Z. Suo, C. Zou, J. Runt, S. Liu, S. Zhang, Q.M. Zhang. Electrical breakdown and ultrahigh electrical energy density in poly(vinylidene fluoride-hexafluoropropylene) copolymer. Appl. Phys. Lett.2009;94:162901.

173. Palza H, Zapata PA, Pineda CA. Eleectroactive smart polymers for biomedical applications. Materials.2019;12:277.

174. Ferraz N, Stromme M, Fellstrom B, Pradhan S, Nyholm L, Myhranyan A. In vitro and in vivo toxicity of rinsed and aged nanocellulose-polypyrrole composites. Journal of biomedical materials research Part A.2012;100(8):2128-2138.

175. Gomez-Quintero T, et al. Cytotoxicity of polypyrrole and polyaniline matrixes for biosensors. Acta scientific medical science. Avril 2019;81-89.

176. Hitscherich P, Wu S, Gordan R, Xie LH, Arinzeh T, Lee EJ. The effect of pvdf-tref scaffolds on stem cell derived cardiovascular cells. Biotechnology bioengineering. 2016;113:1577-1585.

177. Augustine R, et al. Electrospun poly(vinylidene-fluoride trifluoroethylene) /zinc oxide nanocomposite tissue engineering scaffolds with enhanced cell adhesion and blood vessel formation. Nano Research.2017;10:3358-3376.

178. Ribeiro C, et al. Enhanced proliferation of pre-osteoblastic cells by dynamic piezoelectric stimulation. RSC Adv.2012;2:11504-11509.

179. Nordon I.M, Hinchliffe R.J, Holt P.J, Loftus I.M, Thompson M.M. The requirement for smart catheters for advanced endovascular applications. Proc. Inst. Mech. Eng.2010 ;224 :743-749.

180. Petit L, Guiffard B, Seveyrat L, Guyomar D. Actuating abilities of electroactive carbon nanopowder/polyurethane composite films. Sens. Actuators Phys.2008;148:105-110.

181. Song Y, Guan Z, Nie Y, Guan X. The analysis of the bending stiffness and intensity of cylindrical tubes. Sci. China Ser. E Technol. Sci.2007 ;50 :268-278.

182. Guyomar D, Yuse K, Cottinet PJ, Kanda M, Lebrun L. Focus on the electrical field-induced strain of electroactive polymers and the observed saturation. J. Applied Physics. 2010;108:114910.

183. Cottinet PJ, Guyomar D, Guiffard B, Lebrun L, Putson C. Electrostrictive polymer composite for energy harvesters and actuators. J. Polym. Eng.2011;31.

List of figures

Part I. Bibliographic study

Part II. Objectives of the PhD

PART III. Experiments and results

List of tables

Part I. Bibliographic study

Part II. Objectives of the work and experiments

APPENDICES

1. Marquage CE, directive européenne et classification des dispositifs médicaux

12. 7. 93 Journal officiel des Communautés européennes N° L 169/1

II

(Actes dont la publication n'est pas une condition de leur applicabilité)

CONSEIL

DIRECTIVE 93/42/CEE DU CONSEIL

du 14 juin 1993

relative aux dispositifs médicaux

LE CONSEIL DES COMMUNAUTÉS EUROPÉENNES,

vu le traité instituant la Communauté économique européenne, et notamment son article 100 A,

vu la proposition de la Commission [1],

en coopération avec le Parlement européen [2],

vu l'avis du Comité économique et social [3],

considérant qu'il importe d'arrêter des mesures dans le cadre du marché intérieur; que le marché intérieur comporte un espace sans frontières internes dans lequel la libre circulation des marchandises, des personnes, des services et des capitaux est assurée;

considérant que les dispositions législatives, réglementaires et administratives en vigueur dans les États membres en ce qui concerne les caractéristiques de sécurité, de protection de la santé ainsi que les performances des dispositifs médicaux ont un contenu et un champ d'application différents; que les procédures de certification et de contrôle relatives à ces dispositifs diffèrent d'un État membre à l'autre; que de telles disparités constituent des entraves aux échanges à l'intérieur de la Communauté;

considérant que les dispositions nationales assurant la sécurité et la protection de la santé des patients, des utilisateurs et, le cas échéant, d'autres personnes en vue de l'utilisation des dispositifs médicaux doivent être harmonisées afin de garantir la libre circulation de ces dispositifs sur le marché intérieur;

considérant que les dispositions harmonisées doivent être distinguées des mesures prises par les États membres en vue de gérer le financement des systèmes de santé publique et d'assurance maladie concernant directement ou indirectement de tels dispositifs; que, dès lors, ces dispositions n'affectent pas la faculté des États membres de mettre en œuvre les mesures susmentionnées dans le respect du droit communautaire;

considérant que les dispositifs médicaux doivent offrir aux patients, aux utilisateurs et aux tiers un niveau de protection élevé et atteindre les performances que leur a assignées le fabricant; que, dès lors, le maintien ou l'amélioration du niveau de protection atteint dans les États membres constitue un des objectifs essentiels de la présente directive;

considérant que certains dispositifs médicaux sont destinés à administrer des médicaments au sens de la directive 65/65/CEE du Conseil, du 26 janvier 1965, concernant le rapprochement des dispositions législatives, réglementaires et administratives relatives aux spécialités pharmaceutiques [4]; que, dans ces cas, la mise sur le marché des dispositifs médicaux en règle générale est régie par la présente directive et la mise sur le marché des médicaments est régie par la directive 65/65/CEE; que si, toutefois, un tel dispositif est mis sur le marché de telle sorte qu'il forme avec le médicament une entité non réutilisable destinée à être utilisée exclusivement dans cette combinaison, cette entité est régie par la directive 65/65/CEE; qu'il convient de distinguer les dispositifs médicaux susmentionnés et les dispositifs médicaux incorporant, entre autres, des substances qui, si elles sont utilisées séparément, sont susceptibles d'être considérées comme un médicament au sens de la directive 65/65/CEE; que, dans de tels cas, lorsque les substances incorporées dans les dispositifs médicaux sont susceptibles d'agir sur le corps par une action accessoire à celle du dispositif, la mise sur le marché de ces dispositifs est régie par la présente directive; que, dans ce contexte, la vérification de la

(1) JO n° C 237 du 12. 9. 1991, p. 3.
JO n° C 251 du 28. 9. 1992, p. 40.
(2) JO n° C 150 du 31. 5. 1993.
JO n° C 176 du 28. 6. 1993.
(3) JO n° C 79 du 30. 3. 1992, p. 1.

(4) JO n° 22 du 9. 6. 1965, p. 369/65. Directive modifiée en dernier lieu par la directive 92/27/CEE (JO n° L 113 du 30. 4. 1992, p. 8).

I, IIa, IIb, III: Les classes de dispositifs médicaux

12 septembre 2014 Directive 93/42/CEE

Les classes évoluent avec le nouveau règlement UE 2017/745,

Définir la **classe d'un dispositif médical** (DM) est une nécessité pour tout fabricant, en Europe c'est cette classe qui va permettre de définir les contraintes pour établir la **conformité du produit aux exigences réglementaires**.

Il existe quatre classes pour les DM, par ordre de criticité: I, IIa, IIb et III. La **criticité** est fonction du risquepotentiel pour le patient, le personnel soignant ou toute autre personne intervenant lors de l'utilisation du dispositif.

L'annexe IX de la directive Européenne 93/42/CEE définit le système de classification

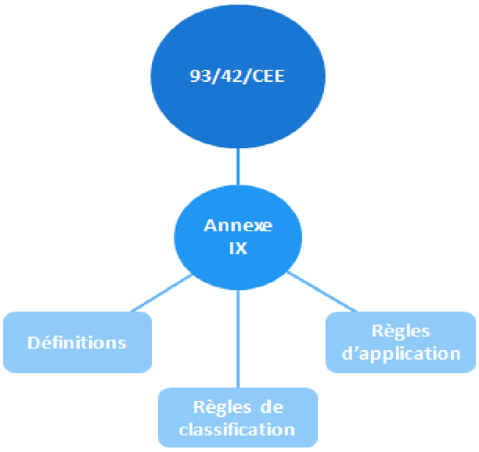

L'annexe IX de la directive 93/42/CEE sur les DM définit les critères utilisés pour la classification, vous pouvez vous reporter au guide MEDDEV 2.4/1 rev.9 qui apporte des précisions et des exemples pour chaque point de l'annexe.
Pour finir, la commission Européenne publie, et met régulièrement à jour, un guide pour les classifications "ambiguës" exemple : dispositif de décontamination de l'air, produits de désinfection des mains, produits de blanchiment des dents ou encore la nouveauté de l'édition 1.16: les **logiciels et applications mobiles**.

L'annexe est divisée en 3 parties:

- **Définitions**: des précisions sur les termes employés dans les critères de classement.
- **Règles d'application**: généralités sur la manière d'appliquer les critères.
- **Règles de classification**: 18 règles qui définissent une cinquantaine de cas de figure.

Les définitions utilisées pour classer les DM

Durée d'utilisation du dispositif

Il s'agit de quantifier la **durée maximale durant laquelle le DM est susceptible d'être utilisé en continu***, il existe 3 niveaux:

- **temporaire** si < 1 heure
- **court terme** si comprise en 1 heure et 1 mois
- **long terme** au delà

Évidement, la criticité augmente avec la durée.

(*) en continu: applicable même si l'on remplace le DM durant l'acte.

Dispositif invasif, dispositif implantable

Les **dispositifs invasifs** pénètrent le corps, par un orifice naturel ou suite à un acte chirurgical auquel cas on parle de **dispositif invasif de type chirurgical**.

Un **dispositif implantable** est lui invasif et destiné à rester dans le corps.
Là aussi la criticité est croissante: l'acte chirurgical introduit de nouveaux risques, tout comme le fait de laisser le DM dans le patient.

Dispositif chirurgical

Tout est dans le nom: il est destiné à accomplir un acte… chirurgical.

Dispositif actif, thérapeutique, destiné au diagnostic

Le nom est trompeur: il s'agit essentiellement des dispositifs médicaux électriques et plus généralement des DM qui utilisent une **énergie** non fournie par un humain ou la pesanteur (un pèse patient électrique et actif, un pèse patient mécanique ne l'est pas).

Ainsi un DM utilisé pour faire du monitoring est passif vis à vis du patient (il ne fait que mesurer) mais actif au sens de la directive.

<u>Précision importante: les **logiciels** sont considérés comme actifs.</u>

C'est donc la source d'énergie qui ajoute de la criticité , le DM étant susceptible de vous électrocuter, de vous écraser, de vous irradier

Ces dispositifs actifs peuvent également être **thérapeutiques** (pour soulager blessures et autres handicaps) ou destiné au **diagnostic**.

Sites critiques: Système circulatoire central et Système nerveux central

Ces sites anatomiques étant particulièrement critiques l'annexe définit clairement les parties du corps concernées: le **système nerveux central** inclut l'encéphale, la moelle épinière, les méninges; la liste des vaisseaux constituants le **système circulatoire** est précisée.

Les Règles d'application

Quelques règles pour comprendre comment aborder la classification.

- Les dispositifs utilisés en **combinaison** sont à classer séparément.
- Un **logiciel** lié à un dispositif hérite de sa classe.
- C'est le cas d'utilisation le **plus critique** qui doit être envisagé pour la classification (ce qui reprend la philosophie appliquée pour la gestion des risques).
- Si **plusieurs règles** s'appliquent alors c'est la plus sévère qui sera appliquée.

La classe du DM, la (les) règle(s) appliquée(s) ainsi que les justifications sont à reporter dans la documentation technique construite en vue du marquage CE, par exemple dans le dossier de gestion des risques puisque c'est la notion de risque qui est analysée ici.

Les Règles de classification

C'est via **18 règles** que la classe va être déterminée, règles qui in-fine établissent une **cinquantaine de critères**.

Les 4 familles de dispositifs

Le système de classification regroupe les dispositifs médicaux selon quatre familles:

- Règles pour les dispositifs **non invasifs**
- Règles pour les dispositifs **invasifs**
- Règles pour les dispositifs **actifs**
- Règles **spéciales**

Hormis les 2 premières, les familles peuvent se recouper, par exemple un dispositif invasif peut être actif.

Les règles particulières

Certaines règles sont très ciblées, la directive a une attention particulière pour les dispositifs destinés à:

- visualiser la distribution de produits radiopharmaceutiques in vivo
- enregistrer les images de radiodiagnostic
- désinfecter les dispositifs invasifs
- désinfecter, nettoyer,(…) des lentilles de contact
- être une poche de sang…

Exemple de classification de dispositifs médicaux

- **Classe I:** Lèves-personne, Seringues (sans aiguille), Scalpels, Électrodes pour ECG, Gants d'examen.
- **Classe IIa:** Tubes utilisés en anesthésie, Tubes de trachéotomie, Aiguilles pour seringue, Pansements hémostatiques, Tensiomètres, Thermomètres.
- **Classe IIb**: Machines de dialyse, Couveuses pour nouveaux nés, Oxymètres, Respirateurs, Préservatifs masculins, Trocarts stériles, Moniteurs de signes vitaux, Implants dentaires.
- **Classe III:** Cathéters destinés au cœur, Spermicides, Neuro-endoscopes, Aiguilles trans-septales, Applicateurs d'agrafe chirurgicale, Pinces souples à biopsie, Pompes cardiaques, Prothèses articulaires de la hanche.

Notez que l'ANSM publie la liste des dispositifs médicaux communiqués par les fabricants (pour les classes IIa, IIb et III), la classe des DM y est précisée, cela peut être une bonne source d'information.

Impact de la classe sur la procédure de marquage CE

Le choix de la procédure de marquage CE dépend de la classe du dispositif, naturellement: les contraintes seront plus importantes lorsque la classe est plus critique.

L'illustration ci-dessous expose les procédures offertes au fabricant :

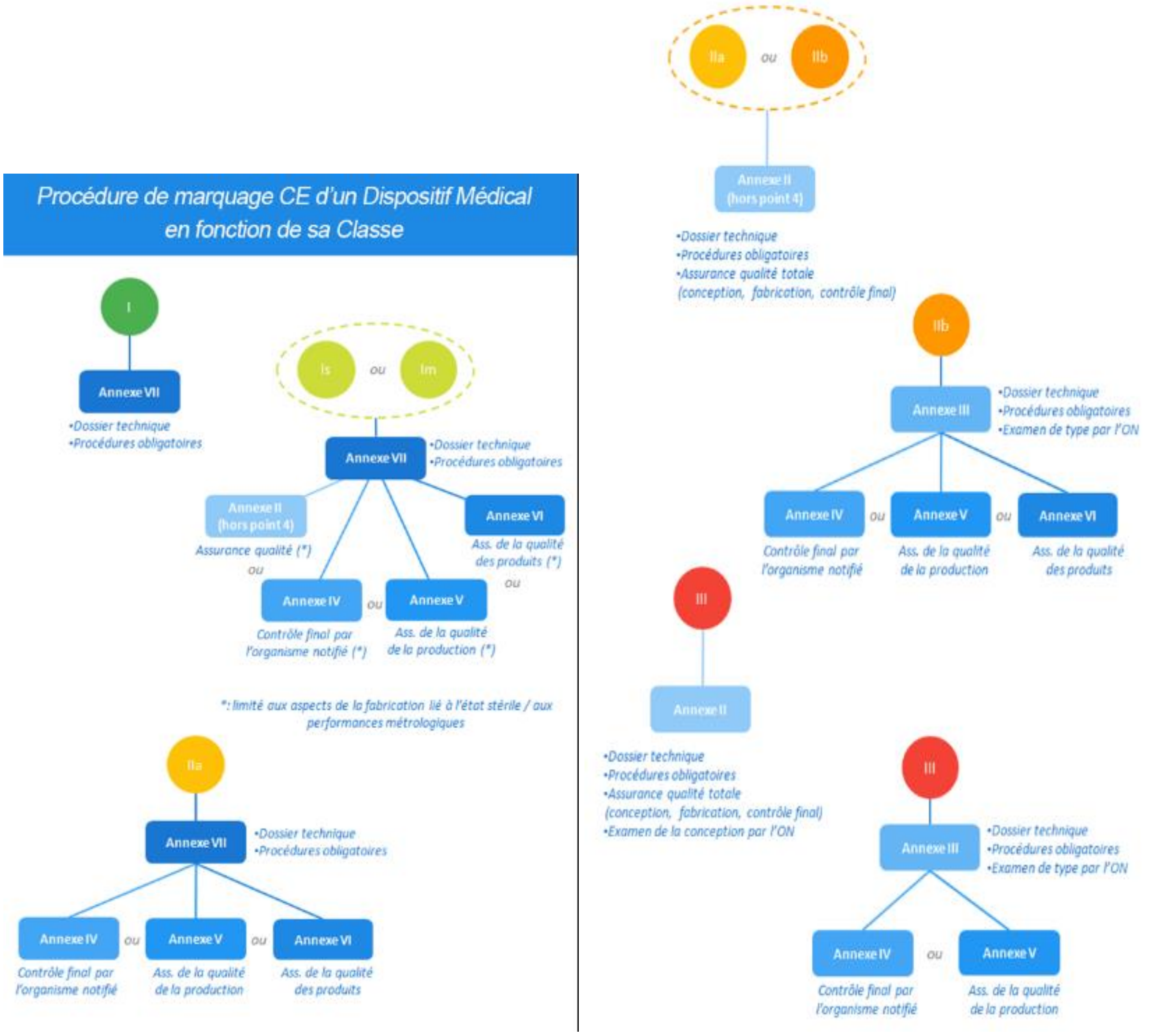

On retiendra que:

- Le [marquage CE des DM de classe I] se fait en “auto-certification”, sans recours à un organisme notifié
- Les classes 1 avec fonction de mesurage ou stérile nécessite une assurance qualité (AQ) de la production (uniquement pour les aspects mesure / stérile)
- Un organisme notifié intervient dès la classe 2a pour, selon les cas, certifier l’AQ complète, certifier l’AQ partielle, effectuer un examen du produit ou réaliser le contrôle final

2.Publications on thesis work

polymers

MDPI

Article

Enhanced Figures of Merit for a High-Performing Actuator in Electrostrictive Materials

Nellie Della Schiava [1,2], Kritsadi Thetpraphi [1], Minh-Quyen Le [1], Patrick Lermusiaux [2,3], Antoine Millon [2,3], Jean-Fabien Capsal [1] and Pierre-Jean Cottinet [1,*]

1 Univ Lyon, INSA-Lyon, LGEF, EA682, F-69621 Villeurbanne, France; nellie.dellaschiava@insa-lyon.fr (N.D.S.); Kritsadi.Thetpraphi@insa-lyon.fr (K.T.); minh-quyen.le@insa-lyon.fr (M.-Q.L.); jean-fabien.capsal@insa-lyon.fr (J.-F.C.)

2 Groupement Hospitalier Edouard Herriot, 69003 Lyon, France; patrick.lermusiaux@insa-lyon.fr (P.L.); antoine.millon@insa-lyon.fr (A.M.)

3 Université Claude Bernard Lyon 1 (Univ Lyon), 8 Avenue Rockefeller Lyon, F-69621 Villeurbanne, France

* Corresponding author: pierre-jean.cottinet@insa-lyon.fr; Tel.: +33-472-438-833

Received: 8 February 2018; Accepted: 1 March 2018; Published: 3 March 2018

Abstract: The overall performance of an electrostrictive polymer is rated by characteristic numbers, such as its transverse strain, blocking force, and energy density, which are clearly limited by several parameters. Besides the geometrical impact, intrinsic material parameters, such as the permittivity coefficient as well as the Young's modulus and the breakdown electric field, have strong influences on the actuation properties of an electroactive polymer and thus on the device's overall behavior. As a result, an analysis of the figures of merit (FOMs) involving all relevant material parameters for the transverse strain, the blocking force, and the energy density was carried out, making it possible to determine the choice of polymer matrix in order to achieve a high actuator performance. Another purpose of this work was to demonstrate the possibility of accurately measuring the free deflection without the application of an external force and inversely measuring the blocking force under quasi-static displacement. The experimental results show good electrostrictive characteristics of the plasticized terpolymer under relatively low electric fields.

Keywords: electrostrictive unimorph cantilever; deflection; blocking force measurement; actuators; material optimization; figure of merit

JOURNAL OF POLYMER SCIENCE Polymer Physics WWW.POLYMERPHYSICS.ORG FULL PAPER

Influence of Plasticizers on the Electromechanical Behavior of a P(VDF-TrFE-CTFE) Terpolymer: Toward a High Performance of Electrostrictive Blends

Nellie Della Schiava,[1,2] Minh-Quyen Le,[1] Jeremy Galineau,[1] Fabrice Domingues Dos Santos,[3] Pierre-Jean Cottinet,[1] Jean-Fabien Capsal[1]

[1]LGEF INSA de Lyon, 8 rue de la Physique, Villeurbanne, 69100, France
[2]Groupement Hospitalier E. Herriot, Chirurgie vasculaire Pavillon M, 5 Place d'Arsonval, 69437 Lyon Cedex 03, France
[3]Piezotech SA, Arkema Group, Rue Henri Moissan, Pierre Benite, 69310, France
Correspondence to: P.-J. Cottinet (E-mail: pierre-jean.cottinet@insa-lyon.fr)

Received 18 August 2016; accepted 10 November 2016; published online in Wiley Online Library
DOI: 10.1002/polb.24280

ABSTRACT: This work aims at providing a complete analysis of the effect of plasticizers on the electrostrictive terpolymer performance. To achieve this, several plasticizing agents such as 2-ethylhexyl phtalate (DEHP), diisononyl phtalate (DINP), and palamoll 652 have been incorporated in the polymer matrix. Experimental results demonstrate that the proposed novel materials exhibited excellent electromechanical enhancement in terms of transverse strain and mechanical energy density under a moderate electric field, which is definitively critical in recent microscale actuation. Another objective of this article was to explore material characteristics as a function of the DINP content, and it was found that the plasticizer weigh fraction was the key parameter determining performance of the modified fluorinate terpolymer blends. Accordingly, it was revealed that high performance flexible actuators can be achieved merely by employing a simple and cheap plasticizer, thus making it possible to overcome the current technological barrier of conventional electroactive polymers that suffer from the high applied electric field usually required to reach sufficient strain. © 2017 Wiley Periodicals, Inc. J. Polym. Sci., Part B: Polym. Phys. **2017**, *55*, 355–369

KEYWORDS: actuators; blends; electroactive polymer; ferroelectricity; high performance polymers; printing electronic www.nature.com/scientificreports

SCIENTIFIC REPORTS

natureresearch

OPEN

Effect of beta-based sterilization on P(VDF-TrFE-CFE) terpolymer for medical applications

Nellie Della Schiava[1,2], Francesco Pedroli[1], Kritsadi Thetpraphi[1], Annalisa Flocchini[2], Minh-Quyen Le[1], Patrick Lermusiaux[1,2,3], Jean-Fabien Capsal[1] & Pierre-Jean Cottinet[1]✉

Electroactive polymers (EAP) are one of the latest generations of flexible actuators, enabling new approaches to propulsion and maneuverability. Among them, poly(vinylidene fluoride-trifluoroethylene-chlorofluoroethylene/chlorotrifluoroethylene), abbreviated terpolymer, with its multifunctional sensing and actuating abilities as well as its impressive electrostrictive behavior, especially when being doped with an plasticizer, has been demonstrated to be a good candidate for the development of low-cost flexible guidewire tip for endovascular surgery. To minimize the possibility of bacterial, fungal, or viral disease transmission, all medical instruments (especially components made from polymers) must be sterilized before introduction into the patient. Gamma/beta (γ/β) irradiation is considered to be one of the most efficient techniques for targeted reduction of microbials and viruses under low temperature, often without drastic alterations in device properties. However, radiation may cause some physical and chemical changes in polymers. A compromise is required to ensure sufficient radiation for microbial deactivation but minimal radiation to retain the material's properties. The main idea of this study aims at assessing the electromechanical performances and thermal/dielectric properties of β-irradiated terpolymer-based sterilization treatment. Ionizing β-rays did not cause any significant risk to the neat/plasticized terpolymers, confirming the reliability of such electrostrictive materials for medical device development.

Endovascular surgery is an innovative, less invasive procedure that is used to treat problems affecting the blood vessels. An alternative to open surgery, endovascular surgery offers many advantages including a shorter recovery period, less discomfort, local or regional anesthesia, smaller incisions, less stress on the heart, and fewer risks for patients. Thus, endovascular techniques become most of time the first line treatment in vascular surgery even for very complex procedures[1–3]. These methods have currently propelled the growth and technical development of numerous intravascular guides and catheters to navigate different targeted arteries. Electroactive polymers (EAPs) have recently attracted a great deal of researcher interest because of their fascinating properties and high potential in medical application, particularly for active catheters or guidewire designs[4–7]. In previous studies, we demonstrated the feasibility of P(VDF-TrFE-CFE/CTFE) terpolymer to create a new generation of intravascular steerable guidewires[8,9]. Several advantages of the developed polymers are easy preparation, simple process, and high bending angle under relatively low input voltages, which makes them suitable materials for future generations of active guidewires. The proposed material likely allows some of the current technological issues relating to the development and control of the steerable guidewire to be overcome, such as the high cost, complex integration of micro-motor, and delayed response. The actuator device used in previous research contains di(2-ethylhexyl) phthalate (DEHP) plasticizer, which is not certificated as biocompatible for surgical procedures. To meet this medical requirement, diisononyl phthalate (DINP) plasticizer was chosen instead for this study because of its biocompatibility and safety for the patients and because of its exceptional ability to significantly enhance the electromechanical performances of the terpolymer[10].

Medical devices today are multifunctional and are manufactured from a very wide variety of materials. Despite their frequently complex geometrical structures, each part has to be sterile. Particularly for invasive medical tools, sterilization becomes mandatory to avoid infections in patients. There are several methods of sterilization for endovascular surgery devices, and irradiation with γ/β rays and autoclaving with steam are the most frequently used

[1]Univ Lyon, INSA-Lyon, LGEF, EA682, F-69621, Villeurbanne, France. [2]Groupement Hospitalier Edouard Herriot, 69003, Lyon, France. [3]Université Claude Bernard Lyon 1 (Univ Lyon), 8 Avenue Rockefeller Lyon, F-69621, Villeurbanne, France. ✉e-mail: pierre-jean.cottinet@insa-lyon.fr

3. Communications on thesis work

-One poster at EuroEAP, juin 2018, abstract adopted by the reading committee.

-An oral communication at the European congress of vascular and endovascular surgery, 2016, abstract adopted by the reading committee.

-An oral communication at the congress of the French society of vascular and endovascular surgery, juin 2019, abstract adopted by the reading committee.

FOLIO ADMINISTRATIF

THESE DE L'UNIVERSITE DE LYON OPEREE AU SEIN DE L'INSA LYON

NOM : DELLA-SCHIAVA DATE de SOUTENANCE : 03/12/2020

Prénoms : Nellie, Laurence

TITRE : Development of electrostrictive P(VDF-TrFE-CFE) Terpolymer for medical applications.

NATURE : Doctorat Numéro d'ordre : 2020LYSEI112 Ecole doctorale : MEGA

Spécialité : Acoustique

RESUME : Pour traiter les maladies artérielles périphériques, les techniques endovasculaires sont devenues le traitement de première ligne car elles permettent une réduction considérable de la morbi-mortalité et des coûts de santé. Pour tout geste endovasculaire, un guide est nécessaire pour la navigation intra-artérielle. Il existe de nombreux guides mais aucun d'entre eux n'est orientable. Or le système artériel humain comporte beaucoup de bifurcations, d'angulations, ce qui oblige à utiliser des cathéters angulés. Ces manipulations peuvent entraîner des complications artérielles graves et les coûts globaux sont élevés. Un guide orientable serait donc un dispositif très intéressant pour le chirurgien, le patient et la santé publique. Les polymères électroactifs sont un des matériaux intelligents les plus intéressants du XXIè siècle. Parmi eux, les poly(fluorure de vinyle) ont été grandement étudiés pour leur haute performance électromécanique. Mais ils nécessitent un champ électrique élevé pour obtenir les réponses souhaitées, ce qui n'est pas envisageable pour des applications médicales. L'objectif de ce travail de thèse est de développer un guide orientable pour la navigation intra-artérielle basé sur le terpolymère électrostrictif P(VDF-TrFE-CTFE). Après avoir expliqué les raisons ayant fait choisir ce terpolymère, nous décrirons le processus de fabrication et sa caractérisation. Nous présenterons les figures de mérite des polymères utilisées pour développer une méthode pour obtenir des performances matérielles élevées, méthode utilisée ensuite pour évaluer celles du terpolymère. Ensuite, pour obtenir de meilleures performances électromécaniques, nous avons évalué l'influence de différents plastifiants sur le terpolymère. Nous avons ensuite évalué la possibilité d'utiliser le terpolymère à des fins médicales en testant sa résistance à la stérilisation et sa compatibilité cellulaire. Pour chaque étape, nous avons évalué le terpolymère pur et modifié en vérifiant toutes leurs performances électromécaniques. Enfin, nous avons travaillé sur la modélisation de la structure afin de concevoir un prototype du guide sous forme tubulaire.

MOTS-CLÉS : Terpolymer, P(VDF-TrFE-CFE), electroactive material, sensor, smart guide wire, endovascular navigation

Laboratoire (s) de recherche : LGEF, EA 682

Directeur de thèse: Pierre-Jean COTTINET, co-directeurs Jean-Fabien CAPSAL, Minh-Quyen Le

Président de jury :

Composition du jury : Pr Annie COLIN, Pr Richard LIANG, Dr Masae KANDA, Dr Frédéric DEMOLY, Pr Olivier ROUVIERE, Pr. Pratrick LERMUSIAUX, Dr. Pierre-Jean COTTINET, Dr. Jean-Fabien CAPSAL, Dr. Minh-Quyen Le